THE AMERICAN UNIVERSITY IN CAIRO
الجـامـعة الأمـريكيـة بالقـاهـرة

School of Sciences and Engineering

ANTI-SCHISTOSOMA SINGLE-DOMAIN ANTIBODY – NANOPARTICLES CONJUGATE: A NOVEL TOOL FOR DIAGNOSTIC AND THERAPEUTIC APPLICATIONS

A Thesis Submitted to

The Nanotechnology Graduate Program in partial fulfilment of the requirements for the Degree

of Master of Science in Nanotechnology

By: Mohamed Abdelazim Sallam

B.Sc. Biochemistry / Chemistry, Faculty of Science, Ain Shams University

Under the supervision of

Prof. Dr. Suher Zada

American University in Cairo, Department of Biology

Associate Prof. Dr. Adham Ramadan

American University of Cairo, Department of Chemistry

Prof. Dr. Serge Muyldermans

Vrije Universiteit Brussel, Department of Molecular & Cellular Interactions, Laboratory of Cellular and Molecular Immunology

Fall 2012

The American University in Cairo

School of Sciences and Engineering

ANTI-SCHISTOSOMA SINGLE-DOMAIN ANTIBODY – NANOPARTICLES CONJUGATE:

A NOVEL TOOL FOR DIAGNOSTIC AND THERAPEUTIC APPLICATIONS

A Thesis Submitted by Mohamed Abdelazim Sallam

To the Nanotechnology Graduate Program

Fall 2012

In partial fulfilment of the requirements for the degree of Master of Science in Nanotechnology

has been approved by:

Prof. Dr. Suher Zada

Thesis Committee Chair / Adviser _____

Affiliation _____

Associate Prof. Dr. Adham Ramadan

Thesis Committee Reader / Adviser _____

Affiliation _____

Prof. Dr. Serge Muyldermans

Thesis Committee Reader / Adviser _____

Affiliation _____

Prof. Dr. Wael Mamdouh

Thesis Committee Reader / Examiner _____

Affiliation _____

Prof. Dr. Eman Elahwany

Thesis Committee Reader / Examiner _____

Affiliation _____

_____   _____   _____   _____

Program Director   Date   Dean   Date

Abbreviation

Fe@C-MNPs	carbon-coated magnetometallic iron nanoparticles
®	registered mark
µCi	microcurie
^0C	degree Celsius
^{99}Mo	isotopes of molybdenum-99
^{99m}Tc	metastable nuclear isomer of technetium-99
a.u.	absorbance unit
Ab	antibody
Ag	antigen
AP	alkaline phosphatase conjugate
Arg	arginine
bp	base pair
cDNA	complementary DNA
CDR	complementarity determining region
CEA	carcinoembryonic antigen
CH	constant heavy chain domain
CL	constant light chain domain
CNT	carbon nanotube
Cys	cystine
DNA	deoxyribonucleic acid
DTT	dithiothreitol
ECD	1-ethyl-3-(3-dimethylaminopropyl)carbodiimide
eGFP	enhanced green fluorescent protein
ELISA	enzyme linked immunosorbent assay
Fab	antigen binding fragment
Fc	fragment crystallizable region
FR	framework regions
GBq	giga becquerel
Gln	glutamine

Glu	glutamic acid
Gly	glycine
GPI	glycosyl-phosphatidyl-inositol
HCAb	heavy-chain only antibody
HER2	human epidermal receptor 2
HPRI	human placental RNase inhibitor
hPSA	human prostate specific antigen
HRP	horse radish peroxidase
IFA	indirect immunofluorescence assay
Ig	immunoglobulin
IgG	immunoglobulin G
IgG-Nb	Nb of the IgG-isotype (with known antigen specificity)
IMAC	immobilized metal affinity chromatography
IPTG	isopropyl-β-D-thiogalacto-pyranoside
ITLC	instant thin layer chromatography
ka	association constant
kb	kilo base
kBq	kilo becquerel
KD	equilibrium dissociation constant
kd	dissociation constant
kDa	kilo dalton
Leu	leucine
mAb	monoclonal antibody
MBP	mannose binding protein
MITI	microwave induced thermoacoustic imaging
MNP	magnetic nanoparticles
mRNA	messenger ribonucleic acid
MUC	mucin
MW	molecular weight
MWCO	molecular weight cutoff
MWNT	multi-wall carbon nanotube

Nb	Nanobody[®]
NHS	N-hydroxysuccinimide
NP	nanoparticles
OD	optical density
PBL	peripheral blood lymphocyte
PBMC	peripheral blood mononuclear cell
PE	periplasmic extract
Phe	phenylalanine
pI	iso-electric point
RDT	rapid detection test
RT-PCR	reverse transcriptase-polymerase chain reaction
SEC	size exclusion chromatography
SmCB	*Schistosoma mansoni* cathepsin-B
SmSE	secretory execratory *Schistosoma mansoni*
SPR	surface plasmon resonance
SWNT	single-wall carbon nanotube
Taq	*Thermus aquaticus*
TAT	thermoacoustic tomography
TCT	thermoacoustic computed tomography
Trp	tryptophane
Tyr	tyrocine
™	trademark
Val	valine
VH	variable domain of the heavy chain of a conventional antibody
VHH	variable domain of the heavy chain of a heavy-chain only antibody
VHH2	bi-valent VHH
VL	variable domain of the light chain of a conventional antibody

Acknowledgments

First and foremost, I would like to thank my advisors, Prof. Dr. Suher Zada, Prof. Dr. Adham Ramadan and Prof. Dr. Serge Muyldermans for giving me the opportunity to work on such an interesting project. Their expertise, critical insight, and advice made the completion of this research thesis possible. More importantly, I am grateful for their support, attention to my work and for putting their confidence in me.

I specially want to thank Jan Van Gompel for the technical expertise, training and assistance throughout my practical work. I sincerely thank Dr. Christine Mikhael for her outstanding support all through the entire work. In addition, I sincerely thank Prof. Dr. Seham El-zeedy the director of veterinary serum and vaccine research institute for her admirable cooperation. I would like to express my appreciation to Dr. Cécile Vincke for her valuable comments and advices during my work. I would like to convey my thanks to Dr. Pieter De Pauw for his great support and very helpful conversations and discussions, Dr. Ibrahim Rabee from TBRI for providing us the antigens used throughout the research work, Dr. Emanuele Pesavento and Dr. Nick Devoogdt for assisting me with the experimental designs, biomolecules and protocols optimizations. Thanks are also extended to Prof. Dr. Wendelin Stark, Prof. Dr. Robert Grass and Dr. Evagelos Athanassiou from the Functional Materials Lab, ETH Zurich, and TurboBeads Inc. Zurich, for their support and providing us with all the needed reagents and materials.

I gratefully acknowledge the assistance provided by all the CMIM members. Thank you for creating the friendly atmosphere surrounding the laboratory and for giving me the feeling of belonging. My special thanks to Hassanzadeh, Benoit, Inge, Steve, Flor, Carol, Camille, Sam, Sanna, Steven, Yanick, Steven, and Liese. I thankfully acknowledge the assistance provided by Prof. Dr. Tony Lahoutte, Dr. Catarina Xavier and all the Nuclear Medicine In vivo Cellular and Molecular Imaging Lab members at the academic hospital, UZ Brussel. Thank you for giving me the opportunity to join your labs and enjoy every moment together. Finally, I would like to thank my family, my wife, Hagar, for her love, endless patience and support that have inspired me to do my best. I could never thank enough Sanaa, Afaf, Hanan, Hayam, Dalia, Ahmed, Mai, Aya and Salah. Their unconditional love and consistent faith in me helped me to be confident and determined to always follow my dreams.

Dedication

I sincerely dedicate this research thesis to the soul of Abdelazim Sallam, the father and the friend.

Table of Contents

List of Figures

List of Tables

Abstract

Nanotechnology has enthused excessive expectations in recent years, particularly in the biology and biomedical fields. Carbon-coated metallic nanomagnets reveal significant physicochemical properties, which are referred to as superparamagnetism, that when designed appropriately can be utilized to generate novel diagnostic and therapeutic applications for a wide range of biologically hazardous species. Schistosomiasis is a chronic parasitic disease that can infect both humans and animals, particularly cattle. It is caused by a trematode blood fluke of the genus *Schistosoma* which belong to the schistosomatidae family. At least 200 million individuals are infected in 75 countries while 600 million people are exposed to infection and are potentially victim of this parasite. Schistosomiasis is still recognized as one of the most neglected disease, the current available diagnostic techniques are deficient in accuracy and are incapable of identifying the disease in its early stages. Moreover, they suffer from prolonged examination time. Besides, the poorly available therapeutic drugs started to lose their efficacy and the parasite started to develop resistance against most of them, which create an imperative need for developing novel diagnostic and therapeutic tools. The humoral immune response of the Camelidae is unique since these animals possess functional heavy-chain only antibodies in addition to the classical antibodies. Thanks to recombinant DNA technology, a series of single-domain antigen binding entities can be produced against specific schistosome's parasite antigens. These binders possess a number of distinctive biophysical properties that offer particular advantages in various theranostic applications. Finally, nanomagnetism was selected to represent a certain phenomena through which we demonstrated, to our knowledge for the first time, the successful construction of effective and functional bioconjugate system which is appropriate for a plethora of diagnostic and therapeutic applications. The main thrust of this research work was towards the developing of single domain antibodies against *Schistosoma mansoni* gut specific antigen and execratory secretory antigen. In parallel, state-of-the-art methodologies were implemented for constructing a bioconjugate system composed of sdAb and graphene-coated metallic nanomagnet tagged with a carboxyl terminal. Finally, the well-established metastable technetium-99 (^{99m}Tc) is used for labeling the conjugate for studying the possibility of active and magnetic targeting of the nano-structured system – i.e. ^{99m}Tc-sdAb-Fe@C-MNP conjugates.

Aim of this research

In this study, we aimed at studying the possibility of generating single domain antibodies (hereinafter referred to as sdAb, VHH, Nb or Nanobodies®) against species-specific antigens of *Schistosoma mansoni* for diagnostic and therapeutic applications. Our interest has been focused on two antigens (i) *S. mansoni* Cathepsin B, and (ii) *S. mansoni* Execratory Secretory antigen. Furthermore, proving the concept of constructing novel conjugate systems through a distinctive bio-conjugation approach:

- Constructing of sdAb-Metallic Graphene-Coated Magnetic Nanoparticles for a variety of *in vitro* and *in vivo* diagnostic and therapeutic applications (i.e. TAT and MRI imaging, active/magnetic targeting and magnetic hyperthermia).

Specific objectives of the study

First Chapter:

- Camel immunization with *Schistosoma mansoni* native antigens of Cathepsin B (SmCB) and secretory execratory (SmES).
- Construction of Nanobody® immune cDNA and phage display libraries.
- Generation of SmCB binding Nanobodies®
- Generation of SmES binding Nanobodies®
- Characterization of Nb-Ag binding interaction via ELISA assays

Second Chapter:

- Generation of Nb-Graphene-Coated MNP
- Radio-labeling of Nb-Graphene-Coated MNP system and studying of magnetic targeting

Concluding Remarks and Future Challenges

CHAPTER 1: GENERATION OF CAMELIDAE'S SINGLE-DOMAIN ANTIBODIES AGAINST *Schistosoma mansoni*

1 Schistosomiasis: The Disease and the Cure

1.1 Background

Schistosomiasis is a parasitic disease commonly known as bilharzia, the infection caused by one of the five different species of the parasite (trematode helminthes) of the genus *Schistosoma*. The species of prevalent seriosity are *S. haematobium* (dominant in Africa), *S. japonicum* (dominant in Japan, Southeast Asia and Western Pacific) and *S. mansoni* (dominant in Africa, Southwest Asia, Brazil and Caribbean). *Schistosoma intercalatum and S. mekongi* are recognized as the two less significant species that parasitize humans. The route of infection takes place during direct skin contact with the free-swimming stage (i.e. cercariae) while swimming or bathing in slow-moving fresh water streams which are inhabited by intermediate host (Adel, 2001).

The world health organization WHO estimates that there are about 200 million people worldwide infected with Schistosomiasis, 120 million symptomatic patients and 600 million individuals live at risk (WHO, 1993). In sub-Saharan Africa the estimated fatality related to *S. mansoni* and *S. haematobium* is about 280,000 people per year (Pearce & MacDonald, 2002). The range of endemicity of the disease may change either throughout movements of infected persons to endemic areas, or through the creation of artificial new habitat for infected snails (i.e. dams, canals and fields irrigated by flooding, for instance, rice fields).

Schistosomiasis is endemic to over 70 countries, and about 85% of the 200 million people infected with schistosoma live in Africa (WHO, 2010). **Figure 1.1** represents the recent distribution of the diseases worldwide and primarily highlighting the following regions:

- Africa: Southern, Sub-Saharan, Lake Malawi.
- Asia: Philippines, Laos, Cambodia, Japan, Central Indonesia, Mekong Delta, Southern China.
- Caribbean: Antigua, Dominican Republic, Guadeloupe, Martinique, Montserrat, Saint Lucia.
- Egypt: Nile River Valley.
- Middle East: Iran, Iraq, Saudi Arabia, Syrian Arab Republic, Yemen.
- South America: Brazil, Suriname, Venezuela.
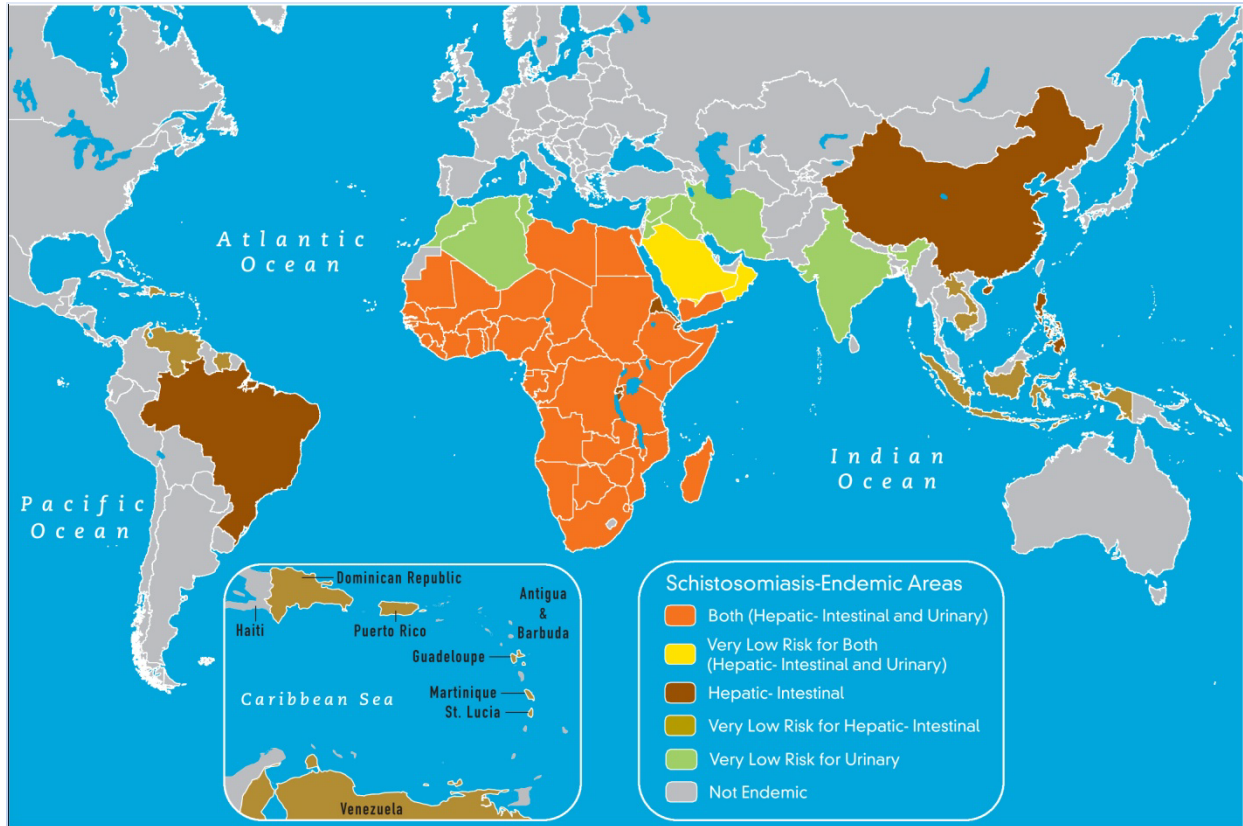
Figure 1.1. Geographic Distribution of Schistosomiasis. *(CDC, 2011)*

There are four trematode species in the genus Schistosoma, *Schistosoma mansoni, S. haematobium, S. japonicum, and S. mekongi*, cause a series of related diseases in humans referred to as schistosomiasis. Additionally, *S. intercalatum* is a parasite of cattle in West Africa which occasionally causes the disease in humans. Schistosomiasis is also known as: Katayama fever, Bilharzia or Schistosome blood-dwelling fluke worms.

The effect of Schistosomiasis on human health was early characterized at least 4,000 years ago in early Egyptian papyri, recent analysis could reveal immunological clues as to its existence in ancient mummies (Adel, 2001). In 1851, Theodor Bilharz discovered the etiology of Schistosomiasis in humans while he was working out of Cairo, Egypt. The German physician successfully identified adult male and female *Schistosoma haematobium* during autopsy examinations. Furthermore, for more than half a century the clinical symptoms of *Schistosoma japonicum* was described as a syndrome until the species was discovered in 1904.

In 1907, Sir Patrick Manson was the first scientist who discovered *Schistosoma mansoni* and could identify the differences in egg morphology – i.e. terminal versus lateral spine, and excretion pathways – i.e. fecal versus urinary, of the two separate species *S. mansoni* and *S. haematobium*. The life cycle details of *S. japonicum* were clearly elucidated in 1913 by Keinosuka Miyairi and Masatsuga Suzuki, they could describe the route of infection into human hosts and the exact dynamics of the parasite life cycles (Bigwan et al., 2012).

The life cycles of all schistosoma species are quite comparable, all the adult worms live in mesenteric venules nearby liver, with the exception of *S. haematobium* in which adults migrate to urinary bladder and live in venous plexus, where it discharges eggs into fresh water sources through urine. All the species share the same mode of infection, infection starts in fresh water where snails are shedding cercaria – i.e. infective form, which penetrates the patient skin – e.g. human and cattle, after that cercaria develop into schistosomula which migrates to the lung. Afterward, schistosomula continue to migrate to the liver through the blood stream. Finally, the eggs enter the small intestine and excreted in the feces and deposited in fresh water where they hatch and release miracidium that penetrate snails.

The schistosomes feed on their host blood (blood fluke) and are attached to the mesenteric venous plexus. The females secrete eggs with ciliated miracidium larva in the urine or stool. The miracidia are released from eggs, and they start to search for their related freshwater snails that serve as the intermediate host. Subsequently, the infected snails produce thousands of cercariae which remain in the water for months. Rivers, lakes, ponds, man-made reservoirs and flooding irrigation systems become typical sources of infection and have resulted in regional increases in schistosomiasis. On finding a host, the cercariae penetrate the host skin and migrate into the liver where they transform into young worms over several weeks before migrating to the mesenteric destination (WHO, 2010). **Figure 1.2** illustrates the general life cycles of the three widespread schistosoma species – i.e. *Schistosoma mansoni, S. haematobium, S. japonicum*.
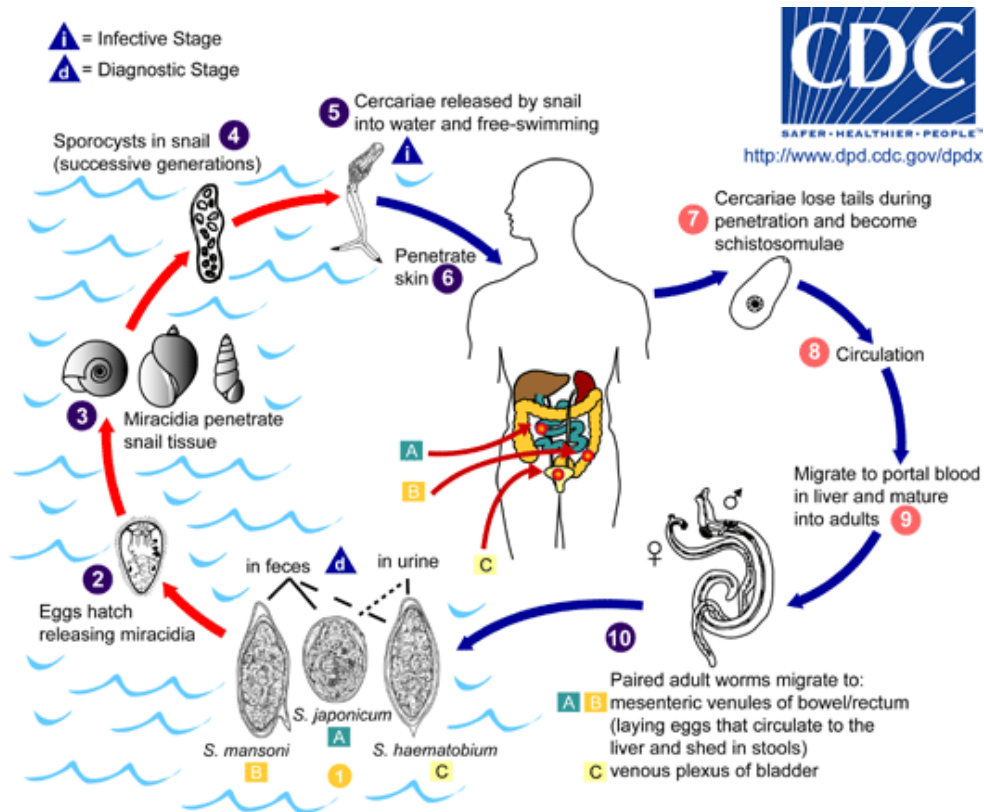
Figure 1.2. Life Cycle of Schistosoma mansoni, S. haematobium, S. japonicum. (CDC, 2010)

There are three genera of freshwater snails which host miracidia of the key human schistosomes, *Oncomelania (S. japonicum)*, *Bulinus (S. haematobium)* and *Biomphalaria (S. mansoni)*. *Schistosoma japonicum* has competent reservoirs in many domesticated animals including cats, dogs, horses and cattle. Whereas, *S. haematobium* has no identified animal reservoirs, recently *S. mansoni* has been found to rarely parasitize monkeys and some rodents, but does not have any genuinely established non-human hosts (Pearce & MacDonald, 2002).

Symptoms differ with respect to the infectious species of worm as well as the phase of infection. In the very beginning, itching and rash at site of percutaneous penetration of the cercariae is often recognized as the earliest sign of infection (usually known as Swimmer's Itch). Immediately afterward, fever, localized oedema and allergic reactions may occur (John & Petri, 2006). The invasion of cercariae might initiate a wide variety of pathologies, the acute pathology also known as Katayama fever which is very common in tourists, travelers and other people accidentally exposed to transmission that include sudden fever, myalgia, fatigue and malaise. **Figure 1.3** illustrates the foremost symptoms of cercariae penetration (i.e. Swimmer's Itch).

4

Figure 1.3. Initial Symptoms of Cercariae Penetration *(Education, 2011)*

The acute phase is usually manifested after one to three months of infection, when the mature flukes start laying eggs in the mesenteric or vesical venules, patients start on complaining of fever and abdominal pain. The deposition of eggs in the small hepatic venules causes the formation of granulomas in the liver and initiation of pipestem fibrosis of the portal and associated veins. Later on, hepatosplenomegaly and lymphadenopathy usually occur (Pearce *&* MacDonald, 2002; Bigwan et al., 2012).

Chronic schistosomiasis stages may be presented in a wide variety of forms, intestinal chronic schistosomiasis typically caused by *S. japonicum* and *S. mansoni*, where large intestines are habitually the site of the infection. Patients experience diarrhea with or without blood, dyspnoea, weight loss, diffuse abdominal pain and discomfort and hepatosplenomegaly might occur. However, the main lesions (situated in large bowl and rectum, bladder, kidney and liver) are not due to the worms but due to the trapped eggs in tissues secreting proteases that provoke eosinophylic inflammatory and granulomatous reactions. **Figure 1.4** shows 6-year-old boy with gross reactive hepatosplenomegaly (left side) and 19-year-old symptomatic man (right side) with chronic fibrotic hepatic schistosomiasis, it illustrate sever splenomegaly, external varices, ascites, and growth retardation (Gryseels et al., 2006).

Figure 1.4. Intestinal and Hepatic Schistosomiasis (Gryseels et al., 2006)

Urinary chronic schistosomiasis, typically caused by *S. haematobium,* is associated with painful urination (dysuria). Given that, these eggs rupture the bladder wall and cause the damage that can contribute to blood in urine (haematuria). In addition, they are also associated with greatly increased incidence of squamous cell carcinoma of the bladder. Cerebral schistosomiasis is most commonly caused by *S. japonicum*, in which the egg deposits cause local damage and lesions in the host central nervous system (CNS). Moreover, severe problems rooted in capillary blockage and subsequent ischemia (John & Petri, 2006). **Figure 1.5** represents two different urine samples, the right sample is for normal patient, whereas, the left sample is for a patient with macro-haematuria due to ulceration of the bladder wall in urinary schistosomiasis (Gryseels et al., 2006).

Figure 1.5. Haematuria Urinary Schistosomiasis (Gryseels et al., 2006)

Hepatic chronic schistosomiasis can lead to liver fibrosis, gastrointestinal varices. The genital schistosomiasis, which is quite common in endemic areas, is regularly found in travelers

and might lead to haemospermia or ovarian lesions causing infertility. However, in schistosomiasis the organ function and indices remain largely unaffected for a long time when the infection might no longer be detectable. Many of the unspecific and multifactorial morbidity symptoms are clinically and epidemiologically hard to differentiate from other infections such as malaria or other poverty-related health problems. Finally, quite a lot of other disorders are usually associated with chronic schistosomiasis, the risk of colon and liver cancer increases with prolonged infection. It is also possible that the chronic bacterial (e.g. chronic salmonellosis) and trematodes infections are more than accidentally connected (John & Petri, 2006; WHO, 2010; Bigwan et al., 2012).

1.2   Diagnosis and Therapy

1.2.1   Diagnostic Tests

The classical standards of diagnosing schistosomiasis are still microscopic-based examination of excreta – i.e. urine and stool smears. Nevertheless, concentration steps need to be included for mild infections or poor egg secretions. Unfortunately, the egg count poorly reflects the worm burden inside the host. Nevertheless, bladder or rectal biopsy specimens are also standard practice (Elliott, 1996). Recently, some haematological techniques correlate between the elevated count of eosinophil and schistosomiasis infection (Dajotoy et al., 2004).

Additionally, sensitive antibody-based assays – i.e. methods where the schistosomes-specific host antibodies are detected, are available. However, these approaches are restricted to specialized hospital settings and fail to discriminate exposure to antigens from active infections. Likewise, antibody tests are also available, such tests are able to screen the presence and quantify the somatic schistosomes' antigens as well. Commonly, circulating anodic antigen – CAA and circulating cathodic antigen – CCA with monoclonal antibodies (mAbs) are successfully used. Despite the fact that, such screening tests do not distinguish between present and history infections (Fulford & Keystone, 2002).

1.2.2   Management and Therapy: Current Status and Novel Approaches

Bilharzia is treated symptomatically with various corticosteroids, a number of schistosomytoxic compounds currently exist such as: Praziquantel, Oxamniquine and Artemisinin. Regarding Praziquantel, it has insignificant toxicity to the animals and human while it exhibits an adequate

toxicity to the mature worm stage, it prevents worms from growing or multiplying in the body. Nonetheless, it is ineffective against immature stages, so that constant treatments are compulsory, although, recurrences of infection still highly probable. The imminent threat of an omnipresent resistance of helminthes to the only available drugs might happen, for this reason, prolonged and massive treatment with these drugs should be avoided. Indeed, Oxamniquine resistance has already been reported and Praziquantel tolerant schistosomes could be found in animals (King et al., 2000).

In 2009, a notable study of the genome of the blood fluke *Schistosoma mansoni* (and *S. japonicum* as well) was published, in which the entire 363 mega-base nuclear genome of the blood fluke was fully analyzed, this genome encodes at least 11,809 genes (Berriman et al., 2009). The bioinformatics approaches could successfully identify numerous metabolic chokepoints, in addition, via thorough chemogenomic screens a series of the parasite proteins, for which existing and future drugs may be effectively developed, has been pinpointed. Thus, such information provides a giant resource for the research community from countless aspects in order to develop new control tools, early diagnostic methodologies and therapeutics for the eradication of this serious, and yet, neglected disease.

Without delay, it is clear that there is an urged need for developing totally new and potent anti-schistosomes drugs, as well as, novel and sensitive diagnostic tools either applicable in field tests or to mass-screening the worm burden *in vivo* in human and cattle. Nevertheless, identifying the worm location in patients is greatly required and would positively affect the entire process of developing robust, efficient, reliable and cost friendly theranostic endeavors. For these objectives, the research group set a plan up to developed highly specific, soluble, stable and monovalent single-domain antibodies (sdAbs) from immunized camel's library against *Schistosoma mansoni* parasite – i.e. fully functional antibody fragment. Comprehensive enlightenment of the reasons behind selecting such unique antibody type is concluded from studying their exceptional properties which will be resourcefully described in the next section. Furthermore, a proof of concept experiment was developed for constructing of bioconjugate system of radio-labeled graphene-coated metallic magnetic nanoparticles to various sdAbs for diagnostic and therapeutic applications.

2 Camelidae's Single-Domain Antibodies: Current Status & Numerous Possibilities

2.1 Introduction

The intensity of the natural immune system has gained much interest because of its importance in a wide range of both fundamental and applied sciences. The immunoglobulins are soluble glycoproteins in blood and tissue liquids that play a basic and essential role in the humoral immune system of vertebrates. Antibodies are synthesized by B-lymphocytes in response to foreign biological and chemical substances – i.e. antigens, of enormous structural variations with an intention to counteract, or neutralize, them. Owing to their high specificity and high binding affinity of antigens and to the possibility of generating antibody against practically limitless repertoire of antigens, antibodies and their derivatives are recognized among the most imperative reagents for fundamental, applied and medical research (Tillib, 2011).

Notwithstanding the fact that camelids are economically important in the Middle East, North African and South American countries, their immune system was barely investigated until the mid-1990s. Systematically, camelid species belong to the family of *Camelidae*, suborder of *Tylopoda*, order of *Atiodactyla* (Conrath et al., 2003). **Table 1.1** gives an idea about the normal average haematological values of camelid sera, in which it is so observable there are no significant disparities among different camelidae species.

Table 1.1. *Haematological values of camelid sera (Wernery et al., 1999)*

	Desert dromedary	Bactrian camel	Llama
Platelets	240-310 x 10^3/μL	Not available	240-310 x 10^3/μL
Red blood cells	7.1-10.9 x 10^6/μL	10.2-13.2 x 10^6/μL	10.5-17.2 x 10^6/μL
White blood cells	10.2-21.5 x 10^3/μL	10.0-15.8 x 10^3/μL	8.0-21.4 x 10^3/μL
Neutrophils (%)	35-60	28-83	41.7-72.9
Lymphocytes (%)	29-55	19-56	9.2-23.2
Monocytes (%)	2-5	0-7	0-4.6
Eosinophils (%)	2-12	0-18	0.2-21.4
Basophile (%)	0-2	0-3	0-14

Although various kits are in use to estimate the actual immunoglobulins concentration, they generally fail to concede consistent results (Wernery, 2001). Therefore, it is rather premature to propose a standard table with a reliable range of concentrations of the various

immunoglobulins' isotypes, and only a qualitative description can be merely provided. Nevertheless, the average values from the few published data affirm that the dromedary immunoglobulins-G IgG includes (i) IgG1 fraction purified from sera by protein A and protein G chromatography of approximately 3 mg antibody per mL serum (Hamers-Casterman et al., 1993), (ii) the IgG2 and IgG3 fractions' concentrations are about 1 and 2 mg antibody per mL of serum, respectively (Nguyen et al., 2001).

Classification of the camelid IgG is typically achieved based on the subject of characteristic differences in the ranges of their heavy chain molecular weight's values. Epigrammatically, the conventional IgG1 is a dominant isotype of IgG antibodies comprising of two heavy chains (H-chains) of about 50 kDa each, and two light chains (L-chains) of 25 kDa each. The other two IgG fractions were named IgG2 and IgG3 which represent the camelid heavy chain antibodies. The absence of the constant heavy chain domain (CH1-domain) which was confirmed via complementary DNA (cDNA) analyses explains the H-chain molecular weight difference of the IgG2 and IgG3 weighed against IgG1. Characteristically, the H-chains of IgG2 and IgG3 are about 10 kDa lighter than those of the conventional IgG1 (De Genst et al., 2006a).

The average concentration of the IgG2 and IgG3 in the serum of camelids is different for each species. For instance, in dromedary approximately half of the concentration of the serum IgG repertoire corresponds to the heavy-chain antibodies. However, their concentration in llama serum is much lower (Muyldermans et al., 2001a; De Genst et al., 2006a).

2.2 Heavy Chain only Antibodies: Discovering the Phenomena

In 1993, a Belgian scientific group could find, by serendipity, (in the course of performing a set of electrophoretic analysis of immunoglobulins for the sera of assorted representatives of camelidae's), that these animals incorporate in their serum a unique class of antibodies that lack L-chains in presence of the conventional ones, they were called heavy-chain only antibodies HCAbs (Hamers-Casterman et al., 1993). The antigen-binding domains of these exceptional camelid HCAbs consist of only one domain, termed variable domain of the heavy chain of the heavy-chain antibodies VHH. Such feature offers a large number of technological advantages in the generation of engineered antibodies, as compared with conventional antibodies which require

both the variable domain of the heavy chains (VH), in addition to that of the light chains (VL) to bind their specific antigen appropriately (De Genst et al., 2006b).

The innate supremacy of HCAbs together with their small size, ability to recognize unique epitopes, sub-nanomolar binding affinity, outstanding solubility, great stability, high expression yields and scalable production in broad variety of expression systems have combined together to make them an interestingly useful class of biomolecules for various medical diagnostic and therapeutic applications.

2.3 The Camelidae HCAbs: Originality and Unique Features

The presence of such unique type of intrinsic antibodies as a component of the humoral immune system is well established, not only for camelidae's species but also for an assortment of other animals. For instance, several notable studies were able to confirm the occurrence of distinctly unconventional antibodies in the serum of wobbegong sharks (*Orectolobus maculatus*), nurse sharks (*Ginglymostoma cirratum*) and in ratfish as well (Greenberg et al., 1995; Nuttall et al., 2001). However, in these cartilaginous fishes they are commonly known as the IgNARs (Ig new antigen receptors). The original nature of IgNARs is visible in their gross structure organization. Nonetheless, HCAbs in sharks have a fairly different structure compared to camelidae's, they are disulfide-bonded homodimers consisting of five constant domains and one variable domain, this single variable domain V-NAR is responsible for targeting antigens (Nuttall et al., 2001). Given that, all the work in this research study have been carried out while utilizing only camelidae HCAbs, from now, only details about camelidae's will be discussed in an ample level of details.

2.3.1 Originality: Introduction

In the beginning, it was strongly suggested that these distinctive camelidae HCAbs will suffer huge deficiency in engendering an extensive antigen-binding complexity. Plausibly, the expansion of conventional forms of antibodies repertoire is formed, at first, by the random association of heavy and light chains. Conversely, the prominent study established by Hamers-Casterman et al. could primarily analyze the immune response of naturally infected dromedaries, with *Trypanosoma evansi*, in which a very diverse HCAbs response against different natural proteins of the parasite was confirmed (Hamers-Casterman et al., 1993). Later and without a doubt, numerous studies could establish the possibility to generate diverse HCAbs that can target

a wide range of antigens (Cortez-Retamozo et al., 2004; De Genst et al., 2006b; Klooster et al., 2007). It can be speculated that, the high frequency of mutation hotspots and the extended structural repertoire of antigen-binding loops along with the longer complementary determining regions (CDRs) contribute to the complexity of VHHs repertoire and balance, in some way, for the lack of the combinatorial diversity between the heavy and light chains (Nguyen et al., 2000).

Unlike the pathological case of heavy-chain disease in which conventional antibodies devoid of L-chains, these abnormalities are generated due to unusual deletion of large and various parts of the VH and CH1. As a result, they fail to bind antigen properly and are recognized as non-functional antibody fragments (Seligmann et al., 1979). In contrast, the camelid HCAbs evidently contribute to the immune response of the camelidae species during the course of infections. Thus, the VHHs derived from camelid HCAbs are fully functional and active in antigen recognition. In addition, their inherent features make them superior to other engineered variable heavy chains VH antigen-specific fragments from murine or human origins.

In conclusion, there have been relatively few studies that could successfully isolate functional domains of VH from conventional antibodies (Tanaka et al., 2003) with the intention of minimizing their sizes, however their practical implementation was usually mired by the low antigen-binding affinity, poor solubility, low expression yields and unfavorably limited stability features (Davies & Riechmann, 1995).

2.3.2 Original Amino Acids Sequence

In camelidae's, despite the fact that the VH and VHH are similar, to a certain extent, in their amino acid sequence, the most evident and reproducible remarkable distinction between the VH and VHH comes from the substitution of four amino acids in the framework-2 region. Such substitution is responsible for providing the VH with more hydrophobic characteristics – i.e. anchoring place for VL, than the VHH in which all the replaced amino acids residues are relatively more hydrophilic. Precisely, the VH's highly conserved residues Val37, Gly44, Leu45, and Trp47 are substituted in VHH by Phe37 (or Tyr37), Glu44 (or Gln44), Arg45 (or Cys45) and Gly47 (or Leu47), as per Kabat numbering (Muyldermans, 2001b; Conrath et al., 2001a; De Genst et al., 2006b).

Compared to humans, camelidae's VHH amino acid sequence closely resembles that of human's VH of family III. Nevertheless, there are still some notable differences in its

framework-2 and CDRs regions (Muyldermans et al., 1994; Vu et al., 1997; Harmsen et al., 2000). As for the framework-2 region, the hydrophobic and highly conserved residues Val42, Gly49, Leu50 and Trp52 of the human and also of mouse VHs' are substituted in VHHs by Phe42 (or Tyr42), Glu49, Arg50 (or Cys50), and frequently Gly52. However, these substitutions do not induce any momentous conformational rearrangements of the molecular backbone as revealed by many crystallographic analyses (Muyldermans et al., 2001a).

The conversion of hydrophobic surface into a more hydrophilic one will certainly resist the preserved-native hydrophobic pairing with the VL (Chothia et al., 1985). Subsequently, the natural existence of highly conserved hydrophilic substitutions will, by all aspects, enhance the solubility of the isolated VHH domain compared to classical antibodies. Indeed, grafting these camelidae's VHH hallmark residues onto the murine or human single domain VH (a process called 'camelization') would render the domain more soluble (Davies & Riechmann, 1994). This can explain the low immunogenicity of VHHs which primarily originates from their small size, in addition to the high homology between them and human VH of family III. Considerable bioinformatics' studies confirmed the occurrence of about 80-90% homology (Desmyter et al., 1996). Moreover, a remarkable study by Vincke and colleagues reported successful humanization of camelidae's derived VHHs without compromising neither their specific function nor their antigen-binding kinetics (Vincke et al., 2009).

2.3.3 Unique Features: Ontogeny vs. Structure and Functionality

The structure of HCAbs' is quite unique, the whole molecule is composed of a single variable domain, in which the hinge region and the two constant domains CH2 and CH3 are homologues to those from the classical antibodies. HCAbs are naturally devoid of light chains and also lack the first domain of the constant region CH1 of conventional antibodies. The variable domain of the HCAbs represents the anchoring site for the constant CH2 and CH3 domains. Moreover, the absence of the three antigen-binding loops provided by VL of VH reasonably authenticates the responsibility of the VHHs' hypervariable loops for antigen recognition. Hence, there was a priori no reason to question the protruded elongation of the hypervariable regions, particularly the CDR1 and CDR3, in VHHs more than in VHs (Muyldermans et al., 2009).

CDRs of HCAbs are very distinctive, the first amino acid of CDR1 is highly variable (Vu et al., 1997; Nguyen et al., 2000). In addition, the CDR3 loop of VHH contains longer loops (i.e.

in average 16-18 amino acids) than the same CDR of human VH (14-12 amino acids) or mouse VH (7 amino acids) (Muyldermans et al., 2009). The high frequent tethering by an inter-loop disulfide bond, typically between CDR1 and CDR3, (Muyldermans et al., 1994; Harmsen et al., 2000) possibly responsible for assisting in the unique loop structure (Muyldermans, 2001b). In summary, the presence of the additional intra-domain disulfide bond (connecting CDR3 and CDR1 or CDR1 and CDR2) may have two outcomes: (i) anchoring the CDR3 against the former interface and (ii) predispose the orientation of CDR3 for appropriate presentation to the antigen (Bond et al., 2003).
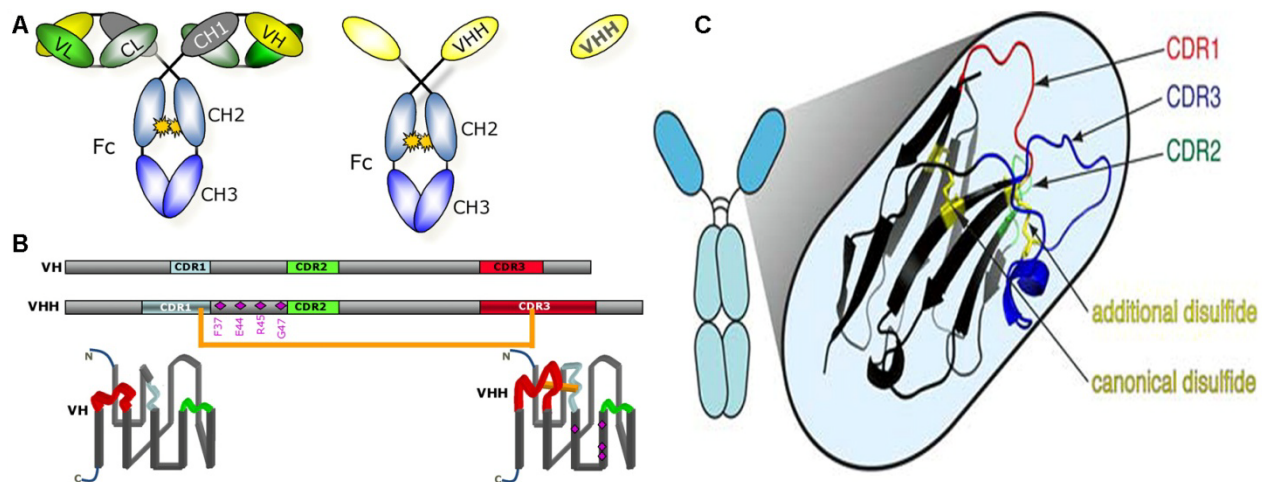
Figure 1.6. Schematic Presentation of the Camelid Conventional and Heavy-Chain IgGs and the Antigen-Binding Fragments thereof. A. From left to right, the composition of a classical antibody (left), a heavy-chain antibody (middle) and a single-domain antigen-binding entity derived from a heavy-chain antibody, the VHH (right). B. The sequence organization of the VH and VHH with framework and CDR's is schematically represented at the top of this panel (Muyldermans et al., 2009). C. The VHH three complementarity determining regions (CDRs) of the antigen-binding paratope are depicted as colored loops: CDR1 red, CDR2 green, and CDR3 blue. (Wesolowski et al., 2009)

The absence of the CH1 Region in VHH while their sequence is present in the genomic DNA signifies that the CH1 sequences are removed during splicing due to a point mutation at the 5' end of the CH1-hinge intron – i.e. at the 3' end of the CH1 exon (Nguyen et al., 1999). Understandably, the instantaneous secretion of camelid HCAbs may account for this absence. In conventional antibodies, the major function of the CH1 domain is to serve as binding site for the

14

H-chain chaperoning protein BiP, which prevents the secretion of the premature antibody from the endoplasmic reticulum (ER). Once the BiP is replaced by the light chain the mature antibodies are secreted (Hamers-Casterman et al., 1993).

Finally, the presence of the fragment crystallizable region Fc part of the camelidae's HCAbs explicates their ability to exert effector functions for target cell destruction through various means: (i) antibody dependent cell-mediated cytotoxicity (ADCC), (ii) antibody dependent cellular phagocytosis (ADCP) and (iii) complement dependent cytotoxicity (CDC) typically as the conventional antibodies (Atarhouch et al., 1997; Nguyen et al., 1999; Chan & Carter, 2010).

2.3.4   Unique Features: Higher Stability, Solubility and Binding Affinity

The remarkable high stability and the ability of refolding of VHHs make them an exceptionally potential agent for numerous possibilities where harsh conditions are habitually encountered. After prolonged heat treatment at relatively elevated temperatures (e.g. 70 ^{0}C and 90 ^{0}C), the VHHs demonstrate high thermotolerance and unique ability to retain more than 80% of their original binding affinity (Van der Linden et al., 1999; Ladenson et al., 2006). Moreover, VHHs exhibit superior degradation-resistance when they exist with various types of protease (protein) enzymes (Hussack et al., 2011). Additionally, VHHs reveal highly stable to extremes pH ranges, Dumoulin and his colleagues confirmed that VHHs could preserve their binding affinity to their target antigens at fairly high concentrations of chaotropic agents (Dumoulin et al., 2002). Such unique feature might endow with ultimate promises for the production of new-fangled generation of oral antibody therapy. Not only the presence of intra-domain disulfide bonding between the CDRs is the reason behind their outstanding stability features, additionally is owed to their gifted ability to properly refold after enforced unfolding in case they are exposed to different thermal or chemical denaturation – e.g. high temperature, urea and guanidinium chloride (Dumoulin et al., 2002; Ladenson et al., 2006).

Solubility, VHHs can be concentrated up to 10-20 mg/mL without any significant aggregation, their superior solubility is partially dependent on the amino acid adaptations in their framework-2 which grant them more hydrophilic characteristics than other VHs (Muyldermans et al., 1994; Vu et al., 1997). The well-conserved hydrophobic VH residues which represent the binding site with the light variable domain VL are responsible for the aggregation tendency of

VHs when existing in aqueous solutions – i.e. to minimize the whole system free energy. In sharp contrast, VHHs' residues are replaced with more hydrophilic ones (Maass et al., 2007). It is worth mentioning that these residues substitutions are encoded in the germline, and do not occur during somatic hyper-mutation (Nguyen et al., 1998). In addition to the residual substitution some other mechanisms are responsible for increasing the solubility of VHHs. For instance, the CDR3 loop folds over the hydrophobic region and shield it from aqueous environment (De Genst et al., 2006b).

Numerous reports deep-rooted the fact that isolated VHHs from immunized libraries often have high binding affinity in the low nanomolar to sub-nanomolar ranges although it was thought that the lack of the VL chain may negatively affect the affinity of VHH in which the antigen-binding site is formed only by a single domain, thus it possesses only three CDR-loops for antigen binding. Consequently, it was expected that the paratope of VHHs would have a lower antigen-binding performance than that of conventional Antibodies (Cortez-Retamozo et al., 2004; Klooster et al., 2007). Moreover, their functional affinities – i.e. avidity, can be tailored for the favor of increasing its value to the optimal limit by constructing bi and multi-valence super molecules (Goldman et al., 2006; Verheesen et al., 2006). In general, VHHs' libraries generated from immunized camelids retain full functional diversity, with high-affinity antigen binding domains that can be isolated through screening a limited number of clones from immune libraries without prior selection using display technologies (Harmsen et al., 2005; De Genst et al., 2010).

2.3.5   Unique Features: Unconventional Epitope Recognition

VHHs are the smallest known protein fragments with the ability to specifically recognize an antigen, these intact antigen-binding fragments measure about 2.4 nm in diameter and 4 nm height. These nanoscale characteristics that made Ablynx laboratories in Belgium call them Nanobodies®. The structural organization of the VHHs is comparable to that of the conventional VH with an Ig fold of two β sheets, one of four strands and one of five strands (Muyldermans et al., 2009).

In conventional antibodies, the paratope – i.e. the antigen-binding site, is composed of both the heavy and light variable domains VH and VL (*see* **Figure 1.6**A). Despite the fact that, in quite few cases, the heavy chain alone can also bind some antigens (Utsumi & Karush, 1964).

The nature of such paratopes' topography does not go well with the antigens' epitopes with grooves or concaved structures. They are either a flat surface or a concave surface which is intimately similar to the cleft in the active sites of enzymes. As a result, the paratopes of conventional antibodies generally evade targeting clefts, the lock and key theory usually plays a critical role in many biological courses of actions. For example, almost all enzymatic reactions are based on the interactions between molecules (Lakowski et al., 1996). Hence, conventional antibodies are hardly ever recognized as competitive enzyme inhibitors or activators.

The VHHs' paratope is enlarged via extensions of CDR1 and CDR3 loops which are usually longer than that found in conventional antibodies. Additionally, the hypervariable loops of the VHH seem to vary substantially in conformation and length from the corresponding loops in VH of human and mouse (Nguyen et al., 2000; Decanniere et al., 2000). The longer CDR3 region of the VHH possesses the extraordinary capacity to form finger-like extensions that protrude into antigen cavities, (*see* **Figure 1.7**), which will result in new antigen binding modes and put forward the VHHs to act as ideal enzyme inhibitors or activators (Wesolowski et al., 2009). A considerable fraction of camelid VHHs, were developed against various enzymes, for instance, α-amylase, carbonic anhydrase and lysozyme, where they could act as target substrate and competitively inhibit the target enzymes (Lauwereys et al., 1998; De Genst et al., 2010).
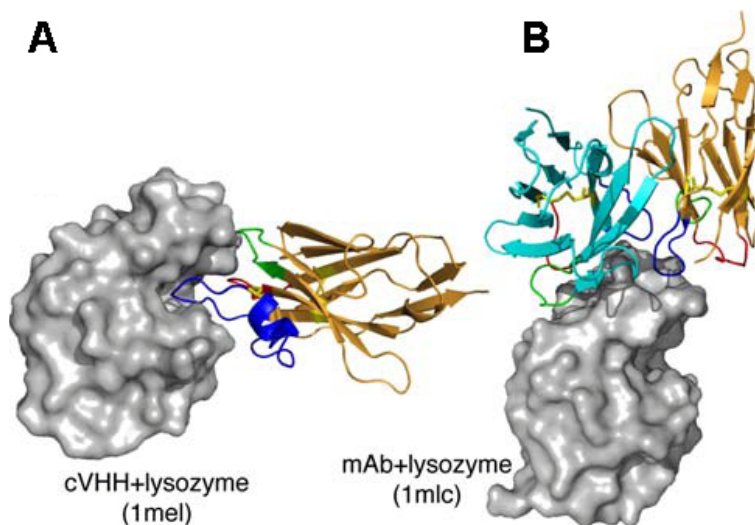
Figure 1.7. 3D-structures of Enzyme-Inhibiting sdAbs Derived from Camel HcAbs and Mouse Fv. The three CDR loops are color-coded as: CDR1 red, CDR2 green, CDR3 blue. A. Chicken lysozyme in complex with an inhibitory camel VHH. B: Chicken lysozyme in complex with the VL and VH domains of a mouse mAb (Wesolowski et al., 2009)

Persuasively, the small size and the longer CDR3 regions have the capacity to reach and recognize cryptic and hidden conformational epitopes that are otherwise inaccessible or not immunogenic for conventional antibodies, which makes them potent alternatives to conventional antibodies. Furthermore, VHHs still share the recognition of planar epitopes which are usually recognized by conventional antibodies (Muyldermans et al., 2009). A notable study by De Genst et al. in which a precise illustration strengthened by thorough crystallographic analysis could show the difference in epitopes recognized by conventional and VHH antibodies, they compared the crystal structures of conventional antibodies-lysozyme complexes with those of VHH-lysozyme complexes (De Genst et al., 2006b).

Collectively, in contrast to antigen-binding entities derived from classical antibodies, the use of recombinant VHH offers numerous advantages in biotechnology and medical applications due to some valuable intrinsic properties such as:

- Smaller size allowing better penetration into dense tissues and neutralization of hidden antigen (Wernery et al., 1999; van Vliet et al., 2002; Stijlemans et al., 2004) or tumors (Cortez-Retamozo et al., 2004),
- Higher thermo and chemical stability (Stok et al., 1999; Frenken et al., 2002),
- Favorable structural features and their ability to form unique paratopes (De Genst et al., 2006b; Wesolowski et al., 2009),
- Superior specificity and affinity for the antigen due to the *in vivo* affinity maturation (antigen-specific VHHs can bind to their corresponding antigens with sub-nM affinities),
- There are various efficient methods of VHH generation with a high yields and selection in a variety of expression systems (e.g. bacteria or yeasts) (de Geus et al., 2000; Harmsen & Haad, 2007),
- A stringently monomeric behavior with no sign of spontaneous dimerisation, so that VHH samples are more homogeneous.

Finally, the compulsory nature of VHHs makes them the best candidate to develop bi-and multi-specific antibodies or immuno-conjugates by fusing the genes of a VHH with another VHH, an enzyme and/or a toxin in one expression unit (Conrath et al., 2001b). Recently, a genuine method has been proposed by a group in the National Research Council of Canada, in order to obtain penta-valent VHH molecules that could increase their apparent affinity by introducing the avidity effect (Zhang et al., 2003).

2.4 Induction, Isolation, Expression and Purification of Camelidae VHH

Recombinant DNA technology in addition to the vast development of various powerful selection strategies allowed the fast and efficient cloning of the harvested pool of VHHs from an immunized dromedary library and the selection of the antigen specific binders from this pool. Accordingly, it became feasible to have access to single domain antigen-binding entities.

The most popular approach to select recombinant antigen-recognizing protein fragments – i.e. VHH binders, is the modified method of the biopanning of phage display libraries. Phage display is a technology in which genotype and phenotype of various types of bacteriophages are physically linked via inserting the gene of interest, which expresses a protein, within the phagemid technology for displaying it on the surface of a filamentous bacteriophage. Displaying a protein, such as VHH fragment, on the surface of a bacteriophage enables the utilization of these modified bacteriophages to select and enrich antigens specific binders through consecutive panning rounds (Ghahroudi et al., 1997; Verrips et al., 2000; Brissette & Goldstein, 2007).

In an alternative strategy, Tanha et al., it was possible to generate a large single pot of naïve VHH library, cloned from a number of healthy llamas, from which binders were retrieved after multiple rounds of biopanning (Tanha et al., 2001). Furthermore, the framework-2 region of a human VH was adapted with the intention of mimicking the camelidae VHH, a process known as "camelization" (Davies & Riechmann, 1994). After that, the CDR3 codons of these camelized VH were then randomized and cloned in a phage display phagemid to retrieve binders from this obtained synthetic library (Davies & Riechmann, 1995). Noteworthy, the latter two strategies have the advantage that the immunization was totally avoided, however, the selected binders are usually of lower affinity and they need further mutagenesis steps to arrive at valuable kinetics. Therefore, it might be more convenient to use immune libraries to arrive at antigen-specific VHHs with appropriate characteristics for detailed applications (Tillib, 2011).

2.4.1 Induction of HCAbs

The Immunization procedures to elicit HCAbs in camelids are, in principle, similar to those in use to raise conventional antibodies in other animals (e.g. rabbit or goat immunization). In general, about five repetitive subcutaneous injections of antigen volume, of concentration about 50-500 µg, mixed with equal volume of Freund or Gerbu adjuvant, are carried out in the course of 5-6 weeks. The initial immunization dose, as a rule, is using complete adjuvant and the rest of

booster doses use incomplete one (Conrath et al., 2001a). Worth mentioning, widely divergent antigens can be used all together for a single immunization (Lauwereys et al., 1998; Van der Linden et al., 2000). Likewise, subcutaneous injection of whole cells (10^8 cells in phosphate buffered saline PBS per shot) and other types of adjuvant is still successfully used to raise an HCAbs response (Maass et al., 2007). The bargain of selecting HCAbs from synthetic or naïve libraries is well-studied, it is confirmed that the HCAbs generated from immune libraries can recognize antigens with a higher affinity (i.e. binding affinity is from nanomolar to sub-nanomolar range) since they undergo *in vivo* affinity maturation progression (Muyldermans et al., 2009; Ghassabeh et al., 2010). In spite of this limitation, the non-immune and synthetic libraries are still considered as attractive alternatives in a number of cases: (i) when only limited amount of antigen is available and/or (ii) in case of the antigen being toxic or non-immunogenic to camelids.

2.4.2   Isolation of antigen specific VHHs

Polyclonal, mono- and bi-valent, VHH antibodies can be isolated from the inborn HCAbs using primitive, simple and yet efficient proteolysis method. A prominent study by Lauwereys et al. could generate polyclonal monovalent VHHs containing α-amylase-specific binders by digesting the harvested HCAbs isotype IgG3 from Protein G chromatography with endo-Glu V8 protease. Afterward, the binders were separated from the cleaved Fc part by running chromatography on protein-A which is able to retain the Fc part. It is worth noting that, a considerable fraction of the dromedary VHHs still firmly bind to protein-A, which drastically affects the applicability of this method. In 1998, Muyldermans and his group at VUB laboratories could successfully obtain bi-valent VHH (i.e. VHH_2) by digesting the purified IgG3 isotype of HCAbs with pepsin, trypsin or papain (Lauwereys et al., 1998). These protease enzymes could cleave the hinge region primarily following the first disulfide bond linking the γ3 heavy chains, although, these methods can generate polyclonal VHHs from HCAbs IgG3 isotype, hitherto, the generation from IgG2 isotype is still calling for further development.

     Monoclonal antigen-specific VHHs of compulsory specificity can be easily identified via phage display method and can be produced in bacterial expression systems in relatively high amounts compared with the conventional antigen binding fragments Fabs (Nguyen et al., 2001; Olichon & Surrey, 2007). Isolation of VHHs includes the cloning of the full repertoire of VHH

genes extracted from the β-lymphocytes isolated from the peripheral blood (about 100 mL of whole blood) of immunized camel. Multiple sequential biochemical procedures are carried out: (i) total RNA isolation from white cells of blood, lymph node or spleen, (ii) complementary DNA (cDNA) synthesis, (iii) two-step polymerase chain reaction PCR using specific primers to amplify VHH sequences, (iv) constructing a VHH library of a satisfactory size. The construction of large immune libraries with the purpose of picking up the perfect antigen-specific binder has been proven redundant, this is elucidated by the fact that VHH unlike the conventional antibodies can bind to their target antigens by asset of only one single domain. Whereas, the antigen binding of the conventional forms usually depends on the presence of heavy and light chains. Accordingly, construction of conventional antibodies' libraries should have room for all possible random association between heavy and light chains. Hence, it is highly favored to construct very large libraries to acquire all possible combinations of VH–VL chains, in order to find few of them which are similar to the original pairing scheme generated *in vivo* (Lauwereys et al., 1998; Alvarez-Reuda et al., 2007). Afterward, (v) the selection procedure and the identification of specific binders from VHHs libraries is done by the enrichment via phage display consecutive rounds of biopanning against the antigen of interest (Nguyen et al., 2001).
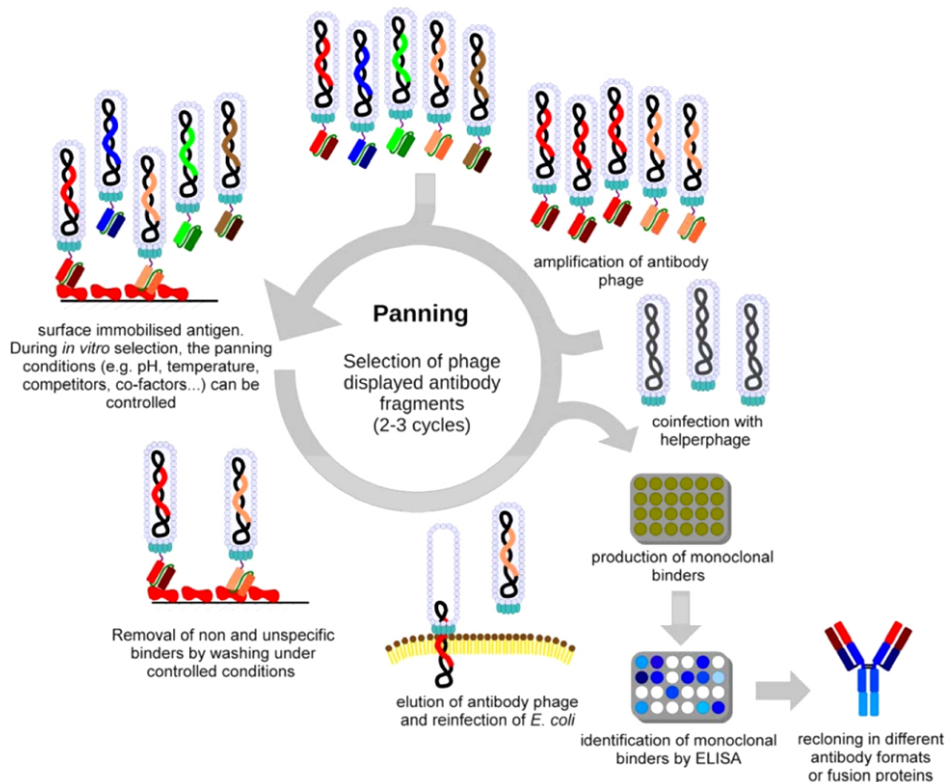
Figure 1.8. Schematic Illustration of Phage Display Biopanning (Schirrmann et al., 2011)

Recently, it was suggested by Tillib et al. to use, in parallel, both conventional helper phage (M13KO7) and a modified helper phage which has an N-terminal deletion in the phage surface protein gIII which would greatly improve the selection procedure (Tillib et al., 2010). Up to date, all the available data obtained from diverse studies point out that the differential character of the selection of particular variants of VHH sequences in the process of biopanning procedure are independent of the number of panning rounds. Although one kind of clones can be successfully picked just right after the first panning round, yet, it can be lost during the following rounds. Nonetheless, other clones can be selected only after three or four panning rounds. In conclusion, it is important to set up the right design of the selection and monitoring procedure so as to improve the possibility of finding appropriate binders with explicit properties, such as the higher affinity, higher solubility and/or superior expression yield (Ghahroudi et al., 1997; Verrips et al., 2000; Tillib, 2011).

2.4.3   Expression Systems: Factors Affecting the Yield

The expression of VHHs in different expression systems has been well established, some studies could obtain high expression yields ranging from 5-10 mg/L in *E. coli* baffled shake flask cultures (Rahbarizadeh et al., 2005). Moreover, there are several reports of VHH production in plant and animal cells, for instance, tobacco and Chinese hamster ovary cells, respectively (Ismaili et al., 2007; Rajabi Bazl et al., 2007). VHH have also been produced in yeasts (Thomassen et al., 2002; Rahbarizadeh et al., 2006), although, most of such VHHs are (i) occasionally N-glycosylated (Frenken et al., 2000; Harmsen et al., 2005), which can severely affect their antigen binding properties (Van der Vaart et al., 2006), (ii) suffering from limited therapeutic application due to the increased immunogenicity resulting from the addition of yeast-specific high-mannose oligosaccharides, and (iii) of short serum half-life, due to the binding of the N-glycosylated VHH to specific mannose receptors found in the reticuloendothelial system RES (Sethuraman & Stadheim, 2006).

The production levels of VHHs in various microorganisms may vary radically among different clones such differences depend on (i) their specific sequences, (ii) the host and (iii) even nutrients in host growth media (Rahbarizadeh et al., 2006; Olichon et al., 2007; Van de Laar et al., 2007). As for sequences, it seems that sequence patterns of VHHs can affect their production level as follows: (a) production rate of conventional-like VHH is generally reduced in

yeast (Harmsen & Haad, 2007), (b) unpaired C-terminal cysteine residues result in a decrease in the expression level (Simmons et al., 2006), and (c) hydrophilic residues found in positions interacting with CH1which results in high expression levels (Harmsen & Haad, 2007).

Regarding the host and nutritional media factors, VHHs' production rate in baker's yeast is related to the host growth rate (Thomassen et al., 2005), in addition, it can be increased by changing the medium (Van de Laar et al., 2007). Furthermore, supplementation of the medium has also been reported to improve VHHs production in *Pichia pastoris* (Rahbarizadeh et al., 2006). In conclusion, the lack of post-translational modifications and the limitations of the folding machinery make the overexpression and production of conventional antibodies in bacteria and yeast almost impossible. Whereas, VHH are active without such modifications, and as being a single chain without the fragment crystallizable region Fc domain they are easily expressed in bacteria and yeast (Arbabi-Ghahroudi et al., 2005). It is worth mentioning that, the expression levels for camelid VHHs in some yeast, for instance, *Saccharomyces cerevisiae* have been reported to be 100 mg/L from shaking flask and 1 g/L from a fed-batch fermentation (Frenken et al., 2000), with scalable expression yield reaching 1.3 kg from a 15 m^3 fermentation (Thomassen et al., 2002).

2.4.4 Purification Methods

VHHs can be simply purified via various procedures. In 1999 Van der Linden et al. reported a simple ultrafiltration of the supernatant of yeast cultures with purity of about 80-90% just by passing through membranes with cut-off limits of 50 and 5 kDa in that order (Van der Linden et al., 1999). In addition to the ultrafiltration, the utilization of the intrinsic characteristic of subfamily III nanobodies[®] which bind to protein-A, many studies could purify nanobodies[®] by simple chromatography methods, however not all properly folded antibodies bind protein-A (Ghahroudi et al., 1997; Frenken et al., 2000).

Recently, the possibility of including a C-terminal $(His)_6$-tag paved the way for using the cost-effective chelating group-columns, nickel-nitrilotriacetic acid Ni-NTA products, a well-known technique called immobilized metal affinity chromatography (IMAC), which frequently produce nanobodies[®] with satisfactory purities for most applications (Lauwereys et al., 1998; Alvarez-Reuda et al., 2007). Furthermore, an interesting study confirmed the practicability and reproducibility of a simple straightforward one-step heat treatment process to purify

Nanobodies® to a comparable level of purity to that obtained via IMAC; such swift and low-cost alternative to conventional chromatography process can still conserve the natural functionality of the produced antibodies (Olichon et al., 2007).

2.5 Applications of Single-Domain Antibodies

2.5.1 Medical applications: Emergence of Immunotherapy

About a century ago, Paul Ehrlich announced that "since normal cells and cancerous cells differ in their staining properties, there should be a "magic bullet" to target only cancer cells". This presumption did not come to realization until 1975 when Köhler and Milstein introduced the first mouse hybridoma technique (Köhler & Milstein, 1975) and, ever since, the production of monoclonal antibodies mAbs became a fact. In reality, the constant domains within the antibodies are not essentially involved in the antigen recognition mechanism. In view of that, a range of smaller antibody fragments which still preserve the antigen-binding affinity have been designed. **Figure 1.9** illustrates various antibody fragments; mono- and bi-valent fragment antigen binding Fab, F(ab′)2, fragment variable Fv, single chain fragment variable scFv and eventually, the domain antibodies dAbs. Nevertheless, added to the technical difficulties, such as, spontaneous aggregation and poor expression yields in heterologous systems, which constantly face the generation of these antibody fragments from conventional antibodies; these produced biomolecules additionally suffer from pathologically relevant immune responses. The latter is responsible for their rapid clearance from the system and makes them unable to effectively interact with effector functions cells (Lee et al., 1998).
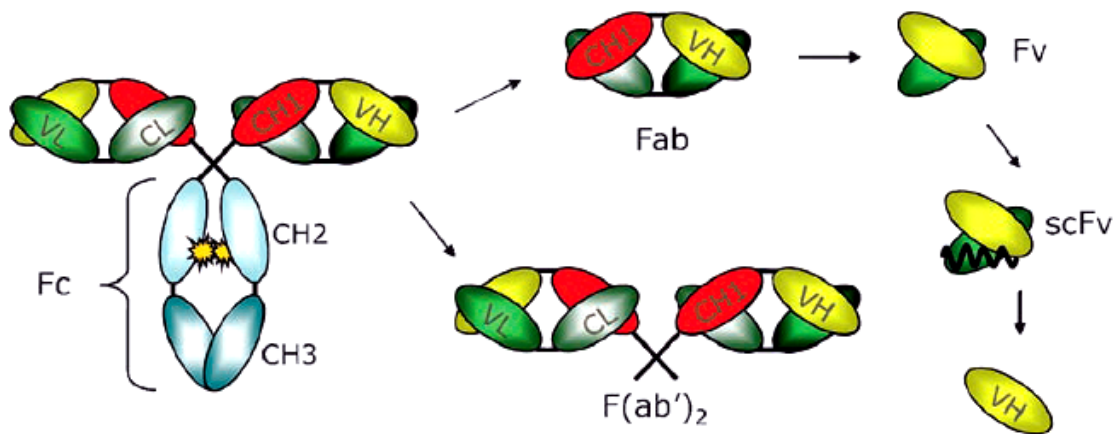
***Figure 1.9. Schematic Presentation of Various Antibody Fragments** (Ghassabeh et al., 2010)*

In 1980, Gabrielle Boulianne and his colleagues from Toronto University and Ontario cancer institute could design and produce the first chimeric antibodies (Boulianne et al., 1984), which was built from a variable antibody part from murine origin fused to the constant region of conventional human antibody. Noteworthy, after this primal experiment many attempts could effectively reduce the human anti-mouse antibody (HAMA) immune response (Hwang & Foote, 2005). Loads of engineered designs of these murine antibodies were developed utilizing numerous ways for the sake of resolving the antigenicity concerns, from controlling the initial and terminal serum half lives to preventing the anti-globulin responses in order to fully exploit their immune effector functions.

Humanization approach is the most common in which the CDRs regions are grafted into the human IgG backbone. In addition, the resurfacing approach shows enhanced results, in which the original human amino acids are only being replaced by the surface exposed murine residues (Zhang et al., 2005). On the other hand, this approach suffers from a significant reduction or complete loss of binding affinity since some of the residues in the removed framework are critical for maintaining the CDRs' conformation (Chothia et al., 1989; Foote & Winter, 1992). Practically, the complex structure of full-length antibodies limits their use in only some of medical applications, such as imaging and active targeting. Financially, the production of mAbs also suffers from the very high costs which are increasingly becoming a burden for the healthcare sector.

Nature has provided an inimitable answer, thanks to the exceptional repertoire of fully functional heavy chain only antibodies of the dromedaries and llamas. All of the previously conferred unique features of these antibody fragments imply that they will put forward remarkable promises to be exploited as robust reagents for presenting superior therapeutic and diagnostic applications as well as multipurpose biological properties.

2.5.2   Medical Applications: Therapeutics

Currently, there are various operational VHHs for different clinical settings, a notable study by Baral et al. demonstrated that the generation of VHH against the sleeping sickness inducing parasite *Trypanosome rhodensiensis* variance surface glycoprotein (VSG) fused to trypanolytic factor apolipoprotein L1 (APOL1) would establish a novel generation of anti-parasitic treatment strategies (Baral et al., 2006). In addition, toxin neutralizing VHHs have been generated against

lethal scorpion envenoming, these venom-neutralizing antibodies could successfully provide much higher efficacy and immunological advantages over conventional anti-venoms (Hmila et al., 2008; Hmila et al., 2010). Moreover, Tremblay and colleagues demonstrated that the VHHs have potential as components of therapeutic agents for reversal of botulism intoxication. The generated VHHs could act as neuronal cell intrabody binding agents and inhibitors of *Clostridium botulinum* neurotoxin proteases (Tremblay et al., 2011).

VHHs have been used as an anti-pathogens either as a direct therapeutic agent such as the fused form used for the treatment of trypanosomiasis (Baral et al., 2006) or, indirectly, for preventing drug degradation by the pathogen (Conrath et al., 2001a). Moreover, VHH could reduce the morbidity of rotavirus induced diarrhea in mice (Van der Vaart et al., 2006). Furthermore, Antagonistic anti-TNF-β nanoantibodies established an outstanding therapeutic efficiency in a murine rheumatoid arthritis model. The therapeutic outcome was much higher than the effect of the conventional antibodies that are already in the use for the treatment of rheumatoid arthritis (Coppieters et al., 2006). **Table 1.2** points up various selected therapeutic applications of VHHs (i.e. sdAbs) developed from different sources including immune, non-immune and synthetic libraries.

Table 1.2. *sdAbs for Various Therapeutic Applications*

Target	Source	Application	Reference
FcgRIII (CD16)	Immune Llama	Cancer immunotherapy, Recruitment of NK cells	(Behar et al., 2008)
TNF-alpha	Immune Llama	Rheumatoid arthritis	(Coppieters et al., 2006)
HIV-1 Subtypes	Immune Llama	Anti-viral therapy	(Strokappe et al., 2012)
Methotrexate	Immune Llama	Cancer therapy	(Alvarez-Reuda et al., 2007)
Hepatocyte growth factor	Immune Llama	Molecular cancer therapy drug discovery	(Vosjan et al., 2012)
Trypanosoma evansi	Immune Dromedary	Trypanosomiasis diagnosis and therapy	(Saerens et al., 2008)
Scorpion toxin	Immune Dromedary	Neutralization	(Hmila et al., 2008; Hmila et al., 2010)

2.5.3 Medical Applications: Diagnostics

In addition to therapeutics, VHHs were effectively used in developing a range of novel diagnostic applications. Such as, accurate determination of tumor epidermal growth factor receptor EGFR such as human epidermal growth factor receptor 2 (HER2), a tumor-associated molecule over expressed in about 30% of breast cancer patients. The detection was possible via imaging the radio labeled anti-HER2 VHH with ^{99m}Tc and [68]Ga (Vaneycken et al., 2011; Vosjan et al., 2011). Noteworthy, the radio-labeling of VHHs facilitates the design of innovative biomolecules conjugates for drug discovery, immunotherapy and diagnosis of different biomarkers – positive tumors. As well, a notable study by Behar et al. demonstrated that high affinity sdAbs were successfully directed against nonconventional epitopes of human carcinoembryonic antigen (CEA), these antigen-binding sites totally differ from those defined by contemporary murine monoclonal antibodies (Behar et al., 2009).

Chromobodies are fusion proteins that comprise an antigen binding VHH and a fluorescent protein. For instance, green fluorescent protein GFP, have been already generated making them proficient candidates for tracking the target antigen *in vivo* and *ex vivo*. This allows dynamic tracing and modulating the changes of target antigens at all stages of cell-cycle in living cells using various techniques, such as, the live cell microscopy (Rothbauer et al., 2006; Kirchhofer et al., 2010). In conclusion, such fluorescent-VHH conjugate show high potential for further theranostic applications. For example, the tracing of the fate of a certain antigen of interest (e.g. parasitic antigen) inside the living host, that possibly will pave the way for discovering a novel drug based on blocking a critical stage of the parasite life cycle. Finally, **Table 1.3** points up different selected diagnostic applications of VHHs.

Table 1.3. *sdAbs for Various Diagnostic Applications*

Target	Source	Application	Reference
Dendritic cells	Immune Camelid	*in vivo* imaging	(De Groeve et al., 2010)
Taenia solium	Immune Dromedary	Cysticercosis	(Deckers et al., 2009)
Trans-sialidase	Immune Llama	Trypanosomiasis	(Ratier et al., 2008)
CEA	Immune Llama	Tumor targeting	(Behar et al., 2009)
HER2	Immune Llama	*in vivo* imaging	(Vaneycken et al., 2011)
hPSA	Immune Dromedary	Cancer Diagnosis	(Saerens et al., 2004)
MUC1	Immune Camelid	Tumor targeting	(Rahbarizadeh et al., 2006)

3 Materials & Methods

3.1 Materials

3.1.1 Reagents, Buffers and Media

Table 1.4. Reagents, Buffers and media utilized in this research (Vincke et al., 2012)

Reagents, Buffers and Media	Composition	Supplier
Dithiothreitol DTT	0.1 M DTT	Sigma-Aldrich
Complete Freund adjuvant[1]	killed Mycobacterium tuberculosis non-metabolizable oils	Sigma-Aldrich
Incomplete Freund adjuvant	non-metabolizable oils	Sigma-Aldrich
DiEthylPyroCarbonate Treated Water DEPC	10 μL DEPC in 10 mL H_2O incubate for 2 h at 37 ^0C or overnight at room temp. autoclave	Sigma-Aldrich
Saline solution, 0.9% NaCl	9 g/L NaCl	Merck
TRIzol reagent kit		Invitrogen
Chloroform/ Iso-amylalcohl (24/1)	12 mL Chloroform 0.5 mL Iso-amylalcohol	Sigma-Aldrich
Ethanol alcohol	100 % EtOH	Sigma-Aldrich
QIAquick Gel Extraction kit		Qiagen
QIAquick PCR purification kit		Qiagen
Sodium acetate (pH 5.2)	3 M Sodium Acetate adjust pH with 37% HCl	Merck
GenElute™ Plasmid Miniprep		Sigma-Aldrich
GenElute™ PCR clean-up kit		Sigma-Aldrich
LB medium (Luria-Bertani medium, pH 7.0)	10 g/L Tryptone 5 g/L Yeast extract 10 g/L NaCl adjust to 1 L Milli-Q H_2O autoclave	Duschefa Biochemie Duschefa Biochemie Merck

---

[1] Gerbu adjuvant (LQ#3000, GERBU Biotechnik GmbH, Heidelberg, Germany) can also be used.

Reagents, Buffers and Media	Composition	Supplier
LB agar	15 g/L Microagar	Duschefa Biochemie
	adjust to 1 L with Milli-Q H_2O	
	autoclave	
LB agar Amp/glucose	LB agar	
	100 µg/mL Amp	Duschefa Biochemie
	1/10 20% glucose	Duschefa Biochemie
2xTY medium (pH 7.0)	16g/L Tryptone	Duschefa Biochemie
	10 g/L Yeast extract	Duschefa Biochemie
	5 g/L NaCl	Merck
	adjust to 1 L with Milli-Q H_2O	
	autoclave	
2xTY Amp/Kan	2xTY medium	
	100 µg/mL Amp	Duschefa Biochemie
	70 µg/mL Kan	Duschefa Biochemie
TB (Terrific Broth)	12 g/L Tryptone	Duschefa Biochemie
	24 g/L Yeast extract	Duschefa Biochemie
	2.31 g/L KH_2PO_4	Merck
	12.54 g/L K_2HPO_4	Merck
	4 mL/L Glycerol	Duschefa Biochemie
	adjust to 1 L with Milli-Q H_2O	
	autoclave	
SOB medium	20 g Tryptone	Duschefa Biochemie
	5 g Yeast extract	Duschefa Biochemie
	0,5 g NaCl	Merck
	1,86 g KCl	Merck
	adjust to 1 L with Milli-Q H_2O	
	autoclave	

Reagents, Buffers and Media	Composition	Supplier
SOC medium	25 mL SOB	
	500 µL 1M $MgSO_4$	Merck
	125 µL 2M $MgCl_2$	Merck
PBS (Phosphate Buffered Saline, pH 7.4)	136 mM NaCl	Merck
	2.6 mM KCl	Merck
	10 mM Na_2HPO_4	Merck
	1.5 mM NaH_2PO_4	Merck
PBS-milk	PBS + 2 % milk powder	Nestlé
PBS/Tween PBST	PBS + 0.05 % (*v/v*) Tween-20	Sigma-Aldrich
Tris-HCl (pH 8.0)	1 M Trizma$^®$ base	Sigma-Aldrich
	adjust pH with 37% HCl	
	adjust to 1 L with Milli-Q H_2O	
TES (Tris-EDTA-sucrose) pH 8.0	0.2 M Tris-HCl (pH 8.0)	
	0.5 mM EDTA	Merck
	0.5 M Sucrose	Duschefa Biochemie
10x TBE (Tris-borate-EDTA buffer)	108 g Trizma$^®$ base	Sigma-Aldrich
	55 g Boric acid	Merck
	9.3 g EDTA	Merck
	adjust to 1 L with Milli-Q H_2O	
PEG/NaCl solution	20 % *w/v* PEG-6000	Duschefa Biochemie
	2.5 M NaCl	Fisher Scientific
	adjust to 1 L with Milli-Q H_2O	
	autoclave	
Ampicillin (Amp 100 mg/mL stock solution)	1 g Amp	Duschefa Biochemie
	10 mL 70 % ethanol	Fisher Scientific
	sterilization by filtration through	Millipore
	0.22 µm Express™ Plus-filter	

Reagents, Buffers and Media	Composition	Supplier
Kanamycin (Kan 70 mg/mL)	0.7 g Kan 10 mL Milli-Q H_2O sterilization by filtration through 0.22 µm Express™ Plus-filter	Duschefa Biochemie Millipore
IPTG (Isopropyl-β-*D* thiogalactopyranoside)	1 M IPTG Milli-Q H_2O sterilization by filtration through 0.22 µm Express™ Plus-filter	Duschefa Biochemie Millipore
DNA loading buffer	0.25 % Bromophenol blue 0.25 % Xyleen cyanol FF 15 % Ficoll™ PM400 84.5 % Milli-Q H_2O	Merck Merck Amersham Bioscience
Ethidium bromide (EtBr 10mg/mL)	1g EtBr dissolve in 100 mL of Milli-Q H_2O	Merck
20x MES buffer (pH 8.3)	195.2 g MES (2-(N-morpholino) ethane sulfonic acid) 121.2 g Trizma® base 6 g EDTA 20 g SDS adjust to 1 L with H_2O	 Sigma-Aldrich Sigma-Aldrich Merck Duschefa Biochemie
SDS-PAGE Staining solution	0.125 g Coomassie® Brilliant Blue R250 50% Methanol 10% Acetic acid adjust to 1 L with H_2O	Fluka Lamers & Pleuger Vel
SDS-PAGE Destaining solution	10% Acetic acid 40% Methanol adjust to 1 L with H_2O	Vel Lamers & Pleuger

Reagents, Buffers and Media	Composition	Supplier
AP-blot buffer (pH 9.8)	1 M Diethanolamine 1 mM MgSO$_4$	Merck
Trimethylamine (TEA)	70 µL TEA 5 mL Milli-Q H$_2$O	Sigma-Aldrich
0.5M Imidazole in PBS	3.5 g Imidazole dissolve in 100 mL PBS adjust pH to 7.5 with 37% HCl with sterilization by filtration through 0.22 µm Express™ Plus-filter	Sigma-Aldrich Merck Millipore
HEPES buffer (pH 7.0)	1 mM HEPES Autoclave	Sigma-Aldrich
10X Buffer H	500 mM Tris-HCl, pH 7.5 100 mM MgCl$_2$ 10 mM Dithiothreitol (DTT) 1000 mM NaCl	Roche
10X Buffer R		Fermentas

3.1.2 Equipments and Consumables

Table **1.5.** *Equipments and Consumables used in this research (Vincke et al., 2012)*

Equipment/Consumable	Supplier
Lab centrifuge with swing-out rotor	Eppendorf
Separation tube for whole blood lymphocytes and peripheral monocellular cells Leucosep™	Greiner Bio-One
Falcon tubes	BD Falcon™
RNase-free tubes and Micropipette tips	Eppendorf
Pasteur glass pipette and Ball to aspirate	
Water bath and heating block	
Thermocycler	BioRad

Equipment/Consumable	Supplier
Agarose gel electrophoresis	BioRad
UV trans-illuminator	
Vortex	
Microcentrifuge	
Nanodrop® spectrophotometer	Thermo Scientific
Shaker incubator	
Gene Pulser Electroporation instrument	BioRad
Electroporation cuvettes	BioRad
Cell scraper	BD Biosciences
Large square Petri dishes (243 x 243 mm)	
Glass beads, average size (0.25-0.35 cm diameter)	E&R Chemicals and equipments
Maxisorb 96-well microtiter plate	NUNC
Round bottom 96-well microtiter plate	BD Biosciences
Microtiter plate reader	
Gel-filtration column HiLoad S75 (16/60) On ÅKTA Express	GE Healthcare
HIS-Select® Nickel Affinity Gel	Sigma-Aldrich
Vivaspin-15 (MWCO 5,000 PES)	Vivasciences-Sartorius
PD-10 columns	GE Healthcare

3.1.3 Bacterial Strain

Two bacterial *Escherichia coli (E. coli)* strains were used in this study:

(i) *E. coli* TG1 strain for biopanning and the selection of antigen specific VHH

- *E. coli* TG1:

  K12, Δ(lac-pro), supE, this, hsdD5/F'traD36, proA$^+$B$^+$, lac^q, lacZΔM15

(ii) *E. coli* WK6 strain for the Nanobodies® expression, they are su$^-$ which make them unable to read-through the amber stop codon.

- *E. coli* WK6:

  K12, Δ(lac-proAB) galE, StrA/F', lacI^q, lacZΔM15, proA$^+$B$^+$

3.1.4　Plasmids: pMECS

The pMECS is a pUC derived phagemid vector used for phage display, it is designed for efficient production of soluble Nanobodies® and the selected VHH coding genes are cloned between a *pelB* leader signal sequence, which transports the VHH to the bacterial periplasm. The phagemid has an F1 origin of replication, upstream of a *hemagglutinin* tag (HA-tag), a C-terminal hexahistidine-tail (His$_6$) and gene III from M13 bacteriophage. The pMECS vector contains an ampiciline resistance gene as well. **Figure 1.10** displays the pMECS gene map.
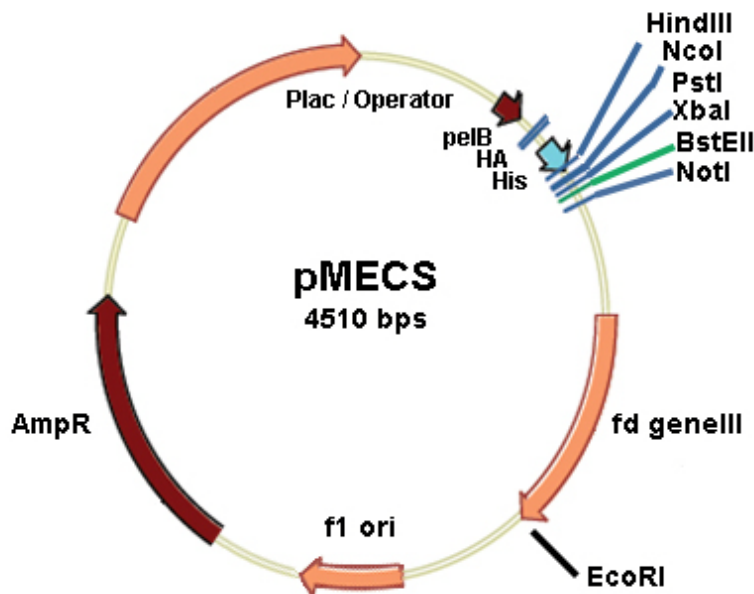
Figure 1.10. Schematic Representation of pMECS Vector (Florea, 2011)

The relevant genes, restriction enzymes and tagging sites are given:

- *Multiple cloning sites*.
- *E coli. Plac promoter*: Isopropyl-β-*D*-thiogalacto-pyranoside (IPTG) inducible.
- *Pectate lyase B* (pelB) signal sequence: bacterial Sec-dependent translocation signal sequence transports the unfolded protein (Nanobody®) into the periplasm.
- *Gene III* (g III): encodes the *phage* coat *protein* (pIII) of phage M13. The protein of interest (the Nanobody®) to be displayed is fussed to pIII and that will allow the VHH to be displayed together with pIII on the phage coat for panning. An amber stop codon (TAG) is located between the HA-tag and gIII, which is partially suppressed in a suppressor strain such as *E. coli* TG1.

- *Polyhistidine tag* (His$_6$): sequence located downstream of the VHH gene. It is used for ease of purification on immobilized metal affinity chromatography (IMAC).

3.1.5 Bacteriophage

M13KO7 helper phage (> 10^{11} plaque forming units/mL), in-house prepared, is an M13 derivative filamentous bacteriophage. The native particle is a thin, cylindrical shape usually 900 nm long and 6–7 nm in diameter (Carmen & Jermutus, 2002). It carries the mutation Met40Ile in geneII, with the origin of replication from P15A and the kanamycin (Kan) resistance gene from Tn903 both inserted within the M13 origin of replication. M13KO7 is capable to replicate in the absence of phagemid DNA**. Figure 1.11** illustrates the schematic diagram of the M13 phage vector. While, in the presence of a phagemid bearing a wild-type M13 of f1 origin a single-stranded phagemid is preferentially packaged and secreted into the culture medium.
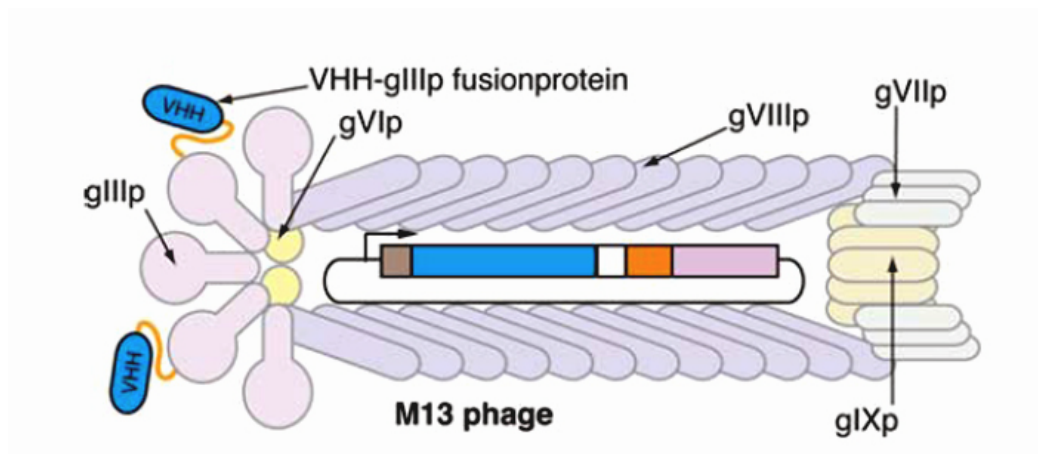
Figure 1.11. Schematic Diagram of the M13K07 Phage Display Vector Used for Cloning Libraries of Immunized Camelids. *VHH are expressed on the phage coatimmunized camelids, afterward the inserted VHHs codons are expressed on the phage coat as fusion to the gIII protein (Wesolowski et al., 2009)*

3.1.6 Primers

Table 1.6. *All used PCR primers utilized for the amplification and sequencing of the VHH genes. Restriction enzyme sites are underlined (Arbabi-Ghahroudi et al., 1997)*

Primers	Sequence (5'- 3')
A6E	GATGTGCAG<u>CTGCAG</u>GAGTCTGGRGGAGG PstI
Call001(20 uM)	GTCCTGGCTGCTCTTCTACAAGG
Call002 (20 uM)	GGTACGTGCTGTTGAACTGTTCC
FP	TTCCCAGTCACGAC
RP	CACACAGGAAACAGCTATGAC
MP57	TTATGCTTCCGGCTCGTATG
GIII	CCACAGACAGCCCTCATAG
Primer38	GGACTAGT<u>GCGGCCGC</u>TGGAGAC<u>GGTGACC</u>TGGGT NotI BstEII

3.1.7 Enzymes

Table 1.7. *All used restriction enzymes utilized for the cloning of the VHH fragments. Restriction enzyme sites are illustrated (Vincke et al., 2012)*

Restriction enzymes	Cutting Site	Supplier
Eco91I (10 u/µL)	5'…G^GTNACC…3' 3'…CCANTG^G…5'	Fermentas
Xba1 (10 u/µL)	5'…C^TCGAG…3' 3'…GAGCT^C…5'	Fermentas
NotI (10 u/µL)	5'…GC^GGCCGC…3' 3'…CGCCGG^CG…5'	Roche
PstI (10 u/µL)	5'…CT GCA^G…3' 3'…GDACGTC…5'	Roche
ExoI (20 u/µL)	Catalyzes the removal of nucleotides from single-stranded DNA in the 3' to 5' direction	Fermentas

Table 1.8. *PCR reagents, DNA polymerase and other enzymes utilized for the cloning of the VHH fragments*

PCR reagents, DNA Polymerase and other enzymes	Supplier
Oligo-dNT12-18	Invitrogen
dNTP mix (10 mM each)	Invitrogen
Superscript II First-Strand Synthesis System, for Reverse Transcriptase RT-PCR(200 u/µL)	Fermentas
Ribolock ™ RNase Inhibitor, Human Placental RNAse Inhibitor HPRI (40 u/µL)	Fermentas
FastStart Taq polymerase (5 u/µL)	Roche
Taq DNA polymerase	Sigma-Aldrich
T4 DNA ligase (5 u/µL)	Fermentas
Shrimp alkaline phosphatase (SAP, 1 u/µL)	Fermentas
DNA smart ladder	Eurogenetec
Hinf (10 u/µL)	Fermentas
ExoSAP-IT	Affymetrix

3.1.8 Antibodies

Table 1.9. *Antibodies utilized for IgG ELISA, PE ELISA and Nanobodies® selection*

Antibody	Supplier
Rabbit anti-camel polyclonal Ab	Sigma-Aldrich
Rabbit anti-VHH polyclonal Ab	Developed in house
Goat anti-rabbit IgG alkaline phosphatase conjugate	Sigma-Aldrich
Mouse anti-M13 horse radish peroxidase conjugate	Amersham Biosciences
Mouse anti-His-tag mAb	Abd Serotec
Goat anti-Mouse IgG	Amersham Biosciences

3.1.9 Animal and Materials used for Immunization and Nanobodies® Selection

- Young adult camel (well behaved[2], three years old, 250-275 kg male).
- Native *Schistosoma mansoni* Cathepsin-B (SmCB) Antigen, 0.5-1mg.

---

[2] The behavior of Camel is considered as a general indicator of its health status (Wernery et al., 1999)

- Execratory Secretory *Schistosoma mansoni* (SmES) Antigen, 0.5-1 mg.

Both proteins are cooperatively provided by Dr. Ibrahim Rabee, Immunology Department, Theodor Bilharz Research Institute TBRI, Giza, Egypt.

Noteworthy, the used antigens are preferred to be well folded/structured proteins. Nevertheless, the proteins used for immunization can be contaminated with other neither non proteases nor toxic antigens, however, it is highly recommended to use high purity proteins for biopanning and binders identification (typically recombinant proteins).

3.2   Methods

In this section, a detailed step-by-step description of the entire processes of developing of the variable domain of the heavy chain of the heavy-chain antibodies VHH, also known as single-domain anti-bodies (sdAbs) and Nanobodies$^{®}$ (Nbs). Part of the steps and methods will not be fully described, those should be carried out as per their manufacturers and suppliers described. Moreover, other parts will be described according to the Department of Molecular and Cellular Interactions Laboratories' (CMIM Lab), Flanders Interuniversity institute for Biotechnology (VIB),Vrije Universiteit Brussel (VUB) in-house protocols. The extent of description will start with a camel's immunization step, going through the expression and purification of the enriched antigen specific binders. Finally, brief estimation of the binding affinity properties of the produced sdAbs will be addressed as well.

3.2.1   Camel's Immunization

A young adult male, well behaved with normal appetite, three years old healthy camel was carefully selected to immunize. The dromedary camel was subcutaneously immunized multiple times with the antigens mixed with (a) Freund complete adjuvant (for first injection) and (b) Freund incomplete adjuvant (for booster injections). The presence of adjuvant is mainly to enhance the immune response of the animal in order to increase the titer of the B lymphocyte cells. After proper amount and doses of immunization doses over an optimum period of time it is highly anticipated to have an affinity-matured antigen-specific HCAbs expressed on the B cells.

The immunization protocol adapted in this work tones with the VIB in-house regular protocol, and other previously reported standard immunization protocols of camels (Conrath et al., 2001a).

Procedure

1. The adjuvant was stored and handled as described by the manufacturer's product information guide.

2. Just before immunization, one aliquot of each -20 ^{0}C frozen antigens was thawed and mixed via vigorous vortex with an equal volume of adjuvant until a thick emulsion was formed.

Critical Step: While using complete Freund's adjuvant for first injection, vortex or shake well to resuspend the Mycobacterium.

3. The emulsion was transferred to a syringe with an appropriately sized needle and injected subcutaneously.

4. The immunization steps were designed as follow:

Table 1.10. Camel Immunization Steps

Injection	Time Interval	Adjuvant Volume	Antigen Volume (1 mg/mL)
First Injection	Day 0	250 µL	250 µL
1st Boost	One Week	250 µL	250 µL
2nd Boost	Two Weeks	200 µL	200 µL
3rd Boost	Three Weeks	150 µL	150 µL
4th Boost	Four Weeks	100 µL	100 µL
5th Boost	Five Weeks	50 µL	50 µL
6th Boost	Six Weeks	50 µL	50 µL

Note: The gradual tapering of the injected doses' concentration was intended to enrich only the B cells which express HCAbs of high affinity.

Caution: Despite the fact that camels are not commonly considered as experimental animals, general regulations concerning to animal welfare, protection and good experimental practices were taken into consideration. During the immunization schedule routine checkups were carried out twice a week to insure the proper supply of nutrition for camel in order to maintain good health, in addition, some developed local tumefactions were watchfully treated.

3.2.2 Preparation of Peripheral Blood Lymphocytes and Extraction of Total RNA

Procedure

1. Approximately 100 mL of peripheral blood was collected four days after the last boost on an anticoagulant EDTA (2g EDTA/100 mL blood).

2. The anti-coagulated blood was diluted with an equal volume of 0.9% NaCl.

3. Carefully, about 30 mL of diluted blood was transferred into each Leucosep™ tube.

4. The tubes were centrifuged at room temperature for 10 min at 1000 g.

Critical Step: The centrifugation must be carried out using a swing-out rotor, while both acceleration and deceleration breaks were disabled.

5. The plasma layer formed in the topmost was carefully removed via Pasteur pipette as much as possible in order to minimize the contamination of the underneath peripheral blood lymphocytes PBLs and transferred to another tubes for further IgGs purification and for evaluation of immune response against antigens.

6. All the procedures followed the recommended experimental practice of the manufacturer's instruction manual, as illustrated in **Figure 1.12-1.15**.
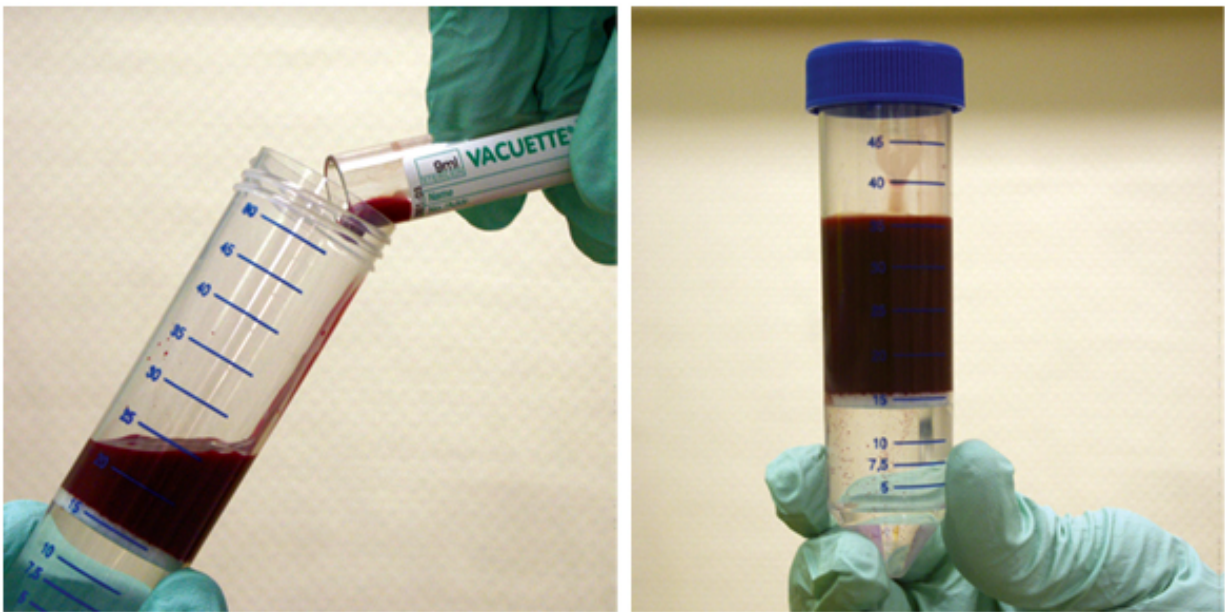
Figure 1.12. Filling with diluted blood before centrifugation. The anti-coagulated and diluted whole blood samples were carefully transferred to each Leucosep™ tube.
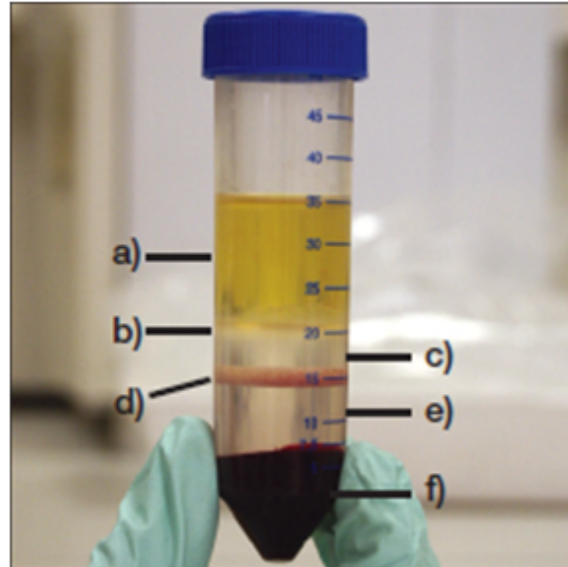
Figure 1.13. Layers Separation after Centrifugation. *After centrifugation the sequence of layers occurs as follows (a) plasma; (b) enriched cell fraction (white ring interphase of lymphocytes and PBMC's); (c) separation medium; (d) porous frit barrier; (e) separation medium, and finally (f) pellet (erythrocytes and granulocytes).*
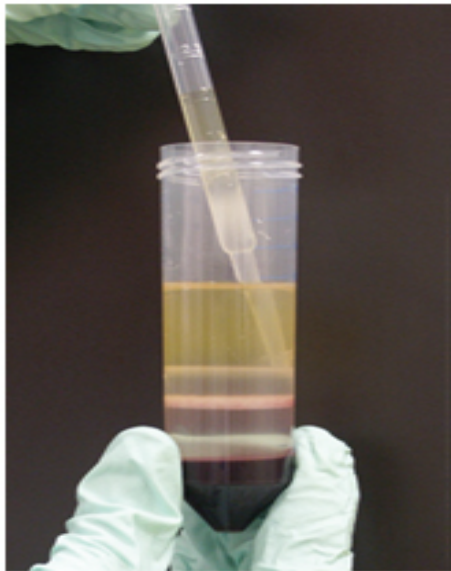
Figure 1.14. Harvest PBLs and PBMCs by means of a Pasteur pipette.
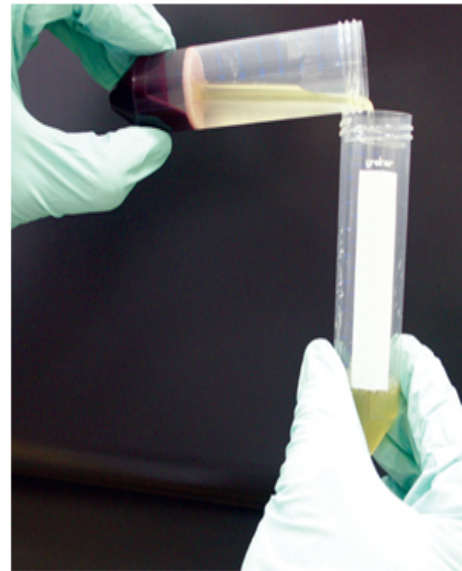
Figure 1.15. Transferring plasma to other tubes for further experiments.

Caution: All blood samples must be handled with care in accordance with the policies and procedures of working facility. In case of any accidental exposure or contamination with blood an appropriate medical treatment must be instantly initiated.

7. The collected PBLs volume was divided into two fresh centrifuge tubes, afterward they were diluted and washed twice with at least 10 times volume of phosphate buffered solution PBS and the tubes were centrifuged at 4 ^{0}C for 10 min at 250 g.

8. The supernatants were decanted, each cell pellet was gently re-suspended in about 5 mL PBS, all the suspension were collected in one tube, afterward, the PBLs washed two more times via centrifugation as described above (*see* **Method 3.2.2.7**).

9. Total RNA was isolated from the prepared PBLs using TRIzol reagent kit, where all the procedures followed the technical instruction manual of supplier.

10. The RNA concentration was measured by UV-spectrophotometer (i.e. OD_{260nm} of 1 approximately corresponds to 40 µg RNA/mL).

Pause Point: The isolated RNA can be used immediately to synthesize the first complementary DNA strand (cDNA) or can be stored at -80 ^{0}C.

3.2.3 Preparation of First Strand cDNA from RNA

Under appropriate sterilization conditions, RNAse free materials and laminar air flow, the extracted total RNA is used as a template to prepare cDNA using commercial reagent   s.

Procedure

1. The secondary structure of the RNA was destabilized by incubating the following mixture for 10 min at 70 ^{0}C:

    - Total RNA_____10 µL ($\approx$ 40 µg)
    - Oligo-dT$_{12-18}$ primer_____11 µL (5.5 µg)
    - DEPC-H$_2$O_____105.5 µL
    - Total volume_____126.5 µL (premix for 5 tubes x 23 µL)

2. The mixture was placed **immediately** on ice for 5 min, then added to it the following mixture:

    - 5x 1st strand buffer_____44 µL
    - 0.1 M DTT_____22 µL
    - dNTPs (10 mM each)_____11 µL
    - HPRI (40 units/µL)_____5.5 µL
    - Superscript™ II Reverse Transcriptase (200 units/µL)_____11 µL
    - Total volume_____93.5 µL

3. In a spinning rotor the mixture was well-mixed and gently centrifuged, the volume was divided over 5 tubes (17 µL each) then incubate the mixture as follows:

- 42 ^{0}C   for   1 h   (annealing time)
- 45 ^{0}C   for   20 min (cDNA synthesis)
- 70 ^{0}C   for   15 min (to inactivate the reverse transcriptase enzyme)
- End cycle: 4 ^{0}C

Pause Point: After the incubation sequence, all the mixture tubes are collected and either stored at -20 ^{0}C or, straight away, used to amplify the VHH sequences.

3.2.4 Nested Polymerase Chain Reaction for VHH Sequences' Amplification

The amplification if the VHH sequences' was carried out through two consequent PCR runs. The first run will yield two distinctive groups of amplicons: group-1, molecular weight 0.7 kb and group-2, molecular weight 0.9 kb. The first group originated from the HCAbs-encoding mRNA (i.e. VHH-hinge-CH2), while, the heavier second group represents the VH-CH1-hinge-CH2. The 0.7 kb fragment is purified from the agarose gel and used as a template for a nested PCR amplification process specific to VHH-only sequences. Corresponding restriction enzymes are introduced for further cloning into the phage display vector (pMECS, *see* **Figure 1.10**).

Procedure

1. Premix volume for about 24 tubes was prepared as follows:

- H$_2$O_____954 µL
- 10x PCR buffer_____120 µL
- dNTPs (10 mM each)_____24 µL
- 20 µM call 01 primer_____24 µL
- 20 µM call 02 primer_____24 µL
- Fast Start Taq DNA Polymerase_____6 µL
- Total volume_____1152 µL

2. The above mixture was divided over 24 tubes from Westburg strips (48 µL/tube), and the cDNA template was added as follows:

- Set 0: 2 tubes, each tube 0.5 µL of 2-fold diluted cDNA
- Set 1: 4 tubes, each tube 1.0 µL of 2-fold diluted cDNA
- Set 2: 4 tubes, each tube 2.0 µL of 2-fold diluted cDNA

- Set 3: 4 tubes, each tube 2.0 µL of non-diluted cDNA

- Set 4: 4 tubes, each tube 3.0 µL of non-diluted cDNA

- Set 5: 5 tubes, each tube 4.0 µL of non-diluted cDNA

- Negative control: no template added, only 48 µL premix

3. PCR runs was executed as per the following design:

- Lid temperature: 105 ^{0}C

- Pre-cycle: 95 ^{0}C for 7 min (to activate the *polymerase*)

- Thirty one cycle as follows:

  - 94 ^{0}C   for   1 min (denaturation)

  - 55 ^{0}C   for   1 min (annealing)

  - 72 ^{0}C   for   1 min (extension)

- Post-cycle: 72 ^{0}C for 10 min (final extension)

- End cycle: 4 ^{0}C

4. The PCR products of each set were pooled, then 8 µL of each set was applied on a 1% (w/v) agarose gel in TBE buffer and EtBr. In addition, 5 µL of DNA smart ladder was used in an adjacent lane.

5. After running the gel at 125 V for 35 min, the DNA bands were visualized under a UV trans-illuminator, where 2-3 fragments are expected, one bigger VH fragment (about 900-1000 bp), and 1-2 shorter bands ($\approx$ 700 bp) for VHH.

6. All the sets in which bands around 700 bp were present and their related PCR tubes were pooled together, then all of the pooled volume was applied on a mini-gel cast with one wide slot of 1% (w/v) agarose gel and the gel was run (*see **above**).

Pause Point: the pooled 1st PCR products can be stored at -20 ^{0}C.

7. After electrophoresis, the agarose gel was put on a well-cleaned UV trans-illuminator for cutting out the specific PCR band ($\approx$ 700 bp) with a sterile blade.

Critical Step: the exposure time to UV must be minimized as much as possible to prevent DNA damage (e.g. pyrimidine dimer formation) that inhibits further PCR amplification.

8. The extracted fragment was weighed then purified from the gel block using the QIAquick Gel Extraction kit. Finally, the purified DNA was eluted in 100 µL H$_2$O, and its concentration was measured at OD$_{260nm}$ using Nanodrop spectrophotometer.

Pause Point: the eluted DNA products can be stored at -20 ^{0}C, or immediately used as template for the subsequent step (i.e. nested PCR).

9. The second step of the nested PCR was carried out by preparing a premix volume sufficient for 10 PCR tubes, as follows:

   - DEPC water_____358 µL
   - 10x PCR buffer_____45 µL
   - dNTPs (10 mM each)_____9 µL
   - 20 µM VHHBACK primer_____9 µL
   - 20 µM PMCF primer_____9 µL
   - Fast Start Taq DNA Polymerase_____2.25 µL
   - Total volume_____432 µL

10. The premix volume kept on ice while dividing equally onto the Westburg strips tubes (≈ 40 µL each), after that, the cDNA template was added as follows:

    - Set 1: 2 tubes, each tube 1.0 µL of 1st PCR purified DNA
    - Set 2: 2 tubes, each tube 2.0 µL of 1st PCR purified DNA
    - Set 3: 3 tubes, each tube 3.0 µL of 1st PCR purified DNA
    - Negative control: no template added

11. PCR runs was executed as per the following design:

    - Lid temperature: 105 ^{0}C
    - Pre-cycle: 95 ^{0}C for 7 min (to activate the *polymerase*)
    - Seventeen cycle as follows:
      - 94 ^{0}C   for   1 min (denaturation)
      - 55 ^{0}C   for   1 min (annealing)
      - 72 ^{0}C   for   1 min (extension)
    - Post-cycle: 72 ^{0}C for 10 min (final extension)
    - End cycle: 4 ^{0}C

12. From each set, 8 µL was applied on a 1% (w/v) agarose gel in TBE buffer and EtBr. In addition, 5 µL of DNA smart ladder was used in an adjacent lane.

13. After running the gel at 125 V for 35 min, the DNA bands are visualized under a UV trans-illuminator, where the presence of 400 bp bands are anticipated, which represents the size of VHHs.

14. All successful PCR sets are pooled together, and the amplified DNA was purified using QIAquick PCR purification kit. Finally the purified DNA was eluted in about 200 μL H_2O and the concentration was measured at OD_{260nm} using Nanodrop spectrophotometer.

Pause Point: the 2nd PCR eluted DNA products can be stored at -20 ^0C, or immediately used for the subsequent steps.

3.2.5 Digestion of VHHs and pMECS and Ligating Same

Procedure

1. The 2nd PCR product was digested overnight at 37 ^0C, as follows:
   - H_2O _____ 250 μL
   - 2nd PCR product (≈ 10 μg) _____ 200 μL
   - 10x H buffer _____ 50 μL
   - PstI (40 units/μL) _____ 5 μL
   - NotI (40 units/μL) _____ 5 μL
   - Total volume _____ 510 μL

2. In parallel, the pMECS vector was digested overnight at 37 ^0C, as follows:
   - H_2O _____ 680 μL
   - pMECS vector (≈ 500 ng/μL) _____ 120 μL
   - 10x H buffer _____ 90 μL
   - PstI (40 units/μL) _____ 9 μL
   - NotI (40 units/μL) _____ 9 μL
   - Total volume _____ 900 μL

3. The restriction enzyme digested 2nd PCR product was purified with QIAquick PCR purification kit protocol, using 3 columns. Finally, the purified VHHs' DNA was eluted in 180 μL H_2O.

4. The eluted DNA is digested again overnight at 37 ^{0}C, as follows:
    - Digested PCR product_____176 μL
    - 10x H buffer_____20 μL
    - PstI (40 units/μL)_____2 μL
    - NotI (40 units/μL)_____2 μL
    - Total volume_____200 μL

5. The restriction enzyme digested pMECS vector was purified with QIAquick PCR purification kit protocol, using 6 columns. Finally, the purified digested vector was eluted in 540 μL H$_2$O.

6. The eluted pMECS vector is digested again overnight at 37 ^{0}C, as follows:
    - Digested pMECS vector_____538 μL
    - 10x H buffer_____60 μL
    - PstI (40 units/μL)_____2 μL
    - NotI (40 units/μL)_____2 μL
    - Total volume_____600 μL

7. Again, the restriction enzyme digested 2nd PCR product was purified with QIAquick PCR purification kit protocol, using 2 columns. Finally, the purified VHHs' DNA was eluted in 100 μL H$_2$O and the concentration was measured at 260 nm using Nanodrop spectrophotometer. Finally, stored at -20 ^{0}C.

8. Then, 2 μL of XbaI (40 units/μL) was added to the pMECS secondary digestion mixture and incubated for 1 hour at 37 ^{0}C. The restriction enzyme digested pMECS vector was then purified with QIAquick PCR purification kit protocol, using 4 columns, where the purified vector was eluted in 300 μL H$_2$O (75 μL H$_2$O each), the concentration was measured at 260 nm using Nanodrop spectrophotometer. Finally, stored at -20 ^{0}C.

    Critical Step: Some DNA molecules are only cleaved by single enzyme, the additional XbaI digestion step for the vector will prevent the self ligation of these molecules.

    Check Point: In order to check the digestion efficiency, 0.5 and 1.0 μL of both 2nd PCR product and pMECS vector were applied on a 1% agarose gel in TBE and EtBr and run at 125 V for 30 min.

9. Three different concentrations of the pMECS vector and insert were prepared in order to get the optimal ratio, as follows:

	Tube 1	Tube 2	Tube 3
pMECS Vector	4.4 µg	4.4 µg	4.4 µg
Insert – 2ⁿᵈ PCR	1.7 µg	3.4 µg	5.1 µg

10. To each of the above tubes, 2.5 µL T4 DNA ligase (5 units/µL) and 15 µL 10x ligation buffer were added, then the final volume was brought up to 150 µL with H_2O, the mixture was gently mixed and span in microcentrifuge, and incubated at 16 ^0C for 4 hours.

11. After incubation, 25 µL of the following mixture was added to each tube as follows:

    ▪ H_2O _____ xx µL

    ▪ 10x ligation buffer _____8.5 µL

    ▪ pMECS (4.4 µg)_____ xx µL

    ▪ Insert - 2ⁿᵈ PCR (8.4 µg)_____ xx µL

    ▪ T4 DNA ligase (5 units/µL)_____3 µL

    ▪ Total volume_____85 µL

Caution: The (xx) volume of the vector and the insert were carefully calculated in order to give a final concentration of about 4.4 µg and 8.4 µg respectively. The final volume was adjusted with H_2O.

12. The mixture was gently mixed and span in microcentrifuge, and incubated overnight at 16 ^0C.

13. Cleaning the ligation reaction was done as follows:

    13.1. The ligation reaction was heated for at 65 ^0C for 10 min, so as to inactivate the ligase enzyme.

    13.2.   All the three tubes were pooled, and then added 100 µL of H_2O to a final volume of about 610 µL.

    13.3. An equal volume of TE-saturated phenol (i.e. ≈ 610 µL from the lower phase) was added, vortex and centrifuged at 18,000 g for 10 min to separate the phases.

    13.4. The upper aqueous phase was transferred to a fresh eppendorf tube, then an equal volume of Chloroform/Isoamyl alcohol (24/1 ratio) was added, vortex and centrifuged at 18,000 g for 10 min to separate the phases.

13.5. Again, the upper aqueous phase was transferred to a fresh eppendorf tube, then added $1/10^{th}$ volume of 3 M sodium acetate (pH 5.2), mixed via in/out pipetting.

13.6. Added three volumes of absolute ethanol (100% EtOH), then mixed via inverting the tubes, and then incubated at -80 ^{0}C for 30 min.

13.7. The content was centrifuged at 18,000 g for 20 min, the upper liquid was carefully removed without disturbing the "invisible" DNA pellets.

13.8. The pellet was air dried, and dissolved in 150 μL H_2O and divided into two tubes (75 μL each), the concentration was measured at OD_{260nm} using Nanodrop spectrophotometer and stored at -20 ^{0}C.

3.2.6 Preparation of Electrocompetent *E. coli* TG1 Cells

Since the main objective is to obtain as large and diverse VHHs library as possible, electroporation was performed to make the cells more receptive for vector. All the procedures of preparing the electrocompetent cells were carried out in the cold room at 4 ^{0}C.

Procedure

1. Buffers (i.e. 1 mM Hepes, pH 7.0) and 10% glycerol were freshly prepared, autoclaved and kept at 4 ^{0}C.

2. A single colony of fresh cells of *E. coli* TG1 was used to inoculate 5 mL 2xTY medium in 50 mL Falcon tube, then incubated overnight at 250 rpm and 37 ^{0}C.

3. About 2 mL of the overnight *E. coli* culture used to inoculate 300 mL 2xTY medium in a baffled flask. Then shacked for about 3-4 h at 250 rpm at 37 ^{0}C until the OD_{600nm} was between 0.8-1.0.

4. Once the desired OD_{600nm} value was reached, the flask was put on ice for 1 h inside the cold room.

5. The TG1 culture was divided over 6 ice-cooled Falcon tubes, and then centrifuged at 2,200 g for 7 min at 4 ^{0}C.

6. The supernatant was carefully decanted and gently resuspended the cells in a volume of ice-cooled 1 mM Hepes buffer (pH 7.0) equivalent to the original culture-volume.

Caution: All the resuspension steps must be carried out very gently (e.g. pipetting up and down very slowly or swirling).

7. The suspension was centrifuged at 2,200 g for 6 min at 4 ^{0}C.

8. The supernatant was carefully decanted and gently resuspended the cells in a volume of ice-cooled 10% glycerol equivalent to the half of the original culture-volume. Then centrifuged at 2,200 g for 6 min at 4 ^{0}C.

9. The supernatant was carefully decanted and gently resuspended the cells in 10 mL of ice-cooled 10% glycerol and all the tubes were pooled together. Then centrifuged at 2,200 g for 5 min at 4 ^{0}C.

10. Finally, the supernatant was carefully decanted and gently resuspended the cells in ice-cooled 10% glycerol to a final volume of 1 mL.

Critical Step: It is highly preferred to use the TG1 cells immediately for transformation. Since storage may significantly reduce their transformation efficiency.

3.2.7 Construction of VHHs Library in Phage Display Vector

The recently prepared *E. coli* TG1 electrocompetent cells were immediately transformed with the previously ligation mixture stored at -20 ^{0}C, and then plated on selective medium in order to generate a minimum VHHs library size of about 10^7 transformants.

Procedure

1. The electroporation apparatus was set at 1.8 kV and about 20 electroporation cuvettes were kept on ice.

2. About 50 µL of the electrocompetent cells was placed in the first electroporation cuvette as a control, and then applied the electric shock. The vulnerable cells were immediately treated with 400 µL SOC medium to recover.

3. The cuvette was rinsed few times by slow in and out pipetting, another 400 µL SOC added to rinse the cuvette once more.

4. About 75 µL ligation mixture was added to the rest of the competent cells, mixed by swirling and kept on ice for 1 min.

5. The total volume was used as follows:
   - Mixture (competent cells + ligation product)_____ 65 µL
   - First rinse (SOC medium)_____400 µL
   - Second rinse (SOC medium)_____400 µL
   - All the used volume was collected in one 15 mL Falcon tube.

6. The negative control and the transformed mixture were incubated at 200 rpm for at least 1 h at 37 ^{0}C.

7. After incubation, a serial dilution was made as follows:

    ▪ Dilution – 1: 900 µL SOC + 100 µL transformed cells

    ▪ Dilution – 2: 900 µL SOC + 100 µL dilution – 1

    ▪ Dilution – 3: 900 µL SOC + 100 µL dilution – 2

    ▪ Dilution – 4: 900 µL SOC + 100 µL dilution – 3

8. About 100 µL of dilution 3 and 4 was placed on a (90 mm) LB/Amp-Glu (i.e. 100 µg/mL Ampicillin and 2% (w/v) Glucose) small round agar plates, glass beads were used to distribute the cells over the agar surface. Finally, plates were inverted and incubated at 37 ^{0}C for overnight.

9. The rest of the competent cells suspension was used to plate about 2 mL/plate all the 6 large square LB/Amp-Glu agar plates (243 x 243 mm). Glass beads were used to distribute the cells over the agar surface. Finally, plates were inverted and incubated at 37 ^{0}C for overnight, these were used to calculate the transformation efficiency.

10. After incubation, the library size was calculated from the number of colonies on the small agar plates as follows:

    ▪ No. of colonies on each plate x 10 x Dilution factor x Volume of transformed cells = CFU/mL

11. The colonies were scrapped from the large square agar plates using 3 mL LB medium/plate with the aid of sterile cell scraper. The scrapped cells were transferred to a 50 mL Falcon tube. Furthermore, each plate was rinsed with 2 mL LB medium and transferred to the tubes. Finally, the cells were pelleted down via centrifugation at 2,200 g for 10 min.

12. The supernatant was carefully decanted and the cells resuspended in LB medium to a final volume of about 20 mL. Then 5 mL of 100 % glycerol was added, afterward, 20 small 1 mL aliquots in eppendorf tubes were prepared, one of the aliquots was diluted 100 times in 2 x TY medium, then measured the OD$_{600nm}$ to estimate the total number of cells within the scraped library (where: OD$_{600nm}$ of 1 corresponds to about 8x10^8 bacterial cell/mL). Finally, all the aliquots and the falcon tubes stored at -80 ^{0}C.

Critical Step: Calculating the library amplification factor (total number of colonies scraped divided by the total number if cells in the small aliquots) will help in estimating the number of presented copies of each individual transformant in the library.

13. Colony PCR was carried out to determine the percentage of colonies from the library which harbors the vector with the right insert size, premix volume for 32 tubes was prepared as follows:

- H$_2$O _____ 676 µL
- 10x PCR buffer _____ 80 µL
- dNTPs (10 mM each) _____ 8 µL
- MP57 primer (20 µM) _____ 16 µL
- GIII primer (20 µM) _____ 16 µL
- FastStart Taq polymerase(5 units/µL) _____ 4 µL
- Total volume _____ 800 µL

14. In each PCR tube (31 tubes) 24 µL was transferred, and to each tube a single colony from the dilution plates (i.e. 10^3 or 10^4) was added with the aid of a sterile micropipette tips. The last 32nd tube kept as negative control.

15. PCR runs was executed as per the following design:

- Lid temperature: 105 ^{0}C
- Pre-cycle: 95 ^{0}C for 6 min (to activate the *polymerase*)
- Twenty eight cycle as follows:
  - 94 ^{0}C for 45 sec (denaturation)
  - 55 ^{0}C for 45 sec (annealing)
  - 72 ^{0}C for 45 sec (extension)
- Post-cycle: 72 ^{0}C for 10 min (final extension)
- End cycle: 4 ^{0}C

16. About 8 µL of each Westburg tube was applied, for electrophoretic analysis, on a 1% (w/v) agarose gel in TBE buffer and EtBr. In addition, 5 µL of DNA smart ladder was used in an adjacent lane.

17. After running the gel at 125 V for 35 min, the DNA bands are visualized under a UV trans-illuminator to find out the number of colonies with the right size (i.e. 700 bp)

out of the 31 lanes. Whereas, the molecular weight of the vector with no insert is about 300 bp. A satisfactory result should be at least 70%.

3.2.8 Screening and Isolation of Nanobodies®: Phage Display and Biopanning

After infecting the *E. coli* TG1 cells with M13K07 helper phage we could generate the library of phages which display VHHs on their tips. The presence of the amber stop codon (TAG) between the VHHs sequences and the M13K07 gene III allowed the generation of a fraction of virions which display the VHHs on their outer tips. These virions are used for a series of consecutive rounds of biopanning against the two antigens used in the research work (i.e. SmCB and SmES). The enriched phages are then used to infect *E. coli* cells for (a) further virions' amplification for the next biopanning round and (b) obtaining single individual colonies of bacteria which would be used for screening antigen-specific VHHs via ELISA.

Procedure

1. In the first day, for each antigen, one well of a flat-bottom ELISA plate was coated with 100 µL of antigen solution at a concentration 100 µg/mL in 100 mM NaHCO$_3$ (i.e. 100 µg/well), the plate covered with Parafilm and kept overnight at 4 ^{0}C.

2. About 1 mL aliquot of the prepared library brought to room temperature and a volume contains number of cells 10-1000 times more than the number of the library size (i.e. the number of independent transformants) was used to inoculate 100 mL 2xTY/Amp-Glu medium (the glucose will prevent the leaky expression of VHH-M13 gene III fused protein from Plac promoter), then incubated at 200 rpm at 37 ^{0}C for about 2.5 h until OD$_{600nm}$ value equal 0.4-0.6 (i.e. the beginning of the exponential growth phase), where, OD$_{600nm}$ of 1 corresponds to $\approx 8x10^8$ cells/mL.

Critical Step: The number of the used cells must be at least 10 times higher than the library size to ensure that each independent transformant is represented and will have the chance to be tested against the antigens while performing the biopanning.

3. Then M13K07 helper phage was added at a multiplicity of infection (MOI) of about 5-20 to infect the TG1 cells, the culture medium was incubated at room temperature for 30 min without shaking.

Caution: The shaking of the culture after adding the helper phage may dramatically reduce the infection susceptibility of *E. coli* cells due to the break off the F-Pilli which is essential for phage infection.

4. The culture volume was divided over two Falcon tubes 50 mL, and centrifuged for 10 min at 1,500 g, then the supernatant was carefully decanted in sodium hypochlorite.

5. The infected TG1 cells pellet was resuspended in 1 mL 2xTY/Amp-Kan medium, and then transferred to 150 mL 2xTY/Amp-Kan medium in a baffled shake flask, then incubated overnight shacked at 225 rpm and 37 ^{0}C.

6. In the beginning of the next day, a single colony of fresh cultured TG1 cells was used to inoculate 10 mL LB medium in Falcon tube 50 mL, then incubated at 37 ^{0}C and 150 rpm for 2-3 h (until it is cloudy turbid) , these cells are used to amplify the eluted enriched phages later on.

7. The overnight 150 mL 2xTY/Amp-Kan culture was centrifuged for 30 min at 2,200 g at 4 ^{0}C. The supernatant containing the phage particles was carefully transferred (without disturbing the TG1 pellets) equally to 4 Falcon tubes 50 mL, then 1/5th volume of PEG/NaCl solution was added to each falcon tube, mixed well by inverting and placed on ice for at least 30 min.

8. After incubation on ice, the tubes were centrifuged for 30 min at 4 ^{0}C and 2,200 g. the supernatant is carefully decanted in sodium hypochlorite, and the tubes were air-dried via inverting on a tissue paper under laminar flow hood.

9. The phage pellets were gently resuspended in PBS (ensure homogenous phage suspension and avoid foaming) to a final volume of 1 mL. Then centrifuged for 2 min at 15,000 g in order to precipitate any existing bacterial cells, cell rubble and phage aggregates. The concentration was measure at OD_{260nm} after 50 to 100 fold dilutions was done, followed by adjusting the final concentration to working concentration of about 2 x 10^{12}/mL in PBS, where, OD_{600nm} of 1 corresponds to $\approx 3x10^{10}$ particles/mL.

10. The overnight-coated ELISA plate is rinsed well 5x with PBST, then 200 µL of blocking milk 2% in PBS was added to the positive well and the non-adjacent negative control well as well in order to block the binding sites of the residual protein. Afterward, incubated at room temperature for 2 h. After incubation the ELISA wells were rinsed at least 5 x with 200 µL PBST.

11. An equal volume of phage particles (2 x 10^{11} particles/mL) and 2% blocking fresh skimmed milk were mixed together (i.e. 100 µL each), then added 100 µL of the mixture to both the positive and control wells. The plate was incubated at room temperature for at least 1 h.

Critical Step: It is preferred to dilute the phage particles in the same blocking buffer to minimize the background and non specific binding between VHH and the buffer components.

12. After incubation, the phage solution was carefully decanted in sodium hypochlorite and subsequently rinsed 10x with PBST.

13. The bound phages were eluted from the wells by adding 100 µL of freshly prepared 100 mM TEA solution (pH 11.5), and incubated same at room temperature for 10 min. The eluted phages are neutralized via transferring them to an equal volume (100 µL) of 1 M Tris-HCl buffer (pH 7.4).

Pause Point: The neutralized solution can be stored at -80 ^{0}C for further procedures. Also, 10 µL of the positive well is stored at -80 ^{0}C as a backup.

14. A serial dilution, 10-folds, was prepared by mixing 10 µL of eluted virions with 90 µL of PBS buffer (the dilution range from 10^{-1} to 10^{-7}) in a round-bottom ELISA plate.

15. In a new round bottom microtiter plate, 10 µL of each phage dilution was mixed separately with 90 µL of exponentially growing *E. coli* TG1 cells (*from* **Method 3.2.8.6**), then incubated without shaking for 30 min at 37 ^{0}C.

16. Using a multichannel pipette 10 µL of each dilution was streaked on a small square agar plate LB/Amp-Glu. The plate is divided into two sides (i.e. positive sample and negative control), then the plates were air-dried under laminar flow hood for a few minutes, finally, the plates are inverted and incubated overnight at 37 ^{0}C.

17. The next day, the estimation of the enrichments was carried out by observing the number of the grown colonies on the square plates, the bacterial growth at each side was compared to the relative dilution of the negative control side.

18. In parallel, 50 µL of the remaining 90 µL of *E. coli* TG1 cells of dilution 10^{-3}-10^{-5} from the positive coated wells was added to small round agar plates LB/Amp-Glu,

then incubated overnight at 37 ^{0}C. The next day all the plates are stored at 4 ^{0}C for further procedures.

19. The remaining≈ 180 µL of the neutralized eluted phages (i.e. from positive and control) was added to about 2 mL of the exponentially growing *E. coli* TG1 cells (*from* **Method 3.2.8.6**) and gently mixed, then incubated at 37 ^{0}C for 30 min without shaking, after incubation, additional 8 mL of 2xTY/Amp-Glu medium was added and the mixture incubated at 37 ^{0}C with shaking at 200 rpm for 45 min.

20. The incubated infected cells were super-infected with about 10^7-10^9 M13K07 fresh phage particles, gently mixed, then incubated without shaking at room temperature for 30 min. After incubation, the cells were pelletized via centrifugation at 800 g for 10 min.

21. The supernatant was carefully decanted in sodium hypochlorite, and the pellet was resuspended in 1 mL 2xTY/Amp-Kan medium then transferred to 150 mL of the same medium in a baffled flask. Finally, the medium was incubated overnight with shaking at 225 rpm and 37 ^{0}C.

22. By the end of the day, another flat-bottom microtiter plate was prepared as explain above (*from* **Method 3.8.2.1**) for the consecutive biopanning rounds onward.

Critical Step: All the available data obtained from different studies indicate the degree of difference of the selection of VHH sequences' variants in the screening process of biopanning procedure, in which one kind of Nanobodies® can be successfully selected after the first biopanning round, though, it can be lost during the subsequent rounds. In contrast, other clones can be successfully picked only after the third or the fourth round. It is crucial to setup the appropriate design of the selection and screening procedures with the intention of improving the possibility to come across proper VHHs with particular properties.

3.2.9 Identification of Phages with Antigen-Specific VHHs Binders: Enrichment Phage ELISA and Periplasmic Extract ELISA (PE–ELISA)

If the selective enrichment was not noticed while performing the consecutive biopanning rounds, enrichment phage ELISA offers an alternative method which is more precise. Nevertheless, if the enrichment was still insignificantly observed, then, random single colonies from the *E. coli* TG1 cells infected with antigen-eluted phages are grown and their periplasmic extracts are screened against the antigen of interest through conventional ELISA procedures. The ELISA-positive colonies are further screened for their redundancy by colony PCR, Hinf-digestion on single colony and DNA sequencing.

Procedure

1. Flat-bottom microtiter plate wells were coated with 100 µL of both antigens (i.e. SmCB and SmSE) at concentration of 1 µg antigen/mL in 100 mM $NaHCO_3$ coating buffer in correspondence to the phage library and all the performed biopanning rounds, the plate was covered with Parafilm and incubated overnight at 4 ^{0}C.

2. After incubation, the antigen solutions were removed and rinsed 5x with PBST, afterward, 200 µL of 2% fresh skimmed milk in PBS was added to all wells (antigen coated and negative control), the plate was incubated at room temperature for 2 h.

3. The blocking buffer was removed and the wells rinsed 5x with PBST.

4. A mixture of 100 µL 2% fresh skimmed milk in PBS and equal volume of phage library and amplified phages from each panning round at concentration 2 x 10^{10} virions was prepared, then 100 µL of the mixture used to coat all the wells. Finally, the plate was incubated in room temperature for 1 h.

5. The coating solutions were removed and the wells rinsed 10x with PBST, then added 100 µL of 1/2000 dilution of anti-M13-HRP monoclonal antibody conjugate. Then, the plate kept in room temperature for 1 h.

6. The antibody solutions were removed and the wells rinsed 5x with PBST, then added 100 µL of HRP substrate solution. The plate was kept in dark and the absorbance was read at 405 nm after 10 min to 30 min with 5 min time step using a microtiter plate reader.

Pause Point: If no enrichment was not observed (i.e. at least 2 folds signal strength difference between the consecutive panning rounds onwards), the random selection of single colonies still a valid approach to be examined.

7. At least 48 single colonies from the panning round which previously showed a relative enrichment for antigen-specific phages were picked and inoculated a 24-well flat-bottom tissue culture plates, each well was previously filled with 1 mL TB medium containing 100 µg/mL of ampicillin. Concurrently, each picked colony was used to streak a reference master agar plat LB/Amp-Glu. These plates incubated overnight at 37 ^{0}C, and afterward, kept at 4 ^{0}C for further procedures.

Critical Step: Each streak must be accurately numbered according to the corresponding well of the 24-well flat-bottom tissue culture plates

8. The inoculated 24-well plates were incubated with shaking at 250 rpm, 37 ^{0}C for 5-6 h (the growth progress can be observed visually), then added 10 µL of 100 mM IPTG for a final concentration 1 mM. Then, incubated overnight with shaking at 250 rpm and 37 ^{0}C.

9. In parallel, a flat-bottom 96-well ELISA plate was coated with 100 µL antigens in 100 mM NaHCO$_3$ at a final concentration of 1 µg antigen/well. The plate was covered with Parafilm and kept overnight at 4 ^{0}C.

10. The next day, the antigen solutions removed and the wells rinsed 5x with PBST, then, the wells coated with 200 µL of 2% fresh skimmed milk in PBS.

11. In a swing-out rotor centrifuge the induced 24-well plates were centrifuged for 15 min at 4 ^{0}C and 2,200 g. The supernatant was carefully decanted without disturbing the bacterial cells, and then resuspended the pellets in 200 µL TES buffer. The plates kept at 4 ^{0}C for 30 min with shaking at 150 rpm.

12. After incubation, 300 µL of 1/4th dilution TES was added to each well, to causing an osmotic shock and extract the Nanobodies$^®$ from the periplasm. The plates incubated with shaking at 150 rpm and 4 ^{0}C for 30 min. Finally, the cells pelletized via centrifugation for 15 min at 4 ^{0}C and 2,200 g.

13. During the centrifugation, the blocking buffer in the 96-well ELISA plates was removed and the rinsed the wells 5x with PBST.

14. The supernatant (i.e. periplasmic extract) from the centrifuged 24-well plates (100 µL) was transferred to the corresponding positive and negative wells on the 96-well ELISA plates. The plates were incubated at room temperature for 1 h.

15. After incubation, the wells rinsed 5x with PBST, then added 100 µL of 1/1000 dilution of mouse anti-His tag antibody in PBS, incubated at room temperature for 1 h.

16. The antibody solution removed and the wells rinsed 5x with PBST, then added 100 µL of 1/2000 dilution of anti-mouse alkaline phosphatase conjugate, incubated at room temperature for 1 h.

17. Finally, the enzyme solutions removed and the wells rinsed 5x with PBST, then added 100 µL of freshly prepared alkaline phosphatase enzyme substrate, the plates kept in dark for 10 min and read the absorbance at 405 nm to 20 min with 5 min step.

18. For the same periplasmic extract, the colony was considered positive only if the absorbance in the antigen-coated well was at least twofold that of the non-coated negative control well.

19. Each positive clone was digested by Hinf restriction enzyme in order to make groups of binders with probable identical sequences.

20. Colony PCR was done, a premix volume for each sample of positive clone was prepared as follows:

    - H_2O _____ 84 µL
    - 10x PCR buffer _____ 10 µL
    - dNTPs (10 mM each) _____ 1 µL
    - MP57 primer (20 µM) _____ 2 µL
    - GIII primer (20 µM) _____ 2 µL
    - FastStart Taq polymerase(5 units/µL) _____ 0.3 µL
    - Total volume _____ ≈ 99 µL

21. On the tip of sterilized yellow-tip a part of each positive single colony from the reference master agar plate was used to streak a numbered agar plate LB/Amp-Glu and then placed inside a PCR eppendorf tube containing 96 µL of the above premix solution, the tips kept for 15 min while the tubes were placed on ice.

22. PCR runs was executed as per the following design:

- Lid temperature: 105 ^{0}C
- Pre-cycle: 95 ^{0}C for 6 min (to activate the *polymerase*)
- Thirty two cycle as follows:
  - 94 ^{0}C   for   45 sec (denaturation)
  - 55 ^{0}C   for   45 sec (annealing)
  - 72 ^{0}C   for   45 sec (extension)
- Post-cycle: 72 ^{0}C for 10 min (final extension)
- End cycle: 4 ^{0}C

23. After PCR reaction, 10 µL from each sample were applied on a 1% agarose gel in TBE and EtBr and run at 125 V for 30 min, and then the gel was visualized under a UV trans-illuminator.

24. Hinf analysis was carried out to make a sub-selection from the positive clones, for each sample a digestion mixture was prepared as follows:

- Hinf (10 u/µL) _____ 0.5 µL
- 10x Buffer R _____ 1.1 µL
- Total volume _____ 1.6 µL

25. After filling the Westburg tubes with 1.6 µL of the premix, 10 µL of the colony PCR reaction was added by means of a multichannel pipette, and then incubated at 37 ^{0}C for 1 h.

26. After incubation, 10 µL from each sample were applied on a 2% agarose gel in TBE and EtBr and run at 110 V for 30 min, and then the gel was visualized under a UV trans-illuminator.

27. According to the results obtained from Hinf analysis, each selected sample was cleaned up for DNA sequencing using MP57 primer, as follows:

- Colony PCR product _____ 10 µL
- ExoSAP-IT _____ 2.6 µL
- The mixture was incubated at 37 ^{0}C for 15 min followed by another 15 min at 80 ^{0}C. Finally, the mixture stored at -20 ^{0}C for sequencing.

28. In addition, a corresponding colony of each positive clone was picked and incubated overnight with shaking at 200 rpm at 37 ^{0}C in LB medium with ampicillin (at final concentration 100 µg/mL).

29. The next day, the recombinant pMECS phagemid (i.e. the plasmid) was purified using GenElute Plasmid Miniprep kit as per the manufacturer protocol.

30. For each successfully identified VHHs sequence, their purified plasmids were used to transform WK6 cells, for the expression of Nanobodies$^®$, as previously described (see **Method 3.2.7.1** to **3.2.7.6**).

Pause Point: A glycerol stock of the transformed WK6 cells must be made for the prolonged storage of the VHHs of interest (Sambrook et al., 1989).

3.2.10   Expression and Purification of Antigen-Specific Binders

After transformation of the recombinant pMECS vector with the VHHs genes of interest into *E. coli* WK6 cells, which lack suppressor (su$^-$). Nanobodies$^®$ fused to HA-tag and His$_6$-tag are expressed and directed to the periplasm of the cells. The induced WK6 cells are exposed to an osmotic shock to extract the periplasm. These extracts are purified via immobilized metal affinity chromatography IMAC, the latter is very sufficient to do basic tests such as ELISA and Western blot. Furthermore, they can be subsequently purified through size exclusion chromatography.

Procedure

1. A single colony of *E. coli* WK6 containing the plasmid of the VHH of interest was used to inoculate a starter culture of 15 mL LB/Amp medium in 50-mL Falcon tube. The culture was incubated overnight at 37 ^{0}C while shaking at 200 rpm.

2. The next day, 1 mL of the starter culture was used to inoculate 330 mL TB/Amp-Glu-Mg medium in a 1 L baffled shake flask and then the culture was incubated for 2-4 h, with shaking at 200 rpm at 37 ^{0}C until the OD$_{600nm}$ value reached 0.6-0.9.

3. Each 330 mL TB/Amp-Glu-Mg medium was induced with 330 µL 1M IPTG for a final concentration 1 mM. Afterward, the culture was incubated overnight with shaking at 200 rpm at 28 ^{0}C until the OD$_{600nm}$ of the undiluted culture reached 20-30. Finally, the culture was transferred to appropriate tubes for centrifugation at 11,300 g for 8 min at 4 ^{0}C.

4. The supernatant of each 330 mL culture was decanted and the cell pellet was fully suspended in 4 mL TES buffer through reciprocating pipetting. Subsequently, the suspension was kept on ice in the cold room, at 4 ^{0}C, on a shaker at 200 rpm for 6 h.

5. While cells still on ice 8 mL of 1/4th dilution TES buffer was added, and kept in the cold room on ice and shaking at 200 rpm overnight.

6. The next day, all the tubes were centrifuged for 30 min at 11,300 g at 4 ^{0}C and then the supernatant containing the periplasmic extract was carefully transferred to 50-mL Falcon tubes.

7. The PD-10 columns were prepared for IMAC purification of the His$_6$-taged VHHs, for each liter of *E. coli* culture 1 mL of the HIS-Select gel was used with binding capacity of about 15 mg His-tag VHH/mL.

8. In the beginning, the HIS-Select gel was equilibrated with 50 mL PBS, then 40 mL of the supernatant was discarded and the rest volume was equally distributed over the 50 mL Falcon tubes with the periplasmic extract. The mixture was incubated at 4 ^{0}C for 30 min with gentle shaking.

9. After incubation, the mixture was poured into the PD-10 column with filter fitted inside and was left to drain by gravity.

10. The His-Select gel washed with 20 column volumes with PBS until the last droplet OD$_{280nm}$ value was close to zero.

11. The Ni-ion bound Nanobodies$^®$ was eluted by adding 5 columns volume of 500 mM Imidazole in PBS, the elution continued until the last droplet OD$_{280nm}$ value was less than 0.15.

12. Finally, the Ni-NTA fractions were ran on 12% sodium-dodecyl-sulfate poly-acrylamide-electrophoresis gel (SDS-PAGE) to confirm Nanobodies$^®$ elution in the samples. The fractions were pooled and their approximate protein concentration was measured at OD$_{280nm}$ at their individual extinction coefficients' values using Nanodrop$^®$ spectrophotometer.

13. The Imidazole was replaced with PBS buffer by using Vivaspin column with molecular weight cut off value MWCO of 5 kDa.

Caution: Nanobodies$^®$ eluted with Imidazole only stored at 4 C, freezing may cause irreversible precipitation.

4 Results and Discussion

4.1 Camel Immunization

In order to generate antigen specific HCAbs, a three years old camel of about 250 Kg weight, was immunized with SmCB and SmES antigens. Medical follow up was performed on regular basis. Evidently, no significant health problem occurred during the entire immunization period until the blood withdrawing date (i.e. 8 weeks).

4.2 Library Construction

Lymphocytes of the immunized camel were extracted from 100 mL of peripheral blood PBL using Leucosep™ tube. A total amount of about 40 µg mRNA was extracted from the PBL and was subsequently used as a template for generating the first complementary strand of complementary DNA. Afterward, the 1st cDNA was as a template to amplify the gene fragments encoding for the variable domain of the heavy chain only antibodies and the conventional antibodies up to the CH2 domain. The resultant fragments bands are corresponding to VH-CH1-hinge-CH2 and VHH-hinge-CH2 regions of corresponding sizes of about≈ 900 bp and ≈ 700 bp respectively. **Figure 1.14** illustrates the 1st PCR products and the resulting bands after separation on 1% agarose gel electrophoresis.
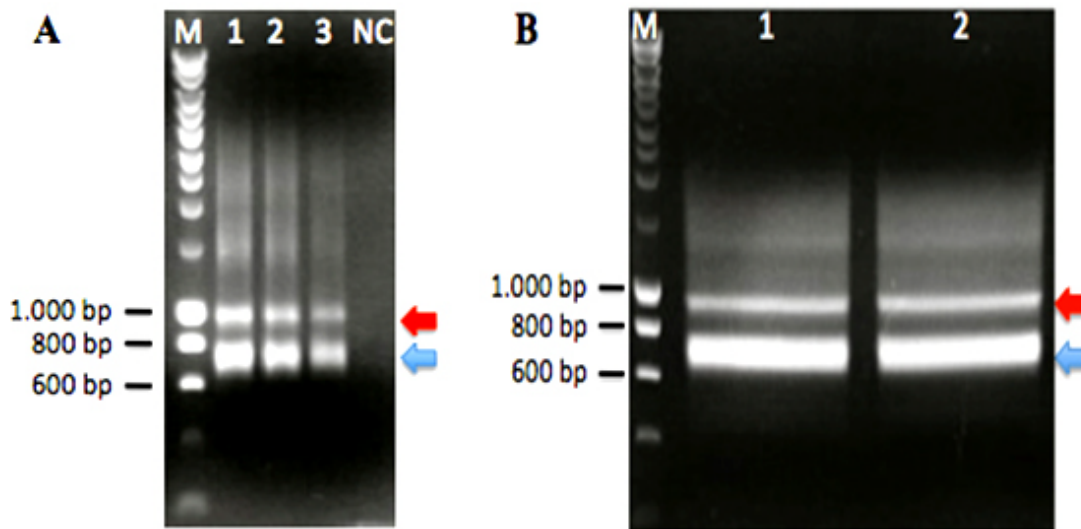
***Figure 1.14. 1st PCR products gel electrophoresis on 1% agarose gel**. Both A & B represent the amplification products of the 1st strand cDNA PCR containing fragments with two different sizes. The red arrow points at the 900 bp fragment corresponds to VH-CH1-hinge-CH2, whereas, the blue arrow points at the 700 bp fragment corresponds to VHH-hinge-CH2.*

The 700 bp fragment band purified from the 1% agarose gel using the QIAquick Gel Extraction Kit (Qiagen), then the purified products used as a template for a nested PCR amplification processes specific to VHH-only sequences producing a corresponding DNA fragment of about 400 bp. **Figure 1.15A** illustrates the purified 700 bp band after purification, while, **Figure 1.15B** represents the product of the 2nd nested PCR.
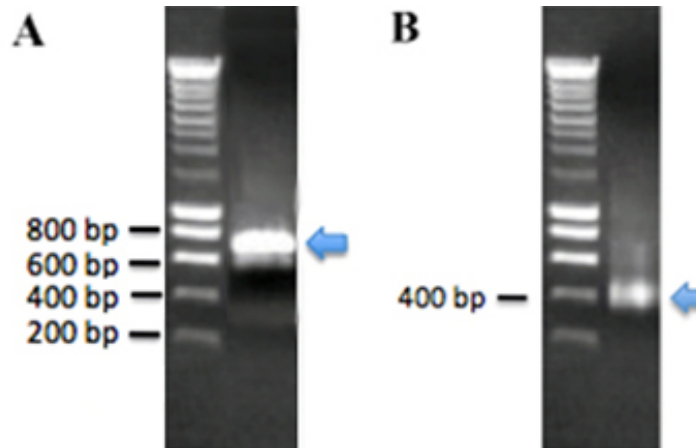
*Figure 1.15. Purified and Nested PCR Products Gel Electrophoresis on 1% Agarose Gel. A. the blue arrow points at the purified 700 bp fragment correspond to the VHH-CH2 region. **B**. the blue arrow points at the product of the 2nd nested PCR of about 400 bp and correspond to the VHH only fragment.*

The PCR fragments and the pMECS vector were digested with the same restriction enzymes via two consecutive digestion sessions. **Figure 1.16** illustrates the digested purified 2nd PCR product and the vector at two different volumes; 0.5 and 1 µL per lane (1 & 2) and (3 & 4) respectively.
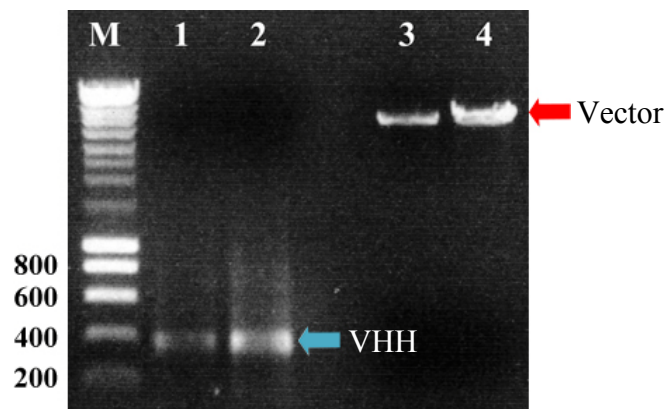
Figure 1.16. Digested VHH Fragment and Vector Gel Electrophoresis on 1% Agarose Gel. The red arrow points at the digested pMECS vector, while, the blue arrow points at the VHH fragment.

The pMECS clean ligation was subsequently transformed into the freshly prepared electrocompetent cells of *Escherichia coli* TG1 strain by electroporation. Finally, a library size of about 1.2 x10^7 transformants (i.e. clones) was obtained. **Figure 1.17** illustrates the products of the colony PCR, from 30 randomly selected single colonies from the dilution plates, which determined about 80 % (i.e. 24 clones with correct insert size out of 30 picked samples) of the clones in the constructed library contained a correct insert size of about ≈ 700 bp encodes for the bacteriophage gIIIp protein (≈ 300 bp) fused to the VHH (≈ 400 bp).
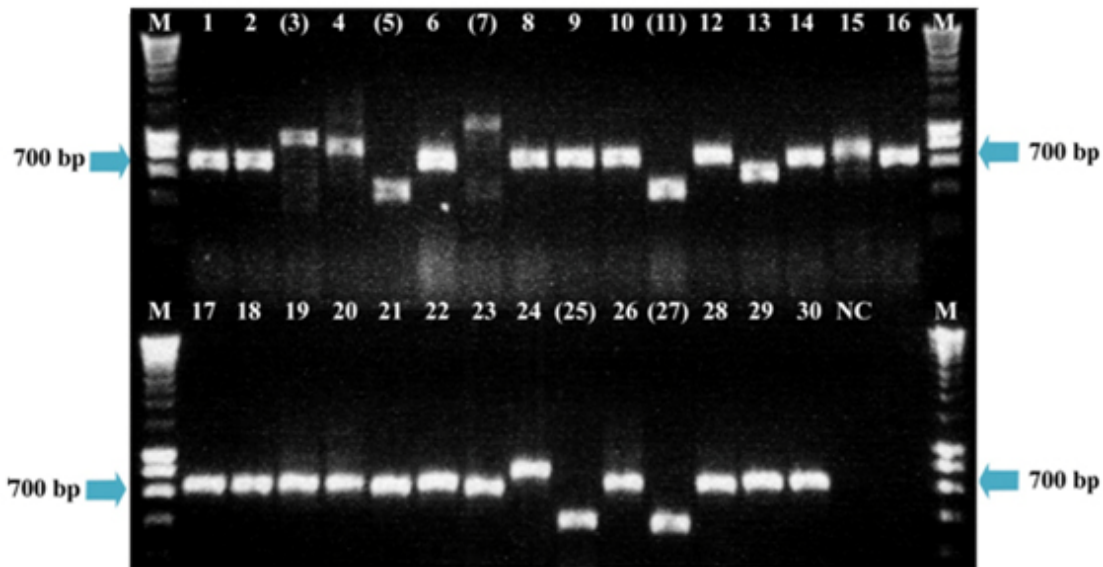
Figure 1.17. Colony PCR for Library with Correct Insert-Size Estimation. *The blue arrows point at the correct size, the lanes numbers between brackets signify those with incorrect sizes.*

4.3 Screening and Isolation of Nanobodies®: Phage Display and Biopanning

After infecting the *E. coli* TG1 cells with M13K07 helper phage, a phage library which displays VHHs on their tips was generated. These virions used for four consecutive rounds of biopanning against the two antigens (i.e. SmCB and SmES). There was no significant enrichment in phages. Nonetheless, random 47 single individual colonies of bacteria for each antigen were used for screening antigen-specific VHHs via Periplasmic Extract ELISA (PE-ELISA). Only two colonies corresponding to SmES gave (≥ 2) the reading absorbance value and were considered positive, whereas, thirty six colonies corresponding to SmCB were considered positive, divided into groups with regard to their absorbance intensities. Furthermore, the redundancy of the ELISA-positive colonies was further screened for their redundancy by colony PCR, Hinf-digestion on single colonies and DNA sequencing.

Table 1.11. *PE ELISA Readings for SmCB Antigen-Specific VHH binders - Plate A & B*

SmCB Plate-A	1	2	3	4	5	6	7	8	9	10	11	12
A	0,085	0,07	0,074	0,086	2,889	0,36	0,126	1,458	0,108	0,1	0,097	3,031
B	0,065	0,067	0,077	0,082	2,821	0,118	0,084	1,406	0,088	0,089	0,088	2,812
C	0,082	0,103	0,154	3,041	0,15	0,18	3,032	2,46	0,091	0,257	0,123	0,13
D	0,063	0,072	0,075	2,764	0,077	0,077	2,918	2,281	0,08	0,078	0,077	0,079
E	0,285	0,081	0,091	0,345	2,771	2,732	0,38	0,319	0,177	0,217	2,802	0,347
F	0,096	0,072	0,081	0,088	3,053	2,359	0,106	0,107	0,083	0,085	2,608	0,118
G	2,763	0,082	0,074	0,099	0,139	0,112	0,074	2,359	0,079	0,139	0,167	0,203
H	2,748	0,079	0,071	0,074	0,082	0,087	0,083	1,821	0,082	0,082	0,075	0,078

SmCB Plate-B	1	2	3	4	5	6	7	8	9	10	11	12
A	0,201	0,346	0,263	0,221	0,196	0,183	0,128	3,158	0,164	0,11	0,262	0,193
B	0,111	0,152	0,115	0,124	0,12	0,157	0,131	2,69	0,147	0,192	0,143	0,122
C	0,112	0,438	0,344	0,837	0,29	0,345	0,334	0,3	0,354	0,224	1,053	0,194
D	0,103	0,219	0,248	0,653	0,234	0,147	0,178	0,149	0,227	0,104	0,709	0,083
E	0,107	0,146	0,302	0,38	0,316	0,445	2,824	0,244	0,259	0,453	0,118	0,163
F	0,081	0,082	0,095	0,125	0,094	0,117	2,321	0,081	0,079	0,245	0,079	0,081
G	3,524	0,095	0,102	0,5	2,229	0,349	0,288	0,098	0,122	0,107	0,303	2,841
H	3,398	0,085	0,083	0,227	1,687	0,082	0,083	0,081	0,078	0,08	0,102	2,563

Where:

Group 1	Group 3
Group 2	Group 4
Negative Control	

Table 1.12. *PE ELISA Readings for SmES Antigen-Specific VHH binders - Plate A & B*

SmES Plate-A	1	2	3	4	5	6	7	8	9	10	11	12
A	1,289	3,069	3,425	3,206	3,004	3,006	0,881	2,868	2,835	0,688	2,823	0,084
B	0,773	3,172	3,397	3,242	2,947	2,708	1,066	3,122	2,888	0,856	2,508	0,087
C	3,459	3,373	0,358	3,398	3,259	2,797	3,178	3,025	2,741	0,945	0,094	3,586
D	3,477	3,373	0,232	3,122	3,346	2,924	2,751	3,022	2,639	0,657	0,087	2,555
E	3,543	3,54	3,268	3,29	0,462	3,089	2,824	2,8	2,912	2,974	2,626	2,745
F	3,312	3,31	3,422	2,93	0,151	3,185	2,919	3,178	2,743	2,729	2,481	2,707
G	3,65	3,479	0,104	3,12	3,242	3,389	3,315	3,212	2,531	2,966	2,854	2,89
H	3,41	3,201	0,086	2,986	3,346	2,94	2,676	2,871	2,629	2,571	2,551	2,649

SmES Plate-B	1	2	3	4	5	6	7	8	9	10	11	12
A	3,349	3,218	2,935	3,282	3,318	1,901	3,249	3,364	3,116	2,628	0,258	2,818
B	3,224	3,423	3,144	2,886	3,32	2,199	3,463	3,59	3,509	3,062	0,283	3,963
C	3,106	3,427	0,374	3,13	3,773	3,515	3,464	1,809	2,538	2,875	1,049	2,839
D	3,382	3,16	0,293	3,052	3,312	3,408	3,277	1,629	3,15	3,108	1,035	2,754
E	3,23	3,224	1,824	2,997	0,375	1,94	3,693	3,46	3,937	3,02	2,469	3,19
F	3,078	3,129	1,752	3,009	0,097	2,012	3,184	2,869	3,139	3,08	2,662	2,786
G	3,26	3,341	3,28	3,193	1,343	3,124	3,451	3,904	3,227	2,972	3,38	2,2
H	3,115	3,228	3,193	3,068	1,046	2,946	3,011	2,787	2,932	3,016	3,158	1,546

Where:

	Group 1
	Negative Control

Figure 1.18 illustrates the colony PCR products of three sample clones for SmES antigen (i.e. two positive binders and one random), and all the positive selected binders of SmCB. Five clones seemed to be contaminated and didn't offer any good candidate, whilst, thirty seven clones were found with the correct insert size and were put forward for further Hinf-digestion analysis.
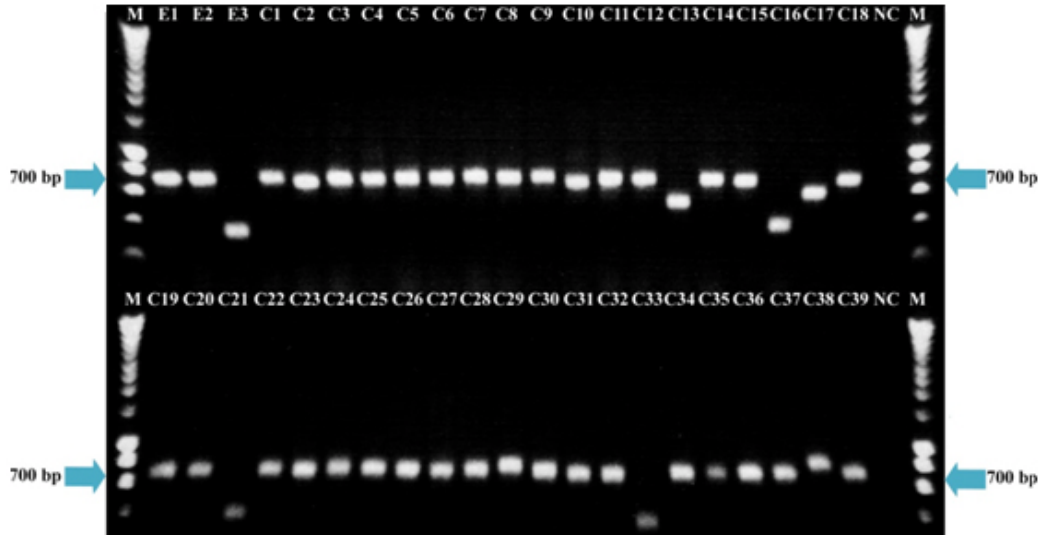
Figure 1.18. Colony PCR for Selected Binders from PE ELISA. From E1 to E3 are colonies for the SmES two positive binders and one negative sample which was randomly selected. From C1 to C39 are colonies for the SmCB positive binders.

All the positive colonies were subjected for further Hinf-digestion in order to assort the positive clones into groups. **Figure 1.19** illustrates the results after digestion.
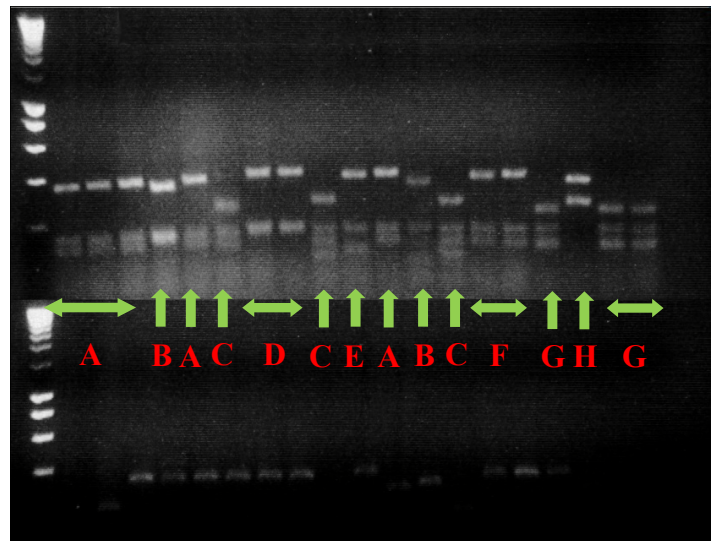
Figure 1.19. The Products of Hinf-Digestion. There are eight different groups of positive clones.

All the positive clones were sent for sequencing and then all sequences were translated into their corresponding amino acids using Clone Manager-6 program. The produced amino acids sequences were aligned and divided into groups, using ClustalW2 multiple sequence alignment program. Noteworthy, some of the binders' retrieved sequences were omitted, and are not shown here in the study, due to inadequacy and erratic manner of their results; mostly it occurs while sequencing, and clones should go for another attempt:

```
              <-----------------FR1----------------->  <---CDR1--->  <-----------FR2----------->   <---CDR2--->
NbSmCB6       QVQLQESGGGSVQAGGSLRLSCTVSG                 ETYRSRY       LAWFRAAPGKEREGVAVI           LPGGGTTY
              <--------------------------FR3-------------------------->  <-----------CDR3------------> <------FR4------>
              YTDSVKGRFTISQDIPKTTVYLQMNSLKPEDTAMYYC                       AASTSMYLYDRKFSADAYNY         WGQGTQVTVSS
```

```
              <-----------------FR1----------------->  <-CDR1->  <-------------FR2------------>   <---CDR2--->
NbSmCB2       QVQLQESGGGSVQAGGSLKLSCTASG                 YIYKTF     WGWFRQAPGKEREGVALF             ATDGIYID
NbSmCB3       QVQLQESGGGSVQAGGSLKLSCTASG                 YIYKTF     WGWFRQAPGKEREGVALF             ATDGIYID
NbSmCB25      QVQLQESGGGSVQAGGSLKLSCTASG                 YIYKTF     WGWFRQAPGKEREGVALF             ATDGIYID
              <--------------------------FR3-------------------------->  <-----------CDR3-----------> <------FR4------>
NbSmCB2       YADSVKGRFTISTDNVKNTVYLMMTNLKPEDTAIYYC                       AAGFGGDYSRRWQIGSWIY         WGRGTQVTVSS
NbSmCB3       YADSVKGRFTISTDNVKNTVYLMMTNLKPEDTAIYYC                       AAGFGGDYSRRWQIGSWIY         WGRGTQVTVSS
NbSmCB25      YADSVRGRFTISTDNVKNTVYLMMTNLKPEDTAIYYC                       AAGFGGDYSRRWQIGSWIY         WGRGTQVTVSS
```

```
              <-----------------FR1----------------->  <-CDR1->  <-----------FR2------------>   <---CDR2--->
NbSmCB11      QVQLQESGGGSVQAGGSLRLSCKASS                 YTGI       MAWFRQSLGKEREGVAAI             RTGTHETY
NbSmCB13      QVQLQESGGGSVQAGGSLRLSCKASS                 YTGI       MAWFRQSLGKEREGVAAI             RTGTHETY
NbSmCB14      QVQLQESGGGSVQAGGSLRLSCKASS                 YTGI       MAWFRQSLGKEREGVAAI             RTGTHETY
NbSmCB15      QVQLQESGGGSVQAGGSLRLSCKASS                 YTGI       MAWFRQSLGKEREGVAAI             RTGTHETY
NbSmCB27      QVQLQESGGGSVQAGGSLRLSCKASS                 YIGI       MAWFRQSPGKEREGVAAI             RTGTHGTY
              <--------------------------FR3-------------------------->  <-----------CDR3-----------> <------FR4------->
NbSmCB11      YHDSVKGRFTISRDNAEKTVYLQMNSLKPEDTAMYYC                       AAARLSVYEWYSDSRYNF          WGQGTQVTVSS
NbSmCB13      YHDSVKGRFTISRDNAEKTVYLQMNSLKPEDTAMYYC                       AAARLSVYEWYSDSRYNF          WGQGTQVTVSS
NbSmCB14      YHDSVKGRFTISRDNAEKTVYLQMNSLKPEDTAMYYC                       AAARLSVYEWYSDSRYNF          WGQGTQVTVSS
NbSmCB15      YHDSVKGRFTISRDNAEKTVYLQMNSLKPEDTAMYYC                       AAARLSVYEWYSDSRYNF          WGPGTQVTVSS
NbSmCB27      YDDSVKGRFTISRDNAENTVYLQMNSLKPEDTAMYYC                       AAARLSVYEWYSDSRYNF          WGQGTQVTVSS
```

	<-----------------FR1----------------->	<-CDR1->	<------------FR2------------>	<---CDR2--->
NbSmCB10	QVQLQESGGGSVQAGGSLRLSCVAST	YTYTS	MGWFRQAPGKEREGVASI	NSRFNTNTY
NbSmCB17	QVQLQESG??SVQAGGSLRLS?VAST	YTYTS	MGWFRQAPGKEREGVASI	NSRFNTNTY
NbSmCB18	QVQLQESGGGSVQAGGSLRLSCVAST	YTYTS	MGWFRQAPGKEREGVASI	NSRFNTNTY
NbSmCB19	QVQLQESGGGSVQAGGSLRLSCVAST	YTYTS	MGWFRQAPGKEREGVASI	NSRFNTNTY
NbSmCB20	QVQLQESG?GSVQAGGSLRLS?VAST	YTYTS	MGWFRQAPGKEREGVASI	NSRFNTNTY
NbSmCB21	QVQLQESGGGSVQAGGSLRLSCVAST	YTYTS	MGWFRQAPGKEREGVASI	NSRFNTNTY
NbSmCB22	QVQLQESGGGSVQAGGSLRLSCVAST	YTYTS	MGWFRQAPGKEREGVASI	NSRFNTNTY
NbSmCB28	QVQLQESGGGSVQAGGSLRLSCVAST	YTYTS	MGWFRQAPGKEREGVASI	NSRFNTNTY
NbSmCB29	QVQLQESGGGSVQAGGSLRLSCVAST	YTYTS	MGWFRQAPGKEREGVASI	NSRFNTNTY
NbSmCB30	QVQLQESGGGSVQAGGSLRLSCVAST	YTYTS	MGWFRQAPGKEREGVASI	NSRFNTNTY

	<-------------------------FR3------------------------->	<-----------CDR3----------->	<------FR4------->
NbSmCB10	YADSVKGRFTISRDSAKNTVYLQMNSLKPEDTAIYYC	AAGPLQGGVTWDKPSGYTR	WGQGTQVTVSS
NbSmCB17	YADSVKGRFTISRDSAKNTVYLQMNSLKPEDTAIYYC	AAGPLQGGVTWDKPSGYTR	WGQGTQVTVSS
NbSmCB18	YADSVKGRFTISRDSAKNTVYLQMNSLKPEDTAIYYC	AAGPLQGGVTWDKPSGYTR	WGQGTQVTVSS
NbSmCB19	YADSVKGRFTISRDSAKNTVYLQMNSLKPEDTAIYYC	AAGPLQGGVTWDKPSGYTR	WGQGTQVTVSS
NbSmCB20	YADSVKGRFTISRDSAKNTVYLQMNSLKPEDTAIYYC	AAGPLQGGVTWDKPSGYTR	WGQGTQVTVSS
NbSmCB21	YADSVKGRFTISRDSAKNTVYLQMNSLKPEDTAIYYC	AAGPLQGGVTWDKPSGYTR	WGQGTQVTVSS
NbSmCB22	YADSVKGRFTISRDSAKNTVYLQMNSLKPEDTAIYYC	AAGPLQGGVTWDKPSGYTR	WGQGTQVTVSS
NbSmCB28	YADSVKGRFTISRDSAKNTVYLQMNSLKPEDTAIYYC	AAGPLQGGVTWDKPSGYTR	WGQGTQVTVSS
NbSmCB29	YADSVKGRFTISRDSAKNTVYLQMNSLKPEDTAIYYC	AAGPLQGGVTWDK?SGYTR	WGQGTQVTVSS
NbSmCB30	YADSVKGRFTISRDSAKNTVYLQMNSLKPEDTAIYYC	AAGPLQGGVTWDKPSGYTR	WGQGTQVTVSS

	<-----------------FR1----------------->	<--CDR1-->	<-----------FR2------------>	<---CDR2--->
NbSmCB8	QVQLQESGGGSVQDGGSLRLSCVASG	YTYSIKW	RGWFRQAPGKEREAVAAI	GTGSGATY
NbSmCB16	QVQLQESGGGSVQDGGSLRLSCVASG	YTYSIKW	RGWFRQAPGKEREAVAAI	GTGSGATY

	<-------------------------FR3------------------------->	<-----------CDR3---------->	<------FR4------->
NbSmCB8	YDDSVRGRFTISQDNAQNTVYLQMSSLKPEDTALYYC	AASDSQSFLLTRSDRYKY	WGQGTQVTVSS
NbSmCB16	YDDSVKGRFTISQDNAQNTVYLQMSSLKPEDTALYYC	AASDSQSFLLTRSDRYKY	WGQGTQVTVSS

```
                <-----------------FR1----------------->   <-CDR1->   <-----------FR2------------->   <---CDR2--->
NbSmCB9         QVQLQESG??SVQAGGSLRLSCEASG                 YNISTYC    MGWFRQAVGKEREGVANI             GSSGGRTY
                <------------------------FR3-------------------------->   <-----------CDR3----------->   <------FR4------->
NbSmCB9         YADSVKGRFTISRDNAKNVVYLQMNNLKPEDTAIYYC                      ATNSLWCPGFQASRWNY             WGQGTQVTVSS


                <-----------------FR1----------------->   <-CDR1->   <-----------FR2------------->   <---CDR2--->
NbSmCB7         QVQLQESG?GSVQAGGSLRLSCAASG                 YTSAPY?    MGWL???VPGKECESVSS?            ?TAGFPN
NbSmCB26        QVQLQESGGGSVRAGGSLRLSCAASG                 YTSAPYL    MGWL?RQVPGKECESVSSM            STAGFPN
                <------------------------FR3-------------------------->   <-----------CDR3----------->   <------FR4------->
NbSmCB7         YADSV??RFTISRDY?KMTVDLQMNNL?PDDTGMYYC                      A?SGRWC                       DGQGTQ?TVSS
NbSmCB26        YADSVKGRFTISRDYAKMTVDLQMNNLKPDDTGMYYC                      AASGRWC                       DGQGTQVTVSS


                <-----------------FR1----------------->   <-CDR1->   <-----------FR2------------->   <---CDR2--->
NbSmES1         QVQLQESGGGSVQAGGSLRLSCAASG                 NSRRPLKY   IGWFRQPPGKEREGIAAI             HLAGGSTW
NbSmES2         QVQLQESGGGSVQAGGSLRLSCAASG                 NSRRPLKY   IGWFRQPPGKEREGIAAI             HLAGGSTW
NbSmES3         QVQLQESGGGSVQAGGSLRLSCAASG                 NSRRPLKY   IGWFRQPPGKEREGIAAI             HLAGGSTW
NbSmES5         QVQLQESGGGSVQAGGSLRLSCAASG                 NSRRPLKY   IGWFRQPPGKEREGIAAI             HLAGGSTW
                <------------------------FR3-------------------------->   <-------------CDR3------------->   <------FR4------->
NbSmES1         YSDSVKGRFTISQDRDKNTVYLQMNSLKPEDTAIYYC                      AALSKSRVGYWRSSREYKY           WGQGTQVTVSS
NbSmES2         YSDSVKGRFTISQDRDKNTVYLQMNSLKPEDTAIYYC                      AALSKSRVGYWRSSREYKY           WGQGTQVTVSS
NbSmES3         YSDSVKGRFTISQDNAKNVVYLQMNSLKPEDTAIYYC                      AALSKSRVGYWRSSREYKY           WGQGTQVTVSS
NbSmES5         YSDSVKGRFTISQDRDKNTVYLQMNSLKPEDTAIYYC                      AALSKSRVGYWRSSREYKY           WGQGTQVTVSS


                <-----------------FR1----------------->   <--CDR1-->   <-----------FR2------------->   <---CDR2--->
NbSmES4         QVQLQESGGGSVQAGGSLRLSCAASG                 NTDN-IYR     MTWFRQAPGKEREGVASM            QRNGRGIY
                <------------------------FR3-------------------------->   <-------------CDR3------------->   <------FR4------->
NbSmES4         YANSVKGRFTISQDNAKNTLYLQMNSLKPEDTGVYYC                      TT-------GWRALRLLP-           DRRGTQVTVSS
```

Where:

FR1,2,3,4: Fram Works 1, 2, 3 and 4

CDR1,2,3: Complementarity Determining Regions 1, 2 and 3

4.4 Expression and Purification of Antigen-Specific Binders

The recombinant pMECS vector with the VHHs genes of interest were transformed into *E. coli* WK6 cells, which lack suppressor (su⁻). Nanobodies® fused to HA-tag and His$_6$-tag are expressed and directed to the periplasm of the cells. The induced WK6 cells are exposed to an osmotic shock to extract the periplasm. These extracts are purified via Ni-NTA immobilized metal affinity chromatography IMAC. The eluted Ni-NTA fractions were pooled and ran on sodium-dodecyl-sulfate poly acrylamide electrophoresis gel (SDS-PAGE), using 12% SDS bistris gel (Invitrogen), to confirm the expression.

As a final point, the approximate protein concentration was measured at OD_{280nm} at their individual extinction coefficients' values using UV Nanodrop® spectrophotometer. **Figure 1.20** illustrates an SDS-PAGE results for one of the produced binders, a systematic follow-up for the presence of the VHH along with the entire processes.
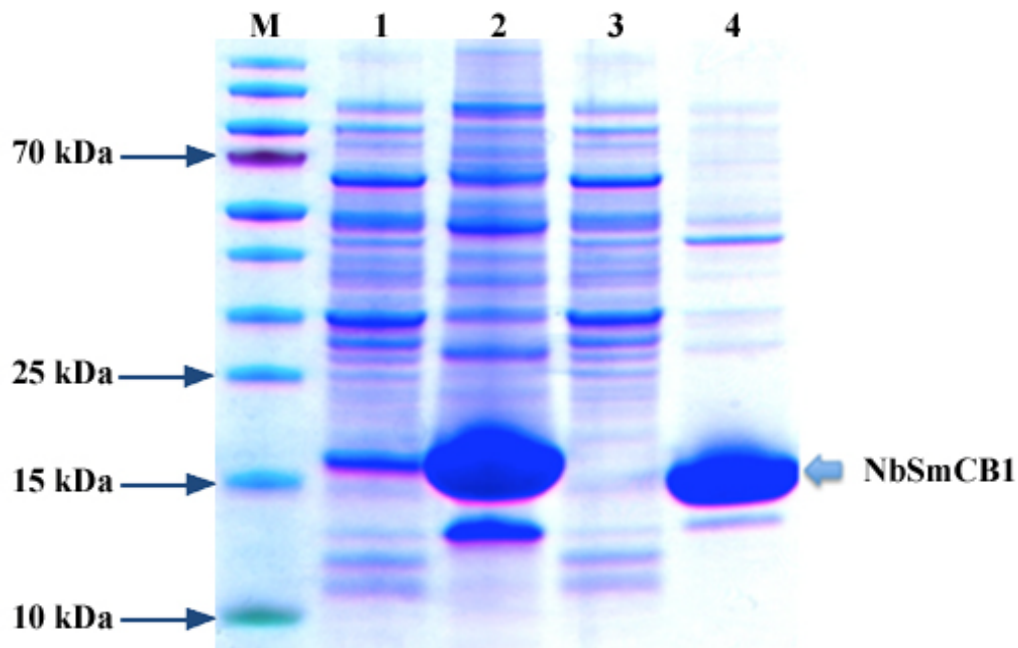
Figure 1.20. VHHs Presence and Purity Confirmation via 12% SDS-PAGE. *M. Page Ruler™ Prestained Protein Ladder (Fermentas).* *1. First flow-through of IMAC,* *2. Native PE extract,* *3. Second flow-through of IMAC,* and *4. IMAC purification of PE extract of one of the expressed Nanobodies®. All the Nanobodies® were displayed as a single band of approximately 15 kDa matching their theoretical molecular weight values.*

Information about the physical properties of the selected Nanobodies[®] is necessary for further experimental set-ups, they were obtained based on the amino-acid sequences of each VHH protein, including the peptide tags, using the ProtParam tool at the ExPASy proteomics server of the Swiss Institute of Bioinformatics.

Table 1.13. *Physical properties & final concentrations of SmCB and SmES specific Nanobodies[®]*

VHH Name	Number of amino acids (including HA & His$_6$ tag)	Molecular weight (Da)	Theoretical pI	Extinction coefficient	Yield (mg/L)
NbSmCB2	144	16004.7	7.17	2.835	8.47
NbSmCB9	141	15624.1	7.86	2.457	5.85
NbSmCB10	144	15734.2	8.56	2.090	8.91
NbSmCB11	141	15809.3	7.25	2.175	8.98
NbSmCB16	144	15843.2	6.64	2.170	2.01
NbSmCB26	133	14387.9	7.16	1.697	12.9
NbSmES4	137	15194.8	9.39	1.606	0.1
NbSmES5	146	16226.9	9.39	2.366	1.2

5   Conclusion

There are over 200 million people worldwide infected with Schistosomiasis, 120 million symptomatic patients and 600 million individuals live at risk, in addition, there are 280,000 of new cases every year mostly among the world's poorest populations where they lack the infrastructure and resources necessary to establish proper equipped laboratories for diagnosis and treatment. Given the high risk of complications, and for further extent, mortality due to Bilharzia, a rapid and accurate schistosoma diagnosis is critical for the appropriate treatment of affected individuals. In the study presented here, we wanted to establish a sensitive technique for detecting parasite specific antigen utilizing Nanobodies® to be used as molecular imaging diagnostic and a therapeutic agent for a novel immunotherapeutic approach.

Currently, there are more than 20 therapeutic mAb products on the healthcare market and more than 100 in clinical trials, it is logical that engineered antibodies have come of age as biopharmaceuticals candidates (Reichert, 2008). Despite various beneficial characteristics of the conventional antibodies, the low intrinsic toxicity of the Nanobodies® together with their size characteristics and their high specificity and affinity for the antigen render them more proficient tools for various approaches – e.g. anti-biomarkers, drug delivery, in addition, physo and chemotherapeutic agents.

In this study, we could successfully generate different Nanobodies® against two representative schistosoma antigens (i.e. *S. mansoni* Cathepsin B and Execratory Secretary antigens). Consequently, the obtained data suggests that these anti-schistosoma Nanobodies® can be properly designed for being used as a premier molecular research tool with the aim of unraveling the *in vivo* molecular mechanism of the host cell invasion. Moreover, wide range of novel Bio-Nano-Conjugate systems can be constructed with metallic, polymeric and magnetic nanoparticles for creating state-of-the-art healthcare theragnostic tools. For instance, rapid lateral flow assays, surface plasmonic resonance, colorimetric tests, magnetic concentrating technique, magnetic targeting and magneto hyperthermia applications.

CHAPTER 2: CONSTRUCTION OF ^{99m}TC LABELED-sdAb-GRAPHENE-COATED-NANOMAGNET BIOCONJUGATE – PROOF OF CONCEPT

## 1 Magnetism: BioNanosystems for Magnetic enforced-Active-Targeting

1.1 Nano-Magnetism from Ferro to Superparamagnets: The Prologue

The etiology of magnetism is an old science that withdrawn an immense attention and interest during the past centuries. The phenomenon exists in a material, commonly a metal, when the electrons of a typical atom rotate around it's nucleus in a certain radius – r and angular velocity – ω. The atomic number – Z determines the total number of electrons and the charge of each electron is given by a value of (e). In general, when a charged particle is in motion around a circular path it generates an electric current with a total amplitude value equals (μ_oIA), where (A) is the area enclosed of the circular motion of each electron, it equals (A = πr2), and (I) is the generated current's intensity, it equals (I = -eω/2π). The produced magnetic moment generated by the motion of the charged electron around the atomic circular path, which is typically an orbital motion, is given by:

$$M = -\frac{\mu_o e \omega r^2}{2}$$

When the outermost shell(s) of an atom are not completely filled they have permanent net magnetic moments. These moments are created from the summation and subtraction of the combination of the total spin and orbital motions of its electron(s). Generally, the actual magnetism of these numerous number of electrons has insignificant values, because of their intrinsic random path orientations inside the magnetic matter. Nevertheless, when exposed to external magnetic/electric fields, the magnetic dipole moments generated from the randomly moving electrons align themselves in a way that creates a net magnetic field in a certain direction matching the one of the externally applied field. A ferromagnetic material has a natural magnetic moment, which implies that the components of the electron moments and the orbital motion's moments are arranged parallel to each other. This spontaneous magnetisation is temperature dependant (i.e. it vanishes above Curie temperature). As the temperature increases, thermal motion, or entropy, competes with the ferromagnetic tendency for dipoles to align, and a ferromagnetic material becomes paramagnetic (i.e. the magnet will lose its magnetism) (Balakrishnan, 2011).

For instance, the Curie temperature of some common materials is: Iron (Fe) 770 $^{\circ}$C, Cobalt (Co) 1130 $^{\circ}$C, Nickel (Ni) 358 $^{\circ}$C and Iron Oxide (Fe_2O_3) 622°C (Buschow, 2001).
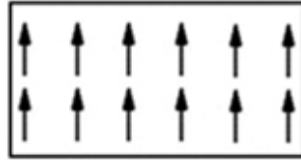
Moments of Individual Atoms Aligned

Figure 2.21. Illustration of Ferromagnetic Domains (Harris, 2002)

A typical ferromagnetic material reaches its magnetisation saturation when it is exposed to external magnetic field. **Figure 2.22** illustrates the classical hysteresis curve obtained throughout the magnetizing and demagnetizing process of a bulk unmagnetized ferromagnetic material. In the absence of any external magnetic field, the magnetic moments of the same orientation are intrinsically organized in regions called magnetic domains which are separated by virtual barriers know as "domain walls". Each of these domains has a permanent net magnetisation (*M*) in a certain direction. Although, the orientation of the domains in the bulk material is random it results in an innate net magnetisation value (**Figure 2.22a**), a more energetically favorable configuration. Upon exposure to a sufficiently large external magnetic field, the domains with magnetisation direction all along the magnetic field axis enlarge while the others get smaller in a phenomenon known as "domain wall displacement" (Gubin et al., 2005) (**Figure 2.22b**). The alignment continues until all moments are aligned in the direction corresponding to that of the external field (**Figure 2.22c**) at this configuration the material reaches its magnetisation saturation (*M*s). When the external field is removed the materials' magnetisation does not relax-back to the initial state. However, some energy is stored maintaining a net magnetisation known as "remanent magnetisation" (*M*r). An external magnetic field of a definite magnitude must be applied in the opposite direction in order to demagnetize the material and reduce its magnetisation back to zero that is known as coercivity field (*H*c). Continuing to expose the material to the opposite field, the same behavior is observed but in opposite manner. Hysteresis refers to the inability of retracing the magnetisation curve, since the material retains a memory of its magnetisation (*M*r) (Balakrishnan, 2011).
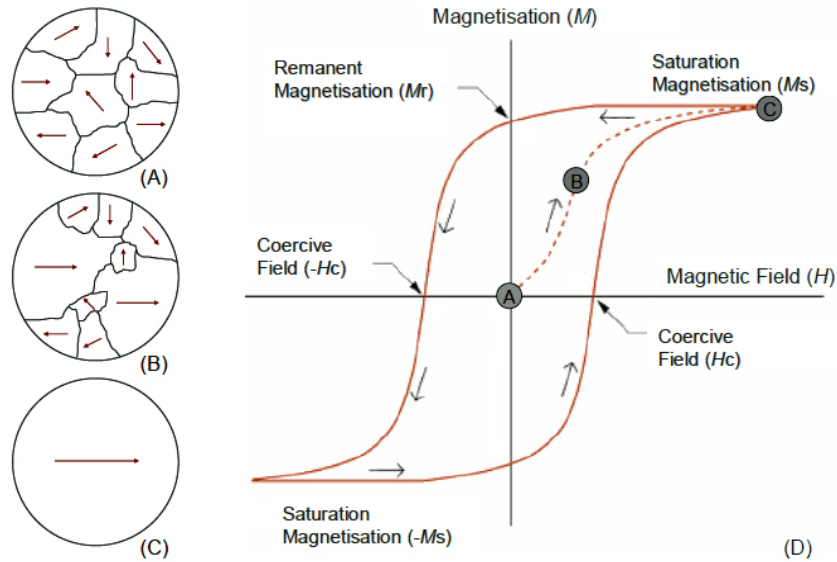
***Figure 2.22. Hypothetical Domain Configuration and Hysteresis Loop of an Unmagnetized Ferromagnetic Material** (Taylor, 2010)*

In nanoscaled magnetic particles, the above scenario diametrically opposed, at a certain nano-size limit particles become so small that they consist of a single domain, leading to the emergence of a distinctive phenomenon known as "Superparamagnetism", in which nanoparticles are found superior to ferromagnetic particles due to the absence of remanent magnetisation. These particles reveal magnetic properties only in the presence of an external magnetic field (Giri, 2003). In the case of single domain magnetic particles the difference between the minimum and maximum potential energy per unit volume of the particle's magnetic moment is significantly smaller than its thermal energy. Consequently, the orientations of these magnetic moments are in constant change due to the thermal agitation. Therefore, thermal energy becomes large enough to cause random fluctuation in the absence of any external fields (Taylor, 2010). Thus, nanosized particles seem to lack hysteresis loss, nevertheless, their coercivity value does not rest at zero, various theoretical calculations indicate that this happens for different particles in different size ranges, for instance, 15-30 nm for Fe, 70 nm for Co and 32-55 nm for Ni (Gubin et al., 2005).

Figure 2.23 illustrates the change in coercivity value as a function of particle diameter. Where: (Dcrt) is the particles' critical diameter and (Dsp) is the superparamagnetic diameter.
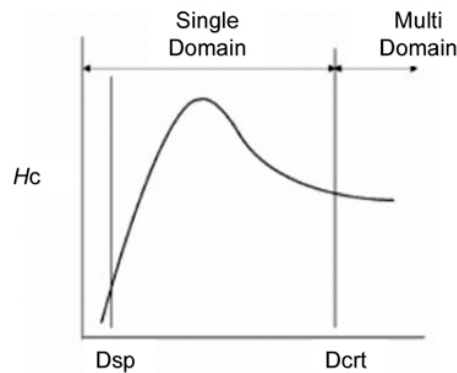
Figure 2.23. Coercivity as a Function of Particle Diameter (Ashby et al., 2009)

Figure 2.24 illustrates the magnetisation curve of superparamagnetic particles, in which, there is no hysteretic nature of the curve and a very small coercivity field magnitude exists (Taylor, 2010).
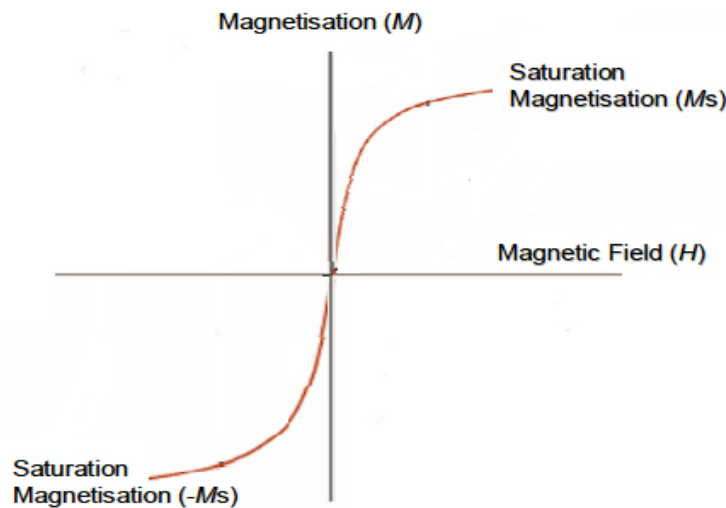
Figure 2.24. Hypothetical Magnetisation Curve of Common Superparamagnetic Nanoparticles (Taylor, 2010)

1.2 Carbon Nanostructures: Graphene-Encapsulated Nanomagnets

The implementation of the extraordinary properties of superparamagnetic nanoparticles is hindered by many factors that limit their applications. The chemical stability is one of the most

critical factors where they are used in complex fluid systems – e.g. biological fluids. In addition, dispersion concerns are also a crucial factor, in view of the fact that, most of the nanoparticles will tend to aggregate in order to minimize their surface free energy. Furthermore, nanoparticles are easily oxidized in presence of free oxygen, therefore, they might lose partially or entirely their significant magnetisation. As a result, numerous attempts have been devoted to furnish these nanomagnets with appropriate protection through encapsulation into an inert chemical compounds – e.g. consecutive graphene layers (Mahmood et al., 2009).

Various coating materials were successfully employed, for example, gold, silica, transition-metal oxides and carbon-encapsulations. The use of gold cannot be recognized as an economic-friendly approach. The covalent bonds on silica and other transition-metal oxides are prone to hydrolysis due to the instability of the silica shells under prolonged exposure to basic conditions. Finally, a carbon coating is considered as the most promising option. Graphene is recognized as one of the most stable materials on earth, in addition, it only requires a single nanometer of carbon encasing the produced nanomagnets (Grass et al., 2007).
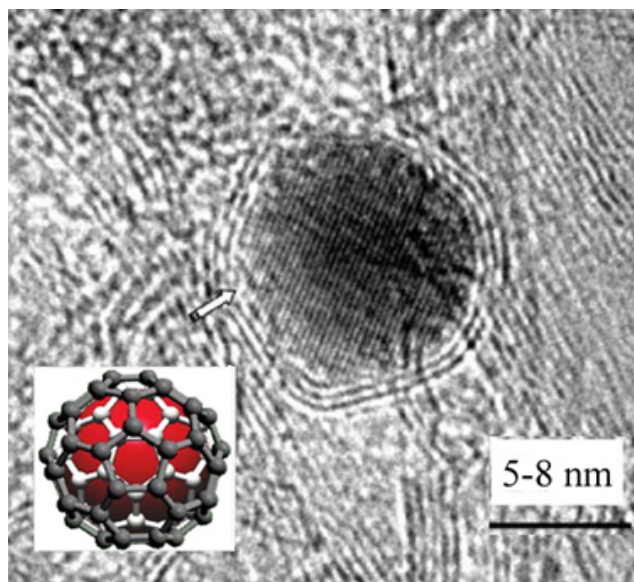
Figure 2.25. Graphene-Coated Nanomagnete. Carbon Encasing Magnetic nanoparticles with two to four layers of graphitic carbon, TEM image of the nanoparticles (Mahmood et al., 2009)

In addition to the protective function of coating to preserve the favorable properties of the magnetic core, graphene also offers a foundation for functionalizing the nanomagnets via attaching complex structures of a huge range of biomolecules. For instance, proteins, antibodies,

DNA and mRNA (Herrmann et al., 2009). The binding strength between the nanomagnet and the surface active molecules is so vital and it determines the overall performance. In actual fact, the carbon-carbon bond which constructs the backbone of almost all biological compounds is recognized as the strongest and most reliable chemical bond (Schätz et al., 2010).

1.3 The Superiority of Graphitic Nanomagnets

Conventional protection via thick polymer layers is available only in the micrometer-size, which is recognized as a sharp contrast to the final size obtained by coating with single nanometer layer of single or multiple graphene layer(s) (Herrmann et al., 2009).

The limited magnetisation strength of the traditionally used metal oxides – e.g. iron oxides, is comparatively much lower than that of pure metals. Whilst, encapsulating pure magnetic metal inside the graphene coating grants an undiluted magnetisation and exceptionally improves the strength and reactivity (Grass et al., 2007).

Graphene-coated nanomagnets have showed exceptionally high chemical stability under sever harsh conditions. Hermann and Stark at ETH Zurich investigated the thermal and chemical stability of the non-oxidic iron core-shell nanomagnets (i.e. iron carbide). About 80 wt % of the as-grown-carbon-coated iron carbide nanomagnets were successfully recovered after incubation for seven days in about 24 v% aqueous hydrochloric acid (i.e. pH<1). X-ray diffraction analysis confirmed that no phase transition occurred. Quite the opposite, naked magnetite readily dissolves within few seconds under similar strong acidic conditions (Herrmann et al., 2009).

Dispersion is considered as one of the main challenging obstacles in biomedical applications, a variety of chemical adaptations have been theoretically and practically studied to exploit the solubility and dispersion of carbon nanostructures and overcome their tendency of aggregation. Well-designed surface engineering not only improves the dispersion efficiency but also develops their biocompatibility and enhances their capability to demonstrate high permeability and retention – EPR, which additionally improves their cellular uptake. The most important approaches for these modifications are generally categorized into two major groups (a) Covalent addition of chemical groups via reactions onto the π- conjugated skeletal structure of the graphene-coat and (b) Non-covalent adsorption of the supra-molecular groups, e.g. bio-molecules, peptides and proteins (Tasis et al., 2006; Liang & Chen, 2010).

Recently, large numbers of *in vitro* and *in vivo* trials were performed in order to evaluate the potential cellular uptake of carbon-coated magnetic nanostructures and explore the relationships between their surface chemistry and biocompatibility. Professor Hwang and his group from Shandong University, in collaboration with St. Jude Children's Research Hospital, USA, established a state-of-the-art experimental design in which they synthesized polymer grafted carbon-coated metallic iron nanoparticles with various surface chemistry modifications and investigated their oxidative stress, dynamic cellular response, cellular uptake and their effects on triggering cell apoptosis. Fruitfully, most of the surface modified carbon-coated iron nanoparticles presented high cellular uptake and insignificant cytotoxic effects which is considered as a great promise for widespread biomedical applications (Mua et al., 2010).

1.4 Bioconjugation: Covalent and Non-Covalent Labeling

1.4.1 Covalent Labeling

Handling the as-produced carbon-coated nanostructures with a mixture of nitric acid and sulfuric acids was found effective to convert most of the terminal carbons, and the carbons at the defect site, into carboxylic groups (Wu et al., 2009). Subsequently, there are countless functional groups can be attached to these carboxylic ends and make possible of a wide range of bioactive compounds. The esterification of these carboxylic terminals may lead to high solubilization. However, these soluble oxidized structures still tend to aggregate in presence of salts because of charge-screening effects. Accordingly, they cannot be straightforwardly used for *in vivo* applications due to the expected high salt-content of most biological fluids, and also because further surface adjustments will be required. (Liu et al., 2009).

Fluorination of the side-walls of the graphene-coated nanostructures takes place via a simple addition reaction. Such approach is considered very useful because further groups still can be attached through substitution of fluorine with various groups. For instance, alkyles, diamines and diols. Such amino alkylated surface can undergo further sophisticated functionalization utilizing these free amino groups in order to bind to many biological molecules for specific bio-medical applications (Wu et al., 2009).

Cycloaddition is considered as one of the most widely used covalent addition reactions used to functionalize and efficiently disperse graphene-based nanostructures for biomedical applications. For instance, addition of azides takes place at the native aromatic side-walls of the

graphene outer-walls. Finally, addition of terminal amine-terminated poly ethylene glycols can be designed for biological applications (Liu et al., 2009).

1.4.2 Non-Covalent Labeling

Non-Covalent functionalization of carbon-coated nanostructures is usually accomplished by coating with surfactants and polymers of amphiphilic nature, given that the chemical structure of the π-network of the outermost graphene-layer is not affected. The characteristic poly-aromatic nature of the graphitic surface is easy to get-linked-to via numerous aromatic molecules by the aid of the π-π stacking. A notable study by Chen and Hongjie Dai at Stanford University showed that proteins can be firmly attached to the surface of hollow cylinders of rolled-graphene-sheet, i.e. single wall carbon nanotubes (SWNTs), functionalized by an amine-reactive pyrene derivative (Chen et al., 2001). Accordingly, aqueous solutions of the non-covalently bio-engineered molecules' show high potential for numerous biomedical applications particularly imaging, ultra high sensitive bio-sensing and therapeutics (Wu et al., 2009; Liu et al., 2009).

1.5 Diagnostic Applications: Thermoacoustic Imaging

A variety of computerized tomographic techniques have had a massive impact on biomedical diagnostics. Furthermore, numerous methods are being developed (e.g., the "common" X-ray, single-photon emission, positron emission, ultrasound, magnetic resonance…etc) (Natterer, 1986). The never-ending strive is to increase the resolution and contrast of the imaging techniques, and at the same time to reduce their cost and negative side-effects. Nonetheless, these objectives are usually contradictory. For example, some economical and significantly harmless techniques with high-resolution methods (e.g. ultrasound imaging) often do not provide good contrast in soft tissues, whereas, other techniques with good contrast (e.g. optical or electrical impedance tomography) suffer from low resolution. Recently, many researchers have been working on developing novel generations of hybrid techniques. Thermoacoustic tomography (TAT) is recognized as the most successful example of such hybridization approaches (Kruger et al., 2003).

In TAT, a short-duration electromagnetic EM pulse is propelled through a biological object (e.g. abdominal cavity, skull or a woman's breast). These EM waves will trigger the

generation of a thermoacoustic signal that can be detected via suitable transducers. **Figure 2.26** illustrates the production of the thermoacoustic signal.
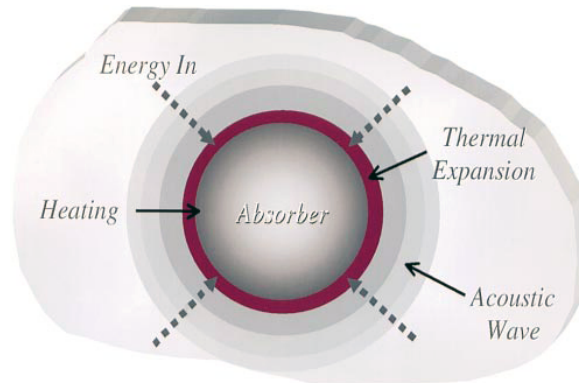
Figure 2.26. Thermoacoustic Signal Production. EM energy in is absorbed, producing heating, followed by sudden thermal expansion, which induces an outwardly propagating acoustic wave (Kruger et al., 2000)

However, as a diagnostic tool neither radiofrequency RF waves nor visual light alone would provide acceptable resolution: (a) in case of RF, this is due to the long wavelength, yet, shorter microwaves still can be used, although this will drastically affect their penetrability, (b) in case of the optical region, the problem is with the multiple scattering of light. The absorption of the EM energy results in thermo-elastic expansion, and thus, a pressure wave which is a function of time and space/distance is generated. Such ultrasound signal can be measured by transducers placed around the object in a three dimensional setup. Indeed, the measuring scheme that utilizes two types of waves combines the high resolution of the ultrasound with the high contrast of EM waves. The advantages of using microwave induced thermoacoustic imaging MITI are utterly based on the simple relation ($\lambda = c \, / \, f$). Where, frequency – f which is inversely proportional to the wavelength – λ – i.e. smaller wavelength results in better resolution, and the speed of light and sound in air are approximately 3 x 10^8 m/s and 330 m/s respectively. Therefore, MITI combines the privilege of both higher frequency and lower speed for better resolution, in addition, takes advantage of both pure ultrasound imaging and microwave imaging in order to obtain good spatial resolution and imaging contrast as well.

In seeking higher resolution and contrast for early, and yet accurate, detection of various diseases many attempts are ongoing for *in vivo* contrast enhancement. A notable study by Nie et al. showed fivefold great thermoacoustic signal enhancement and much longer retention time.

When tumor bearing mice was intravenously injected with superparamagnetic magnetite nanoparticles coated with polyaniline and conjugated to folic acid which serves as a cancer-biomarker-specific targeting ligand FA-Fe$_3$O$_4$/PANI (Nie et al., 2010). In conclusion, optimizing the design of the conjugate system – i.e. targeting ligand (e.g. sdAbs), magnetic material (e.g. Fe@C-MNP) and biocompatible coating (e.g. PEG and others) would have a tremendous impact on the quality of the diagnostic processes and subsequently on the efficacy of the therapeutic applications.

1.6 Therapeutic Applications: Magneto Hyperthermia

Magneto hyperthermia is a noninvasive technique that devastates diseases tissues, for instance, cancer cells, by transferring fatal dose of heat to the actively-targeted site of interest upon exposure to an oscillating external magnetic field while preserving surrounding vicinity of healthy tissues from any significant damage.

1.6.1 Physicochemical Principles of Magneto Hyperthermia

As previously explained, the hysteresis loop of macroscopic, bulk, ferromagnetic materials (*see* **Figure 2.22**) is primarily responsible for the heat generation when an external oscillating electromagnetic field is applied to a colloidal system of magnetic material. Upon exposure to a properly intense alternating field, the material will continuously get magnetized and demagnetized according to its hysteresis loop curve while each cycle leads to the release of energy in the form of heat**.**

In sharp disparity, upon application of an external oscillating magnetic field to superparamagnetic nanoparticles, which are intrinsically in constant rotation due to their very small thermal energy barrier, the heat generated results from two different relaxation mechanisms (i) Néel and (ii) Brownian relaxations. In case of Néel's, the produced heat is due to the occurrence of rapid alteration in the orientation of the magnetic moments correlated to its crystal lattice's arrangement – i.e. it is an internal dynamic process. The continuous change of the directions is hindered by the anisotropic energy barrier of the crystal lattice which will typically tend to direct the magnetic domains in the most energetically favorable orientation. Heat loss in the form of thermal relaxation arises as a result of overcoming these energy barriers (Kumar & Mohammad, 2011). In case of Brownian relaxation, the produced heat is due to the

physical rotation of the particles themselves in the surrounding medium – i.e. it is an external dynamic process, in which the rheological properties of the medium (i.e. viscosity and fluid dynamics) where the magnetic nanoparticles MNPs are placed will, to a great extent, affect the amount of the heat generated since the heat dissipation is mainly created by the frictional forces created during the physical rotation (Kumar & Mohammad, 2011). **Figure 2.27** illustrates the two different mechanism of relaxation. In case of the internal dynamic Néel relaxation mode the crystal lattice configuration of the nanoparticles rotate so as to align themselves according to the external field directions while overcoming the crystal lattice energy barrier. In case of the external dynamic Brownian relaxation mode, the entire particle will continuously tend to align itself in accordance to the external field which typically produce a localized friction forces with the surrounding media and subsequently produces heat (Mornet et al., 2004).

Néel Rotation

Brown Rotation
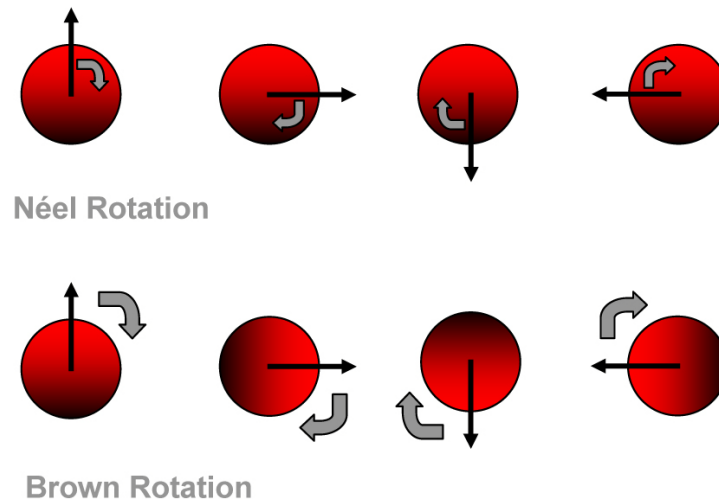
Figure 2.27. Néel and Brownian Relaxation Mechanisms (Mornet et al., 2004)

The specific absorption rate SAR of MNPs represents the slope of the time-dependent temperature curve. The SAR is a useful parameter to contrast the heating capability of different magnetic nanoparticles. In addition, it is used for evaluating their selection.

$$SAR = c\frac{dT}{dt}$$

Where: *c* corresponds to the heat capacity of the solution, T for temperature and t for time.

A new term which was only proposed in 2009, and is not yet well-known defined as intrinsic loss power ILP, the advantage of the new term that it lacks the extrinsic parameters –

i.e. frequency and field amplitude. Therefore, the inherent heating ability of the nanoparticles can be expressively compared. The ILP is more suitable for superparamagnetic nanoparticles and is also valid for frequencies up to 900 kHz, this range is commonly applied for most biomedical applications (Kallumadil et al., 2009; Kumar & Mohammad, 2011).

Multifunctional graphitic magnetic nanomaterials (e.g. cobalt and iron) have been synthesized by different methods. For instance, flame spray (Grass et al., 2007; Herrmann et al., 2009), microwave arch discharge (Hsin et al., 2008; Liang et al., 2008), chemical vapor condensation/deposition (Wang et al., 2003) and ultrahigh sonic power (Nikitenko et al., 2001). All synthesized particles were directly administered to their targets (e.g. cancerous HeLa cell cultures) and lacked the targeting moieties which in general hindered the impracticability of such nanostructures and severely reduced their ability of reaching certain diseased spots where direct injection would not be possible. After a proper incubation time, usually 24 hours, it was found that according to their size ranges, the carbon-coated nanomagnets were up-taken inside various sub-compartments of the target cells. Electromagnetic radiation of radiofrequency ranges 100-1000 kHz typically applied to cell cultures due to their high penetrability (Young et al., 1980) and high bio-tolerance (Nikiforov, 2007). In most of the cases, it was found that the graphitic materials are strong absorbers of the exposed radiation, such absorbance was reflected in an elevated localized heating inside the diseased cells. In addition, the nanoparticles were found to induce localized damage of the cellular DNA and various membranes integrity, which was reflected in the stimulation of cellular apoptosis (Mahmood et al., 2009; Xu et al., 2010). Even so, various MNPs are FDA approved while others are still in the process of getting approved.

Table 2.14. *Commercially Available MNPs Currently FDA Approved (Cole et al., 2011)*

Pre-Clinical Agent	Commercial Name	Target	Status
AMI-25	Ferumoxide, Feridex, Endoderm	Liver	Approved
OMP	Abdoscan	Bowel	Approved
AMI-227	Combidex, Sinerem, Ferumoxtran	Lymph Node	Phase III
CODE 7228	Feraheme, Ferumoxytol	Vasculature	Phase II

1.7 Nano-Magnetism from Ferro to Superparamagnets: The Epilogue

Momentous development has been made with respect to magnetic nanostructures platforms for a huge range of magneto hyperthermia applications, particularly for cancer treatment. However, there are still gaps in the awareness and technical capacity which avert such progresses from being transferred from the lab-bench-tops to the bed-sides in clinic. In addition, limitations exist for targeting effectiveness, predominantly with respect to active/magnetic targeting. Furthermore, there has been recently more focus on understanding the biocompatibility and cellular cytotoxic concerns for the implementation of nanotechnology in biomedical theranostics fields. The majority of the currently ongoing studies still limited to be conducted only for *in vitro* diagnostic applications, whereas, meticulous testing still need to be conducted for *in vivo* diagnostic and therapeutic applications as well.

2 Construction and Radioactive Labeling of sdAbs-Fe@C-MNPs Conjugate

Thanks to the particular properties of single domain antibodies, they have high potential for immuno imaging. A technique has recently been developed at the *In vivo* Cellular and Molecular Imaging (ICMI) Laboratory of the Nuclear Medicine Department, UZ Brussels, to generate highly specific radiotracers based on sdAbs (Vaneycken et al., 2011). The technique takes advantage of the His-tag that these recombinant molecules contain to form a coordination bond with Tri-carbonyl Metastable Technetium $[^{99m}Tc(CO)_3(H_2O)_3]^+$ which is used for obtaining high definition images with the aid of single-photon emission computed tomography SPECT (Xavier et al., 2012).

Another interesting technique in imaging is active/magnetic directing of magnetized tracers to a specific site of interest within the body – i.e. organ or sub-organ's location of interest, using an external focalized magnetic field. In view of a better trespassing, and penetrability, of these markers through physical boarders, the main aim was to bring this technique to the nano-scale. Therefore, a method to conjugate sdAbs to nanosized magnetic graphene-coated particles has been developed at Faculty of Science and Bio-engineering, Vrije Universiteit Brussel (VUB) in collaboration with School of Science and Engineering (SSE), The American University in Cairo (AUC). For this purpose, carbon-coated metallic Iron nano magnetic beads of an average diameter 50 nm and exhibiting terminal carboxyl functional groups are conjugated to sdAbs. The

hereby applied coupling is based on the formation of peptide bonds using water-soluble 1-Ethyl-3-(3-Dimethylaminopropyl)Carbodiimide (ECD) and N-Hydroxysuccinimide (NHS).

2.1 Applied Chemistry

2.1.1 General Principle

The Fe@C-MNPs conjugation reaction is based on the formation of peptide bonds by condensation reaction of terminal carboxyl groups formed on the surface of the MNPs with the amino groups, particularly from lysine, of the sdAb. On the other hand, the chelating of $[^{99m}Tc(CO)_3(H_2O)_3]^+$ is specifically directed to the $(His)_6$ tag of the sdAbs to form a strong coordination bond. In both reactions, amine groups are involved, where the differentiation between histidine and non-histidine coupling is achieved by conducting two consecutive reactions at different pH values. Indeed, the residue of histidine is an imidazole containing molecule in which the double bound nitrogen atom in the aromatic ring is protonated at $pH \leq 6$. As a consequence, there would be no nucleophilic attack on the carbon of a carboxyl group at pH lower than 6. **Figure 2.28** illustrates all the protonation states of the histidine residues at different pH values.
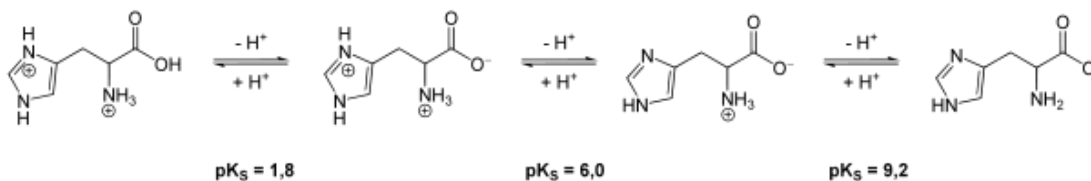
Figure 2.28. Protonation States of Histidine at Different pH Values (Li & Hong, 2011)

In sharp contrast, the amino groups of lysine residues are still unprotonated at pH6, and peptide bonds between terminal functional carboxyl groups of the Fe@C-MNP and the lysine amino groups of a protein can be formed. The coupling system generated between the water-soluble carbodiimide (EDC) / N-hydroxysuccinimide (NHS) has its optimum at (pH 5.5). The hereby presented procedure consists of (a) first performing the condensation reaction at (pH 5.5) with the EDC/NHS system, directed to non-histidine residues (i.e. Lys) amines, then (b) followed by the His-directed radioactive labeling of the sdAb-Fe@C-MNPs complex with$[^{99m}Tc(CO)_3(H_2O)_3]^+$ at relatively higher pH value (i.e. pH 7.4) and temperature 50°C.

Noteworthy, both of the sdAbs as well as carboxylated magnetic beads remain highly stable under in these harsh conditions.

2.1.2 Preparation of His$_6$-Tag Anti-GFP and Ni-NTA Magnetic-Beads Conjugate

The binding affinity of the conjugated sdAb was examined through performing a simple, and straightforward, conjugation between the (His)$_6$-taged sdAb (e.g. anti-GFP sdAb) and the nickel-nitrilotriacetic acid Ni-NTA functionalized magnetic beads from QuickPick™ IMAC. The remaining GFP content is typically estimated through measuring the fluorescence peak which exists at a wave length of about 488 nm. The conjugation conditions of the preliminary test are now used as a basis for this protocol, but should be further optimized.

2.1.3 The Non-His Conjugation of sdAb to Fe@C-MNPs

The non-His conjugation between the antibodies and the graphene-coated magnetic nanoparticles is performed with a classical condensation reaction using carbodiimide as intermediate, whereby the carboxyl groups of the magnetic beads react with the primary amine groups (i.e. terminal or intermediate groups) of the sdAb in order to form a peptide bond.
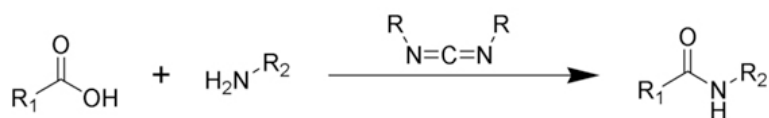
Figure 2.29.General Reaction of the Formation of a Peptide Bond. *Starting from a carboxyl group and a primary amine group, using a carbodiimide, which is taking part in the reaction but does not appear in the final product (Li & Hong, 2011)*

Figure 2.30 illustrates the reaction mechanism involves the presence of carboxylic group from the first molecule and the EDC crosslinker in order to form the first unstable intermediate (o-Acylisourea) which in the presence of N-hydroxysuccinimide (NHS) is transformed into the corresponding urea and a more stable carboxy-succinimide ester. The latter reacts spontaneously with primary amines from another molecule 2 to form the peptide bond.
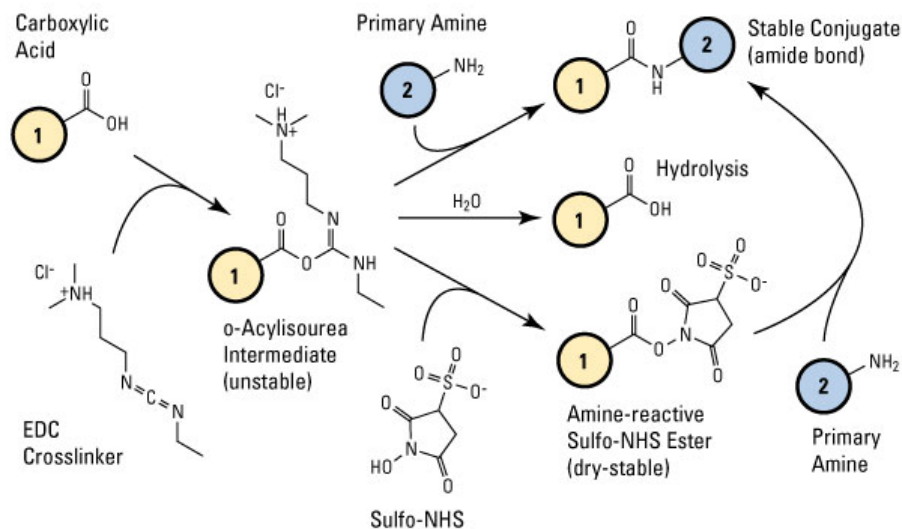
Figure 2.30. Carboxyl-to-Amine Crosslinking Using the Carbodiimide EDC and Sulfo-NHS.
The formed carboxy-succinimide ester reacts spontaneously with primary amines, leading to the
aimed peptide bonds (Pierce, 2012)

The hereby described procedure activates the carboxyl groups of the magnetic beads with the water soluble EDC and NHS. This system has an optimum performance at (pH 5.5), a condition where histidine molecules do not react.

2.1.4 The His-Tag Specific Labeling of sdAb with [99m]Tc

His-tagged sdAbs are particularly suited for ^{99m}Tc-labeling via tricarbonyl chemistry. Indeed, histidines have proven to coordinate efficiently to the tricarbonyl core of ^{99m}Tc-tricarbonyl (Garayoa, 2002; Xavier et al., 2012)
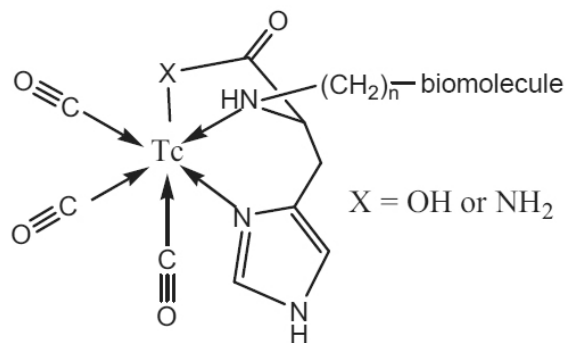
Figure 2.31. Technetium Labelling of a Biomolecule Through the Tc-tricarbonyl Synthon
(Garayoa, 2002)

Crystallography studies have also proofed that the His-tag on sdAbs is located on the opposite side of the paratope (Vincke et al., 2009). Hence, it minimizes the risk of interference with antigen-binding capability. Finally, the high thermal and chemical stabilities have been recognized as essential criteria for efficient complexation of the ^{99m}Tc-tricarbonyl to His-tagged antibody fragments (Broisat et al., 2012), and these high stability properties are a typical feature of SdAb (Dumoulin et al., 2002).

The complete labeling procedure has been described by Catarina Xavier et al., and starts with the generation and purity assessment of the ^{99m}Tc-tricarbonyl precursor. Afterward, it is followed by a set of straightforward procedures for the sake of complexing the precursor with the His-tagged sdAbs. Finally, various ways are applied to evaluate the radiochemical purity of the obtained sdAb-Fe@C-MNP derived radiotracer conjugate (Xavier et al., 2012).

3 Materials and Methods

3.1 Materials

3.1.1 Reagents and Buffers

Table 2.15. Reagents and Buffers used in this research

Reagents and Buffers	Composition	Supplier
Carboxylated Magnetic Beads	25-50 nm Fe@C-MNP concentration 30 mg/mL suspended in 5 mL H_2O 5×10^{13} Particles/mL 8.7×10^{17} mmol (-COOH)[3]/ Particle	TurboBeads®
QuickPick™ IMAC	metal affinity kit for proteins	Bionobile
IMAC Magnetic Particles	IMAC magnetic particles in PBS buffer adjust pH 7.0, 1M NaCl, 0.05 % Tween-20, 0.02 % NaN_3	Bionobile
IMAC Regeneration Buffer	Aqueous $NiSO_4$ solution, 0.05 % Tween-20, 0.02 % NaN_3	Bionobile

---

[3] The beads are functionalized with 2-Phenylethylamine and 3-Phenylpropanoic acid groups respectively

Reagents and Buffers	Composition	Supplier
IMAC Imidazole Buffer, 500 mM	500 mM imidazole in PBS buffer adjust (pH 7.0), 0.02 % NaN_3	Bionobile
IMAC^{2x} Wash Stock Buffer	PBS buffer (pH 7.0), 1 M NaCl, 0.05 % Tween-20, 0.04 % NaN_3	Bionobile
IMAC Wash Buffer 1	1700 µL IMAC^{2x} wash buffer 1700 µL H_2O	Bionobile
IMAC Wash Buffer 2	1700 µL IMAC^{2x} wash buffer 135 µL Imidazole buffer 500 mM	Bionobile
IMAC Wash Buffer 3	1700 µL IMAC^{2x} wash buffer 270 µL Imidazole buffer 500 mM 680 µL 5 M NaCl 750 µL H_2O	Bionobile
IMAC Elution Buffer	20 mM Tris-HCl (pH 8.0), 250 mM NaCl, 300 mM imidazole, 0.05 % Tween-20, 0.02 % NaN_3	Bionobile
MES Buffer (2-(4-Morpholino) ethanesulfonic acid	1.06 g MES dissolve in 90 mL H_2O adjust pH to 5.5 adjust final volume to 100 mL	Sigma-Aldrich
PBS/Tween Buffer	PBS buffer adjust pH to 7.4 0.05 % Tween-20	Sigma-Aldrich
EDC Solution	10 mg/mL EDC in MES buffer	Sigma-Aldrich
NHS Solution	10 mg/mL NHS in MES buffer	Sigma-Aldrich
Lyophilized kit IsoLink^{TM}	4.5 mg of sodium boranocarbonate 2.85 mg of sodium tetraborate.$10H_2O$ 8.5 mg of sodium tartrate.$2H_2O$ 7.15 mg of sodium carbonate, pH 10.5	Covidien
Hydrochloric Acid	1 M HCl in H_2O	Sigma-Aldrich
His-tagged anti-VCAM sdAb	1 mg/mL sdAb in PBS buffer	CMIM, VUB

Reagents and Buffers	Composition	Supplier
His-tagged anti-HER2 sdAb	1 mg/mL sdAb in PBS buffer	CMIM, VUB
His-tagged anti-GFP sdAb	1 mg/mL sdAb in PBS buffer	CMIM, VUB
eGFP protein	1 mg/mL eGFP in PBS buffer	CMIM, VUB
Instant Thin Layer Chromatography ITLC Eluent	acetone	Sigma-Aldrich

3.1.2 Equipments and Consumables

***Table 2.16.** Equipments and Consumables used in this research*

Equipment/Consumable	Supplier
$^{99}Mo/^{99m}Tc$ Generator	Drytec, GE Healthcare
Ventilated hood with leaded-shield	GE Healthcare
PickPen® Magnet	Bionobile
PickPen® tips	Bionobile
Vivaspin® HY 5000	VIVAPRODUCTS
Water bath	Eppendorf
Polycarbonate microtubes	Sigma-Aldrich
Silica gel impregnated glass fiber sheets	Pall Corporation, Life Sciences
Gamma counter	Drytec, GE Healthcare
Ultrasonic homogenizer	Hielscher

3.2 Methods

3.2.1 Preparation of His$_6$-Tag Anti-GFP sdAb and Ni-NTA Magnetic-Beads Conjugate

The main motive behind performing this experiment was to confirm (a) the preservation of the binding affinity of the conjugated sdAb and (b) the absence of any shielding or masking effect on its active paratopes. In order to optimize the ratio between anti-GFP and Ni-NTA magnetic beads (i.e. QuickPick™ IMAC) during conjugation, different concentrations of anti-GFP for a constant amount of magnetic beads were tested.

Procedure

1. In order to avoid any unspecific binding of the His-tagged eGFP protein, the protein sample was washed with IMAC wash buffer 1.

2. Tubes were numbered and filled up with sample/solutions as follows:

- Tube 1: 100 µL IMAC Magnetic Particles
- Tube 2: 400 µL IMAC Regeneration Buffer
- Tube 3: 400 µL IMAC Wash Buffer 1
- Tube 4: 300 µL eGFP Protein Sample
- Tube 5: 400 µL IMAC Wash Buffer 2
- Tube 6: 400 µL IMAC Wash Buffer 3
- Tube 7: 50 µL IMAC Elution Buffer

Caution: Mix the IMAC magnetic particles suspension thoroughly before pipetting into microtubes, in addition, higher yields can be obtained by optimizing the incubation time.

3. The PickPen® was dressed up with its tip and immersed in tube 1 to collect all the magnetic beads, then, released into tube 2 with gentle mixing.

4. The magnetic beads was collected from tube 2 and released into tube 3 and gently mixed using the PickPen® tip.

5. The magnetic beads were collected from tube 3 and transferred to tube 4 where they were incubated for 15 min. The solution was mixed occasionally to avoid sedimentation.

6. After incubation, the beads were collected and washed in tube 5 by gentle mixing for at least 10 sec, followed by further washing in tube 6 for at least 10 sec.

7. Finally, the washed beads were collected and transferred to tube 7 (containing the elution buffer), mixed thoroughly and incubated for at least 2 min. The solution was mixed occasionally to avoid sedimentation.

8. After incubation, the magnetic beads were collected and discarded and the purified His-tagged protein was transferred into new microtube.

9. The fluorescent peak of the remaining solution from tube 7 was measured at OD_{448nm} using Nanodrop® spectrophotometer.

3.2.2   Preparation of sdAb and Carboxylated Fe@C-MNPs Conjugate via EDC/NHS

Based on the above optimization test, a ratio of approximately 10/1 weight/weight is considered between the Fe@C-MNPs magnetic beads and the sdAb. That is to say, 50 µL magnetic beads

suspension (about 1.5 mg magnetic beads) should couple to 50 µg of sdAb (i.e. 50 µL anti-eGFP, anti-VCAM and anti-HER2 sdAbs).

Procedure

1. The carboxylated Fe@C-MNPs magnetic beads was homogenously dispersed using a sonicator with 10 x 5 sec pulses, with interval times of about 10 sec.

2. After sonication, the beads were brought up to room temperature, then 50 µL of the beads suspension was transferred into a new 2 mL polycarbonate microtube containing 200 µL MES buffer for washing via gentle mixing using the PickPen® tip.

3. The beads were collected and washed again after being transferred into another microtube containing 200 µL of MES buffer. Finally, the beaded were collected and transferred into a microtube containing 50 µL of MES buffer.

4. An equal volume of EDC solution was added – i.e. 50 µL EDC. Then immediately followed by addition of another 50 µL NHS solution. Finally, the mixture was incubated at room temperature for 20 min with continuous gentle agitation.

5. The as-produced sdAbs (i.e. sdAb in PBS buffer) were prone to change their buffer into MES buffer via several centrifugation cycles using Vivaspin® HY 5000 tubes, then concentrated up to a final concentration of about 1.0 mg/mL.

6. After incubation, the activated magnetic beads were collected and transferred into the microtubes containing 50 µL of each sdAb. The mixture was incubated with continuous shaking for about 30 min.

7. After incubation, the conjugated beads were collected and washed 3 times in 3 consecutive microtubes containing 200 µL PBS/Tween. Finally, beads were collected and redispersed via vortex in 100 µL PBS/Tween.

8. In order to confirm the preservation of the binding affinity of the sdAb conjugated to the carboxylated magnetic beads via EDC/NHS method. All the conjugated anti-GFP-Fe@C-MNPs were collected and transferred into new microtube containing eGFP protein sample of the same concentration (i.e. Tube 4) as described earlier.

9. The fluorescent peak of the remaining solution from tube 7 was measured at OD_{448nm} using Nanodrop® spectrophotometer.

3.2.3 Radioactive Labeling of sdAb-Fe@C-MNP Conjugate

Utilizing the well established technique of radioactive labeling of the single domain antibodies (Xavier et al., 2012) paved the road for the subsequent labeling of the entire conjugate – i.e. single domain antibodies and the graphene-coated magnetic nanoparticles. Such radio-labeled bio-nanostructure would present a very informative tool for a wide range of applications, for instance: (a) confirming and optimizing the EDC/NHS bioconjugation and (b) enabling the characterization and imaging of the actively targeted magnetic nanoparticles which will possibility impact both *in vitro* and *in vivo* theranostic applications under the gamma camera and MRI machines respectively. The purpose of this section is to show in step-by-step manner the easy way of preparing the radioactive precursors followed by the radioactive labeling with ^{99m}Tc-Tricarbonyl, and then afterwards, instant thin layer chromatography analysis for assessment of radiochemical purity of labeled conjugate and finally the characterization of the capability of magnetic targeting under gamma camera will be addressed as well.

A. Preparation of ^{99m}Tc-Tricarbonyl Precursor

Procedure

1. Exactly 1 mL of the ^{99m}TcO$_4^-$ solution which was previously prepared by the ^{99}Mo/^{99m}Tc generator, with radioactivity of about 0.74 – 3.7 GBq was added to the IsoLink™ kit.

2. The mixture was incubated at 100 °C for about 20 min.

3. After incubation, the reaction mixture was cooled down in water bath and brought to room temperature.

4. Finally, the pH of the reaction mixture was adjusted to 7.4 using 1 M HCl.

B. Radioactive labeling of sdAb-Fe@C-MNP Conjugate with ^{99m}Tc-Tricarbonyl

Procedure

1. Approximately, 50 µL of the sdAbs and free Fe@C-MNPs were added to about 450 µL of *fac*-[^{99m}Tc(CO)$_3$(H$_2$O)$_3$]$^+$ at a pH 7.4.

2. About 250 µL of the sdAb-Fe@C-MNP conjugate in PBS was added to about 250 µL of *fac*-[^{99m}Tc(CO)$_3$(H$_2$O)$_3$]$^+$ at a pH 7.4.

3. The reaction mixtures were incubated at 50 °C for about 60 - 90 min.

Caution: The temperature of incubation depends on the thermostability of the sdAb, it is always recommended to determine, in advance, the melting temperature (Tm) of sdAb to be labeled.

4. The labeled conjugate was separated from the free ^{99m}Tc-Tricarbonyl and ^{99m}TcO$_4^-$ via PickPen® or conventional magnet bar.

C. *ITLC analysis for Assessment of Radiochemical Purity*

Procedure

1. About 2 μL of the ^{99m}Tc-Tricarbonyl labeled conjugate solution was added onto a 15mm x 200 mm silica gel impregnated glass fiber sheet.

2. The ITLC chromatogram was developed in acetone.

3. The distribution of radioactivity was analyzed by scanning with a γ-radiation TLC scanner or counting the strip cut in 3 parts (i.e. application point, middle, solvent front) in a dose calibrator or gamma counter. Knowing that, the ^{99m}Tc-Tricarbonyl precursor and the ^{99m}TcO$_4^-$ reveal a retention factor value (Rf) of 1, whereas, the ^{99m}Tc-Tricarbonyl-Conjugate has an Rf of about Zero.

3.2.4 Magnetic Targeting of the Radio Labeled sdAb-Fe@C-MNP Conjugate

The application of an external magnetic field by using a commercial standard magnet bar (i.e. ≤ 0.55 Tesla) was performed under a gamma camera for two main reasons:

- Confirming the attachment of the radiolabeled sdAb to the graphene-coated magnetic nanoparticles.
- Proofing the concept of magnetic targeting function for the entire conjugate when it is placed in a phosphate buffered saline at the natural physiological criteria.

Procedure

1. The radiolabeled conjugate was transferred to a PBS/Tween (pH 7.4) filled 100mm dia. x 15mm H round Petri dishes and 50 mL Falcon tubes.

Caution: All the radiolabeled solutions must be handled with great care to avoid radioactive contamination.

2. Place the Petri dishes and the Falcon tubes under a gamma camera for capturing images at static conditions for at least 4 min.

3. An external positioned magnet (i.e. < 0.55 Tesla) was placed while running the gamma camera and continued capturing images.

4. The magnet was removed and the gamma camera continued capturing image after removal for at least 1 min.

4   Results and Discussion

4.1   His$_6$-Tag Anti-GFP sdAb and Ni-NTA Magnetic-Beads Conjugate

After conjugating the His$_6$-tagged anti-GFP to the Ni-NTA magnetic beads from QuickPick™ IMAC the concentration of the eGFP protein content was measured using Nanodrop spectrophotometer at OD$_{280nm}$ and OD$_{488nm}$.

Table 2.17 illustrates the initial and final concentrations and absorbance values of the eGFP proteins after purification using NI-NTA magnetic beads.

Table 2.17. Concentration of eGFP Proteins before and after Magnetic Purification

Protein	Initial Conc. (mg/mL)	Initial Absorb. (a.u.) [4]	Final Conc. (mg/mL)	Final Absorb. (a.u.)
eGFP – 25 µL	0.21	0.449	0.00	-0.206
eGFP – 50 µL	0.47	0.945	0.14	0.291
eGFP – 100 µL	0.95	1.798	0.29	0.621

In addition, the fluorescent finger print of the eGFP protein was reduced in equivalence to the above results. Finally, the optimum obtained results came from using a 50 µg of sdAb per 1.5 mg (i.e. 50 µL) of magnetic beads.

4.2   Preparation of Anti-GFP sdAb and Fe@C-MNPs Conjugate via EDC/NHS

The optimized set-up from the previous experiment was used to evaluate the conjugation's efficiency of the anti-GFP sdAb conjugated to 25-50 nm Fe@C-MNPs via EDC/NHS method. **Table 2.18** represents the initial and final concentration of the eGFP protein after magnetic purification using the PickPen® magnet.

---

[4] Absorbance Units

Table 2.18. *Concentration of eGFP Proteins before & after Fe@C-MNPs Magnetic Purification*

Protein	Initial Conc. (mg/mL)	Initial Absorb. (a.u.)	Final Conc. (mg/mL)	Final Absorb. (a.u.)
eGFP – 50 µL	0.44	0.913	0.12	0.314

In the same way, the fluorescent finger print of the eGFP protein at OD_{448nm} was reduced in equivalence to the obtained results. Certainly, both of the Ni-NTA magnetic beads as well as the Fe@C-MNP were able to get conjugated to the anti-GFP sdAb with equal efficiency. In addition, with the aid of an external magnet they could, powerfully, collect their specific target antigen (i.e. the eGFP protein) from the PBS buffer. In conclusion, the EDC/NHS conjugation did not affect the antigen binding capacity of the sdAbs and preserved their immunogenicity.

4.3 Radioactive Labeling of sdAb-Fe@C-MNP Conjugate

After the radioactive precursor was prepared it was incubated with the reagents as follows:

- 50 µL Free Fe@C-MNP + 450 µL $[^{99m}Tc(CO)_3]^{7+}$
- 50 µL Anti-HER2 sdAb + 450 µL $[^{99m}Tc(CO)_3]^{7+}$
- 50 µL Anti-VCAM sdAb + 450 µL $[^{99m}Tc(CO)_3]^{7+}$
- 250 µL Anti-VCAM sdAb-Fe@C-MNP Conjugate + 250 µL $[^{99m}Tc(CO)_3]^{7+}$
- 250 µL Anti-HER2 sdAb-Fe@C-MNP Conjugate + 250 µL $[^{99m}Tc(CO)_3]^{7+}$

Table 2.19 illustrates the initial and final activities of the free graphene-coated magnetic nanoparticles, as well as, those of the different prepared conjugates in accordance to their incubation times.

Table 2.19. *Radioactivity of the Radiolabeled Reagents and Conjugates*

Reagent/Conjugate	Initial Activity (µCi)[5]	Final Activity (µCi)	Incubation Time	Labeling (%)
Free Fe@C-MNP	2.99	0.34	2 hr 03 min	11.4
α-VCAM Conjugate	2.83	0.685	2 hr 29 min	20
α-HER2 Conjugate	2.75	0.89	2 hr 56 min	25
Free α-HER2 sdAb	4.68	3.84	1 hr 46 min	> 99
Free α-VCAM sdAb	5.05	4.1	1 hr 47 min	≈ 93

The naked graphene-coated magnetic beads showed 11.4% labeling capacity which might be considered as non-specific binding to the particles, however, the radioactivity of the magnetic particles will be added to the whole conjugate and will serve for the benefit of the tracing/imaging experiments.

4.4   Magnetic Targeting of the Radio Labeled sdAb-Fe@C-MNP Conjugate

After transferring the radiolabeled content of the conjugated sdAb to Petri dishes and Falcon tubes filled with PBS/Tween, they were placed under dynamic gamma camera (i.e. 1 frame/s) for characterization and visualizing the effect of placing an externally position, commercially standard, magnet bar of an intensity < 0.55 Tesla. **Figure 2.32A** represents the qualitative analysis of the initial static condition of the fully dispersed radiolabeled sdAb conjugates (i.e. α-VCAM- and α-HER2-Fe@C-MNP conjugates), while **Figure 2.32B** represents the focalization effect of placing an external magnet bar. The increase in intensity is mainly concluded by the attraction of the dispersed magnetic particles to the externally positioned magnet, which confirm the binding between the radiolabeled single domain antibody and the graphene-coated metallic Iron magnetic nanoparticles.

---

[5] 1 microcurie (µCi) = 37 kilobecquerel (kBq)
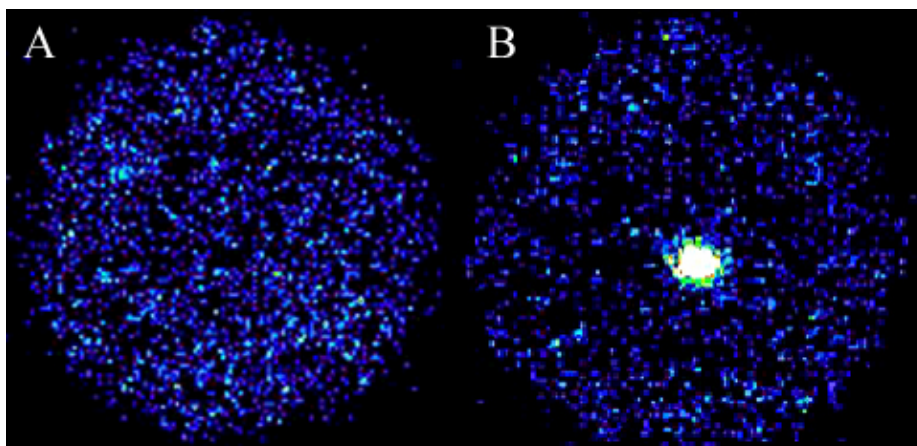
Figure 2.32. Qualitative Analysis of Magnet Focalization of the Radiolabeled Conjugate. A. Represents the initial static condition, while, B. Represents the focalization effected obtained after application of the external magnet.

Figure 2.33 illustrates the quantitative analysis of the focalization effect in the Petri dish, in the beginning, the magnet was placed after one minute of capturing time, a fast focalization took place (i.e. from ≈ 2.5% to 20%), then followed by slow increase over extra four minutes in the radioactivity till it reached about 32% of the total radioactivity sensed in the entire containing medium.
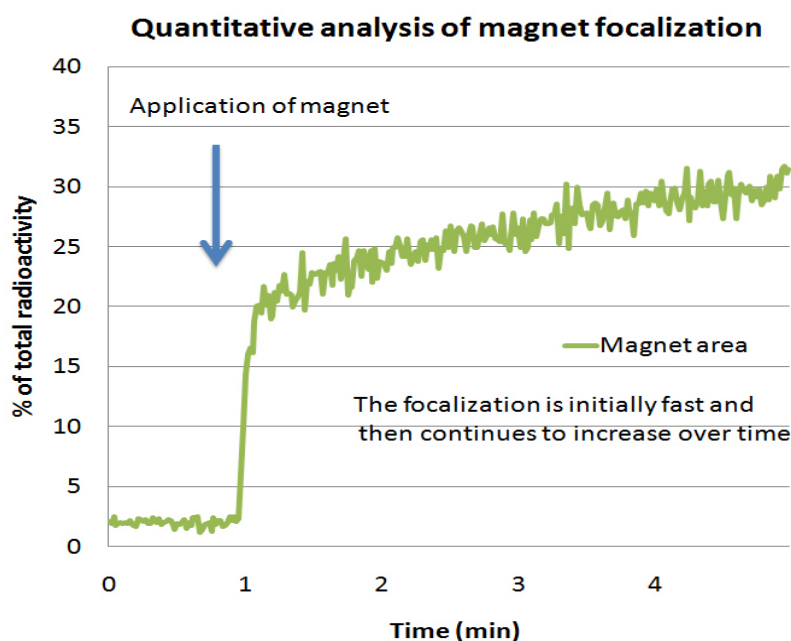
Figure 2.33. Quantitative Analysis of Magnet Focalization of the Radiolabeled Conjugate

5 Conclusion

The properties of the single domain antibodies were combined with the vast growing nanotechnology. In general, any diagnostic and/or therapeutic application will require certain predefine multifunctional criteria, above and beyond is the presence of a smart targeting moiety which is able to deliver the attached loads to its corresponding site with minimal/insignificant non specific targeting. In the current study, sdAbs were selected to represent the specific targeting agent and the nanomagnetism was selected to express the superiority of nanotechnology in constructing such a system of high biocompatibility and easy-tailored physiochemical properties which can be predesigned to serve for diagnostic as well as therapeutic applications.

The distinctive inherent ferro and superparamagnetic properties combined with the superior chemical, thermal and biological stabilities of the multilayered graphene-coating have a wide range of novel and efficient tools for highly multipurpose applications – i.e. diagnostic and therapeutic fields. Worth mentioning, their brilliant properties enable them to effectively impact other different fields as well – i.e. environmental, agricultural, chemical and industrial. The implementation of the currently available simple and mass-scalable synthetic methods would provide high control over size and shape which will supply economic and eco-friendly candidates for future research works. Finally, the development of novel functionalization protocols together with new-fangled smart targeting ligands – e.g. sdAbs, will sincerely lead to the generation of a new epoch of scientific researches which will pave the road for a new era of noninvasive and side-effects' free theranostic means.

Schistosomiasis: the disease, the severity of the gap in the present intensity of applied research workloads and the scarce sensibility of withdrawn attention incited the authors of this research work to conduct the current research. Neglected tropical diseases as "Bilharziasis" infects at least 200 million individuals in 75 countries, while 120 million people are symptomatic patients, a further 600 million people are still exposed to infection and are potentially victim of this parasite (WHO, 2010), which causes brutal debilitating and incapacitating illness in millions of human and cattle. The annual death of Schistosomiasis was recently estimated by 150 – 200 thousand people every year, adding to that the drastic impact on economical and nutritional aspects (Blyther, 2011).

The development of a novel theranostic agent was the main target, in order to get it accomplished the single-domain antibody technology was selected to design a stable and efficient targeting moiety. In addition, the implementation of the vast growing nanotechnology was established via two major joint aspects (a) Nanobodies® technology, which, by itself, can afford a serological and therapeutic tool and (b) Graphene-coated magnetic nano-system, which can provide a complementary diagnostic and therapeutic function. The distinctive combined properties (i.e. high affinity, thermal and chemical stability, efficient synthesis, plus the synergistic active and magnetic *in vivo/in vitro* targeting ability) of the pre-designed system are, so far, confined in a nanoscale dimensions which sequentially added a wide-range of theranostic possibilities and applications.

The research described in this thesis resulted in the following methodological novelties:

- Nanobodies® against two different *Schistosoma mansoni* antigens, gut specific antigen and excretory-secretory antigen,
- Active sdAb-Graphene-Coated-Nanomagnet Bioconjugate,
- ^{99m}Tc Labeled active conjugate.

The research described in this thesis led to the following important biological conclusions:

- SmCB antigen was recognized as a potent immunogenic antigen and could elicit proper immune response in Camelidae's which subsequently lead to the production and purification of antigen-specific sdAbs binders,

- The bioconjugation of sdAb-Fe@C-MNP via EDC/NHS method showed a high preservation of the binding affinity of the attached Nanobodies[®],
- The radiolabeled active bio-nano-system could successfully be externally directed through a simple magnetic targeting process.

The number of reports dealing with bio-nanotechnology applications in different fields clearly indicates that this class of bio-nanostructure system represents an important tool for research as well as biotechnological uses, particularly theranostic ones. Despite the advantages of single domain antibody in terms of unique structural features, stability, and production costs the technology has taken almost twenty years and yet not largely popular in the scientific area. Part of the problem comes from the pretty restrictive intellectual property policy introduced by Hamers' patents which has probably prevented other contributors from participating in the development. In addition, there are quite a lot of technical challenges that still need to be studied in a systematic way, at the recombinant antibody panning level, plus, the level of the pre and post production strategies. For instance:

- Although Nanobodies[®] usually exhibit high expression yield, inadvertently, those of high binding affinity may suffer from very low expression.
- Some of the developed sdAbs may show excellent performance, yet, lack stability upon prolonged storage (e.g. dimerization), which necessitates an afterward genetic engineering intervention.
- The clearance time is a very crucial factor that it may act as a double-edged sword, several techniques need to be developed to control the optimal blood circulating time.
- The undesired accumulation in kidney still requires further investigation for finding the reason and discovering appropriate solutions.
- Tailoring into pluripotent constructs of Nanobodies[®] and their fusion derivates as well as their heterogeneous conjugate systems.

Finally, the single-domain antibody original patents are expiring in the next year along with the recent accessibility of new libraries, protocols, and vectors suitable for different theranostic applications. Therefore, it is strongly expected to have an increase of the interest of both research and industry for this class of sdAb bio-nano-technology in the near future.

Bibliography

Adel, M 2001, *Schistosomiasis: Tropical Medicine Science and Practice*, Imperial College Press, London.

Alvarez-Reuda, N, Behar, G, Ferré, V, Pugnière, M, Roquet, F, Gastinel, L, Jacquot, C, Aubry, J, Baty, D, Barbet, J & Birklè, S 2007, 'Generation of llama single-domain antibodies against methotrexate, a prototypical hapten', *Molecular Immunology*, vol 44, p. 1680–1690.

Arbabi-Ghahroudi, M, Desmyter, A, Wyns, L, Hamers, R & Muyldermans, S 1997, 'Selection and identification of single domain antibody fragments from camel heavy-chain antibodies', *FEBS Letters*, vol 414, p. 521–526.

Arbabi-Ghahroudi, M, Tanha, J & MacKenzie, R 2005, 'Prokaryotic expression of antibodies', *Cancer and Metastasis Reviews*, vol 24, p. 501–519.

Ashby, M, Ferreira, P & Schodek, D 2009, *Nanomaterials, Nanotechnologies and Design: An Introduction for Engineers and Architects*, 1st edn, Butterworth-Heinemann.

Atarhouch, T, Bendahman, N, Hamers-Casterman, C, Hamers, R & Muyldermans, S 1997, 'cDNA sequence coding for the constant region of the dromedary 3 heavy chain antibody', *Journal of Camel Practical Research*, vol 4, p. 177–182.

Balakrishnan, S 2011, *Structural and magnetic properties of polymer coated iron based nanoparticles for biomedical applications*, ProQuest, UMI Dissertation Publishing.

Baral, T, Magez, S, Stijlemans, B, Conrath, K, Vanhollebeke, B, Pays, E, Muyldermans, S & De Baetselier, P 2006, 'Experimental therapy of African trypanosomiasis with a nanobody-conjugated human trypanolytic factor', *Nature Medicine*, vol 12, p. 580–584.

Behar, G, Chames, P, Teulon, I, Cornillon, A, Alshoukr, F, Roquet, F, Pugnie're, M, Teillaud, J, Gruaz-Guyon, A, Pe'legrin, A & Baty, D 2009, 'Llama single-domain antibodies directed against nonconventional epitopes of tumor-associated carcinoembryonic antigen absent from nonspecific cross-reacting antigen', *The FEBS Journal*, vol 276, p. 4305–4317.

Behar, G, Siberil, S, Groulet, A, Chames, P, Pugniere, M, Boix, C, Sautes-Fridman, C, Teillaud, J & Baty, D 2008, 'Isolation and characterization of anti-FcgammaRIII (CD16) llama single-domain antibodies that activate natural killer cells', *Protein Engineering Design & Selection*, vol 21, p. 1-10.

Berriman, M, Haas, B, LoVerde, P, Wilson, A, Dillon, G, Cerqueira, G, Mashiyama, S, Al-Lazikani, B, Andrade, L, Ashton, P, Aslett, M, Bartholomeu, D, Blandin, G, Caffrey, C,

Coghlan, A, Coulson, R, Day, T, Delcher, A, DeMarco, R, Djikeng, A, 2009, 'The genome"qh'ÿj g blood fluke *Schistosoma mansoni*', *Nature*, vol 460, p. 352-358.

Bigwan, E, Tinja, B & Damen, J 2012, 'Prevalrnce of Schistosomiasis amongsecondary school boarding students in Potiskum Metropolis, Yobe State, North-Eastern Nigeria', *Bayero Journal of Pure and Applied Sciences*, vol 5, no. 1, p. 155-158.

Blyther, T 2011, 'Neglected Tropical Diseases: Background, Responses, and Issues for Congress', Prepared for Members and Committees of Congress, Congressional Research Service, CRS Report for Congress.

Bond, C, Marsters, J & Sidhu, S 2003, 'Contributions of CDR3 to VHH domain stability and the design of monobody scaffolds for naive antibody libraries', *Journal of Molecular Biology*, vol 332, p. 643– 655.

Boulianne, G, Hozumi, N & Shulman, M 1984, 'Production of functional chimeric mouse/human antibody', *Nature*, vol 312, p. 643–646.

Brissette, R & Goldstein, NI 2007, 'The use of phage display peptide libraries for basic and translational research', *Methods in Molecular Biology*, vol 383, p. 203–213.

Broisat, A, Hernot, S, Toczek, J, De Vos, J, Riou, L, Martin, S, Ahmadi, M, Thielens, N, Wernery, U, Caveliers, V, Muyldermans, S, Lahoutte, T, Fagret, D, Ghezzi, C & Devoogdt, N 2012, 'Nanobodies Targeting Mouse/Human VCAM1 for the Nuclear Imaging of Atherosclerotic Lesions', *Circulation Research*, vol 110, p. 927-937.

Buschow, K 2001, 'Encyclopedia of materials : science and technology', Pergamon.

Carmen, S & Jermutus, L 2002, 'Concepts in antibody phage display', *Briefings in Functional Genomics and Proteomics*, vol 1, no. 2, p. 189-203.

Chan, C & Carter, J 2010, 'Therapeutic antibodies for autoimmunity and inflammation', *Nature Reviews | Immunology*, vol 10, p. 301-316.

Chen, R, Zhang, Y, Wang, D & Dai, H 2001, 'Noncovalent Sidewall Functionalization of Single-Walled Carbon Nanotubes for Protein Immobilization', *American Chemical Society*, vol 123, p. 5838-3839.

Chothia, C, Lesk, A, Tramontano, A, Levitt, M, Smith-Gill, S, Air, G, Sheriff, S, Padlan, E, Davies, D & Tulip, W 1989, 'Conformations of immunoglobulin hypervariable regions ', *Nature*, vol 342, p. 877–883.

Chothia, C, Novotny, J, Bruccoleri, R & Karplus, M 1985, 'Domain association in immunoglobulin molecules. The packing of variable domains', *Journal of Molecular Biology*, vol 186, p. 651–663.

Cole, A, Yang, V & David, A 2011, 'Cancer theranostics: the rise of targeted magnetic nanoparticles', *Trends in Biotechnology*, vol 1, p. 1-10.

Conrath, K, Lauwereys, M, Galleni, M, Matagne, A, Frere, J, Kinne, J, Wyns, L & Muyldermans, S 2001a, 'Beta-lactamase inhibitors derived from single-domain antibody fragments elicited in the camelidae', *Antimicrobial Agents and Chemotherapy*, vol 45, p. 2807–2812.

Conrath, K, Lauwereys, M, Wyns, L & Muyldermans, S 2001b, 'Camel single-domain antibodies as modular building units in bispecific and bivalent antibody constructs', *The Journal of Biological Chemistry*, vol 276, p. 7346–7350.

Conrath, K, Wernery, U, Muyldermans, S & Nguyen, V 2003, 'Emergence and evolution of functional heavy-chain antibodies in Camelidae', *Developmental & Comparative Immunology*, vol 27, p. 87–103.

Coppieters, K, Dreier, T, Silence, K, de Haard, H, Lauwereys, M, Casteels, P, Beirnaert, E, Jonckheere, H, Van de Wiele, C, Staelens, L, Hostens, J, Revets, H, Remaut, E, Elewaut, D & Rottiers, P 2006, 'Formatted anti-tumor necrosis factor alpha VHH proteins derived from camelids show superior potency and targeting to inflamed joints in a murine model of collagen-induced arthritis', *Arthritis & Rheumatism*, vol 54, p. 1856–1866.

Cortez-Retamozo, V, Backmann, N, Senter, P, Wernery, U, De Baetselier, P, Muyldermans, S & Revets, H 2004, 'Complete remission of solid tumors by a single-domain antibody based conjugate prodrug activation', *Cancer Research*, vol 64, p. 2853–2857.

D'huyvetter, M, Aerts, A, Xavier, C, Vaneycken, I, Devoogdt, N, Gijs, M, Impens, N, Baatout, S, Ponsard, B, Muyldermans, S, Caveliers, V & Lahoutte, T 2012, 'Development of 177Lu-nanobodies for radioimmunotherapy of HER2 positive breast cancer: evaluation of different bifunctional chelators', *Contrast Media & Molecular Imaging*, vol 7, p. 254-264.

Dajotoy, T, Andersson, P, Bjartell, A, Löfdahl, C, Tapper, H & Egesten, A 2004, 'Human eosinophils produce the T cell-attracting chemokines MIG and IP-10 upon stimulation with IFN-', *Journal of Leukocyte Biology* , vol 76, p. 685-691.

Davies, J & Riechmann, L 1994, 'Camelising human antibody fragments: NMR studies on VH domains', *FEBS Letters*, vol 339, p. 285–290.

Davies, J & Riechmann, L 1995, 'Antibody VH domains as small recognition units', *Biology and Technology*, p. 475–479.

De Genst, E, Guilliams, T, Wellens, J, O'Day, E, Waudby, C, Meehan, S, Dumoulin, M, Hsu, S, Cremades, N, Verschueren, K, Pardon, E, Wyns, L, Steyaert, J, Christodoulou, J & Dobson, C

2010, 'Structure and Properties of a Complex of alpha-Synuclein and a Single-Domain Camelid Antibody', *Journal of Molecular Biology*, vol 402, p. 326-343.

De Genst, E, Saerens, D, Muyldermans, S & Conrath, K 2006a, 'Antibody repertoire development in camelids', *Developmental and Comparative Immunology*, vol 30, p. 187–198.

De Genst, E, Silence, K, Decanniere, K, Conrath, K, Loris, R, Kinne, J, Muyldermans, S & Wyns, L 2006b, 'Molecular basis for the preferential cleft recognition by dromedary heavy-chain antibodies', *PNAS*, vol 103, p. 4586-4591.

De Geus, B, Frenken, L, van der Linden, R, Hermans, P, Bos, W & Ruuls, R 2000, 'Isolation of antigen specific llama VHH antibody fragments and their high level secretion by Saccharomyces cerevisiae', *Journal of Biotechnology*, vol 78, p. 11–21.

De Groeve, K, Deschacht, N, De Koninck, C, Caveliers, V, Lahoutte, T, Devoogdt, N, Muyldermans, S, De Baetselier, P & Raes, G 2010, 'Nanobodies as tools for *in vivo* imaging of specific immune cell types', *Journal of Nuclear Medicine*, vol 51, no. 5, p. 782–789.

Decanniere, K, Muyldermans, S & Wyns, L 2000, 'Canonical antigen binding loop structures: more structures, more canonical classes?', *Journal of Molecular Biology*, vol 300, p. 83–91.

Deckers, N, Saerens, D, Kanobana, K, Conrath, K, Victor, B, Wernery, U, Vercruysse, J, Muyldermans, S & Dorny, P 2009, 'Nanobodies, a promising tool for species-specific diagnosis of *Taenia solium* cysticercosis', *International Journal for Parasitology*, vol 39, p. 625–633.

Desmyter, A, Transue, T, Ghahroudi, M, Thi, M, Poortmans, F, Hamers, R, Muyldermans, S & Wyns, L 1996, 'Crystal structure of a camel single-domain VH antibody fragment in complex with lysozyme', *Nature Structural Biology*, vol 3, p. 803–811.

Dumoulin, M, Conrath, K, Van Meirhaeghe, A, Meersman, F, Heremans, K, Frenken, L, Muyldermans, S, Wyns, L & Matagne, A 2002, 'Single-domain antibody fragments with high conformational stability', *Protein Science*, vol 11, p. 500–515.

Elliott, D 1996, 'Schistosomiasis Pathophysiology, Diagnosis, and Treatment', *Gastroenterol Clinical North American*, vol 25, p. 599-625.

Ellis, S, Newlands, G, Nisbet, A & Matthews, J 2012, 'Phage-display library biopanning as a novel approach to identifying nematode vaccine antigens', *Parasite Immunology*, vol 34, p. 285–295.

Florea, R 2011, 'Generation of anti-malaria Nanobodies® as diagnostic and molecular imaging tools', M.Sc. thesis, Faculty of Science and Bio-engineering Sciences Master of Biomolecular Sciences, Vrije Universiteit Brussel, Brussels, Belgium.

Foote, J & Winter, G 1992, 'Antibody framework residues affecting the conformation of the hypervariable loops', *Journal of Molecular Biology*, vol 224, p. 487–499.

Frenken, L, Dumoulin, M, Conrath, K, Van Meirhaeghe, A, Meersman, F & Heremans, K 2002, 'Single-domain antibody fragments with high conformational stability', *Protein Science*, vol 11, p. 500–515.

Frenken, L, van der Linden, R, Hermans, P, Bos, J, Ruuls, R, de Geus, B & Verrips, C 2000, 'Isolation of antigen specific llama VHH antibody fragments and their high level secretion by Saccharomyces cerevisiae', *Journal of Biotechnology*, vol 78, p. 11–21.

Fulford, M & Keystone, J 2002, *Schistosomiasis*, Healthline, New York.

Garayoa, G 2002, 'Preclinical evaluation of a new, stabilized neurotensin(8-13) pseudopeptide radiolabelled with 99mTc', *Journal of Nuclear Medicine*, vol 43, p. 374–383.

Ghahroudi, M, Desmyter, A, Wyns, L, Hamers, R & Muyldermans, S 1997, 'Selection and identification of single domain antibody fragments from camel heavy-chain antibodies', *FEBS Letters*, vol 414, p. 521–526.

Ghassabeh, GH, Muyldermans, S & Saerens, D 2010, 'Nanobodies, Single-Domain Antigen-Binding Fragments of Camelid Heavy-Chain Antibodies', in *Current Trends in Monoclonal Antibody Development and Manufacturing*, Springer, NY.

Giri, J 2003, 'Biomaterials and magnetism', *Sadhana Journal*, vol 28, no. 3, p. 639–656.

Goldman, E, Anderson, G, Liu, J, Delehanty, J, Sherwood, L, Osborn, L, Cummins, L & Hayhurst, A 2006, 'Facile generation of heat-stable antiviral and antitoxin single domain antibodies from a semisynthetic llama library', *Analytical Chemistry*, vol 78, p. 8245–8255.

Grass, R, Athanassiou, E & Stark, W 2007, 'Covalently Functionalized Cobalt Nanoparticles as a Platform for Magnetic Separations in Organic Synthesis', *Angewandte Chemie*, vol 46, no. 1, p. 4909 –4912.

Greenberg, A, Avila, D, Hughes, M, Hughes, A, McKinney, E & Flajnik, M 1995, 'A new antigen receptor gene family that undergoes rearrangement and extensive somatic diversification in sharks', *Nature*, vol 374, p. 168–173.

Gryseels, B, Polman, K, Clerinx, J & Kestens, L 2006, 'Human schistosomiasis', *Seminar*, vol 368, p. 1106-1118.

Gubin, S, Koksharov, Y, Khomutov, G & Yurkov, G 2005, 'Magnetic nanoparticles: preparation, structure and properties', *Russian Chemical Reviews*, vol 74, no. 6, p. 489-520.

Gueorguieva, D, Li, S, Walsh, N, Mukerji, A, Tanha, J & Pandey, S 2006, 'identification of single-domain, Bax-specific intrabodies that confer resistance to mammalian cells against oxidative-stress-induced apoptosis', *The FASEB Journal*, vol 20, p. 2636–2638.

Hamers-Casterman, C, Atarhouch, T, Muyldermans, S, Robinson, G, Hamers, C & Bajyana Songa, E 1993, 'Naturally occurring antibodies devoid of light chains', *Nature*, vol 363, p. 446-448.

Harmsen, M & Haad, H 2007, 'Properties, production, and applications of camelid single-domain antibody fragments', *Applied Microbiology and Biotechnology*, vol 77, p. 13–22.

Harmsen, M, Ruuls, R, Nijman, I, Niewold, T, Frenken, L & De-Geus, B 2000, 'Llama heavy-chain V regions consist of at least four distinct subfamilies revealing novel sequence features', *Molecular Immunology*, vol 37, p. 579–590.

Harmsen, M, van Solt, C, Hoogendoorn, A, van Zijderveld, F, Niewold, T & van der Meulen, J 2005, 'Escherichia coli F4 fimbriae specific llama single-domain antibody fragments effectively inhibit bacterial adhesion *in vitro* but poorly protect against diarrhoea', *Veterinary Microbiology*, vol 111, p. 89–98.

Harris, L 2002, 'Polymer Stabilized Magnetite Nanoparticles and Poly(propylene oxide) Modified Styrene-Dimethacrylate Networks', PhD Thesis, Chemistry, Virginia Polytechnic Institute and State University, Blacksburg, Virginia.

Henderson, K, Streltsov, V, Coley, A, Dolezal, O, Hudson, P, Batchelor, A, Gupta, A, Bai, T, Murphy, V, Anders, R, Foley, M & Nuttall, S 2007, 'Structure of an IgNAR-AMA1 complex: targeting a conserved hydrophobic cleft broadens malarial strain recognition', *Structure*, vol 15, no. 11, p. 1452–1466.

Herrmann, I, Grass, R, Mazunin, D & Stark, W 2009, 'Synthesis and Covalent Surface Functionalization of Nonoxidic Iron Core-Shell Nanomagnets', *Chemistry of Materials*, vol 21, no. 1, p. 3275–3281.

Hmila, I, Abdallah, R, Saerens, D, Benlasfar, Z, Conrath, K, Ayeb, M, Muyldermans, S & Bouhaouala-Zahar, B 2008, 'VHH, bivalent domains and chimeric Heavy chain-only antibodies with high neutralizing efficacy for scorpion toxin AahI'', *Molecular Immunology*, vol 45, p. 3847–3856.

Hmila, I, Saerens, D, Ben Abderrazek, R, Vincke, C, Abidi, N, Benlasfar, Z, Govaert, J, El Ayeb, M, Bouhaouala-Zahar, B & Muyldermans, S 2010, 'A bispecific nanobody to provide full protection against lethal scorpion envenoming', *The FASEB Journal*, vol 24, no. 9, p. 3479–3489.

Hsin, Y, Lin, C, Liang, Y, Hwang, K, Horng, J, Ho, J, Lin, C & Hwu, J 2008, 'Microwave Arcing Induced Formation and Growth Mechanisms of Core/Shell Metal/Carbon Nanoparticles in Organic Solutions', *Advanced Functional Materials*, vol 18, no. 1, p. 2048–2056.

Hussack, G, Hirama, T, Ding, W, MacKenzie, R & Tanha, J 2011, 'Engineered Single-Domain Antibodies with High Protease Resistance and Thermal Stability', *PLoS ONE*, vol 6, p. 1-15.

Hwang, W & Foote, J 2005, 'Immunogenicity of engineered antibodies', *Methods*, vol 36, p. 3-10.

Ismaili, A, Jalali-Javaran, M, Rasaee, M, Rahbarizadeh, F, Forouzandeh-Moghadam, M & Memari, H 2007, 'Production and characterization of anti-(mucin MUC1) single-domain antibody in tobacco (Nicotiana tabacum cultivar Xanthi)', *Biotechnology and Applied Biochemistry*, vol 47, p. 11–19.

Jobling, S, Jarman, C, Teh, M-M, Holmberg, N, Blake, C & Verhoeyen, M 2003, 'Immunomodulation of enzyme function in plants by single-domain antibody fragments', *Nature Biotechnology*, vol 21, p. 77–80.

John, D & Petri, W 2006, *Markell and Voge's Medical Parasitology*, 9th edn, Saunders Elsevier, United States.

Kallumadil, M, Tada, M, Nakagawa, T, Abe, M, Southern, P & Pankhurst, Q 2009, 'Suitability of commercial colloids for magnetic hyperthermia', *Journal of Magnetism and Magnetic Materials*, vol 321, p. 1509-1513.

King, C, Muchiri, E & Ouma, J 2000, 'Evidence Against Rapid Emergence of Praziquantel Resistance in *Schistosoma haematobium*, Kenya', *Emerging Infectious Diseases*, vol 6, no. 6, p. 585-594.

Kirchhofer, A, Helma, J, Schmidthals, K, Frauer, C, Cui, S, Karcher, A, Pellis, M, Muyldermans, S, Casas-Delucchi, C, Cristina Cardoso, M, Leonhardt, H, Hopfner, K & Rothbauer, U 2010, 'Modulation of protein properties in living cells using nanobodies', *Nature Structural & Molecular Biology*, vol 17, no. 1, p. 133-139.

Klooster, R, Maassen, B, Stam, J, Hermans, P, ten Haaft, M, Detmers, F, de Haard, H, Post, J & Verrips, C 2007, 'Improved anti-IgG and HSA affinity ligands: clinical application of VHH antibody technology', *Journal of Immunological Methods*, vol 324, p. 1-12.

Köhler, G & Milstein, C 1975, 'Continuous cultures of fused cells secreting antibody of predefined specificity', *Nature*, vol 256, p. 495–497.

Kruger, R, Kiser, W, Reinecke, D & Kruger, G 2003, 'Thermoacoustic computed tomography using a conventional linear transducer array', *Medical Physics*, vol 30, no. 5, p. 856–860.

Kruger, R, Miller, K, Reynolds, H, Kiser, W, Reinecke, D & Kruger, G 2000, 'Breast Cancer *in Vivo*: Contrast Enhancement with Thermoacoustic CT', *Radiology*, vol 216, no. 1, p. 279-283.

Kumar, C & Mohammad, F 2011, 'Magnetic nanomaterials for hyperthermia-based therapy and controlled drug delivery', *Advanced Drug Delivery Reviews*, vol 1, p. 1-20.

Ladenson, R, Crimmins, D, Landt, Y & Ladenson, J 2006, 'Isolation and characterization of a thermally stable recombinant anti-caffeine heavy-chain antibody fragment', *Analytical Chemistry*, vol 78, p. 4501-4508.

Lakowski, R, Luscombe, N, Swindells, M & Thornton, J 1996, 'Protein clefts in molecular recognition and function', *Protein Science*, vol 5, p. 2438–2452.

Lauwereys, M, Ghahroudi, M, Desmyter, A, Kinne, J, Hölzer, W, De Genst, E, Wyns, L & Muyldermans, S 1998, 'Potent enzyme inhibitors derived from dromedary heavy-chain antibodies', *The EMBO Journal*, vol 17, p. 3512–3520.

Lee, J, Fenton, B, Koch, C, Frelinger, J & Lord, E 1998, 'Interleukin 2 expression by tumor cells alters both the immune response and the tumor microenvironment', *Cancer Research*, vol 58, p. 1478–1485.

Liang, F & Chen, B 2010, 'A Review on Biomedical Applications of Single-Walled Carbon Nanotubes', *Current Medicinal Chemistry*, vol 17, p. 10-24.

Liang, Y, Hwang, K & Lo, S 2008, 'Solid-State Microwave-Arcing-Induced Formation and Surface Functionalization of Core/Shell Metal/Carbon Nanoparticles', *Small Journal*, vol 4, no. 1, p. 405–409.

Li, S & Hong, M 2011, 'Protonation, Tautomerization, and Rotameric Structure of Histidine: A Comprehensive Study by Magic-Angle-Spinning Solid-State NMR', *Journal of the American Chemical Society*, vol 133, no. 5, p. 1534–1544.

Liu, Z, Tabakman, S, Welsher, K & Dai, H 2009, 'Carbon Nanotubes in Biology and Medicine: *In vitro* and *in vivo* Detection, Imaging and Drug Delivery', *Nano Research*, vol 2, p. 85-120.

Maass, D, Sepulveda, J, Pernthaner, A & Shoemaker, C 2007, 'Alpaca (Lama pacos) as a convenient source of recombinant camelid heavy chain antibodies (VHHs)', *Journal of Immunology Methods*, vol 324, p. 13–25.

Mahmood, M, Xu, Y, Li, Z, Dervishi, E, Ali, N, Saini, V, Biris, A, Trigwell, S, Zharov, V & Biris, A 2009, 'Graphitic Materials for RF Thermal Ablation of Tumors', *IEEE Transaction on Inustry Applications*, vol 45, no. 6, p. 2162-2169.

Martin, F, Volpari, C, Steinkuhler, C, Dimasi, N, Brunetti, M, Biasiol, G, Altamura, S, Cortese, R, De Francesco, R & Sollazzo, M 1997, 'Affinity selection of a camelized V(H) domain antibody inhibitor of hepatitis C virus NS3 protease', *Protein Engineering*, vol 10, p. 607–614.

Mornet, S, Vasseur, S, Grasset, F & Duguet, E 2004, 'Magnetic nanoparticle design for medical diagnosis and therapy', *Journal of Materials Chemistry*, vol 14, p. 2161-2175.

Mua, Q, Yang, L, Davis, J, Vankayala, R, Hwang, K, Zhao, J & Yan, B 2010, 'Biocompatibility of polymer grafted core/shell iron/carbon nanoparticles', *Biomaterials*, vol 31, no. 1, p. 5083-5090.

Muyldermans, S 2001b, 'Single domain camel antibodies: current status', *Journal of Biotechnology*, vol 74, p. 277-302.

Muyldermans, S, Atarhouch, T, Saldanha, J, Barbosa, JARG & Hamers, R 1994, 'Sequence and structure of VH domain from naturally occurring camel heavy chain immunoglobulins lacking light chains', *Protein Engineering*, vol 7, p. 1129–1135.

Muyldermans, S, Atarhouch, T, Saldanha, J, Barbosa, J & Hamers, R 1994, 'Sequence and structure of VH domain from naturally occurring camel heavy chain immunoglobulins lacking light chains', *Protein Engineering*, vol 7, p. 1129–1135.

Muyldermans, S, Baral, N, Retamozzo, C, De Baetselier, P, De Genst, E, Kinne, J, Leonhardt, H, Magez, S, Nguyen, V, Revets, H, Rothbauer, U, Stijlemans, B, Tillib, S, Wernery, U, Wyns, L, Hassanzadeh-Gassabeh, G & Saerens, D 2009, 'Camelid immunoglobulins and Nanobody technology', *Veterinary Immunology and Immunopathology*, vol 128, p. 178-183.

Muyldermans, S, Cambillau, C & Wyns, L 2001a, 'Recognition of antigens by single-domain antibody fragments the superfluous luxury of paired domains', *Trends in Biochemical Sciences*, vol 26, p. 230-235.

Natterer, F 1986, *The Mathematics of Computerized Tomography*, Wiley, New York.

Nguyen, V, Desmyter, A & Muyldermans, S 2001, 'Functional heavy-chain antibodies in camelidae', *Advances in Immunology*, vol 79, p. 261–296.

Nguyen, V, Hamers, R, Wyns, L & Muyldermans, S 1999, 'Loss of splice consensus signal is responsible for the removal of the entire CH1 domain of the functional camel IgG2A heavy chain antibodies', *Molecular Immunology*, vol 36, p. 515–524.

Nguyen, V, Hamers, R, Wyns, L & Muyldermans, S 2000, 'Camel heavy-chain antibodies: diverse germline VHH and specific mechanisms enlarge the antigen-binding repertoire', *The EMBO Journal*, vol 19, p. 921–931.

Nguyen, V, Muyldermans, S & Hamers, R 1998, 'The specific variable domain of camel heavy-chain antibodies is encoded in the germline', *Journal of Molecular Biology*, vol 257, p. 413–418.

Nie, L, Ou, Z, Yang, S & Xing, D 2010, 'Thermoacoustic molecular tomography with magnetic nanoparticle contrast agents for targeted tumor detection', *Medical Physics*, vol 37, no. 8, p. 4193-4200.

Nikiforov, V 2007, 'Magnetic induction hyperthemia', *Russian Physics Journal*, vol 50, p. 913–924.

Nikitenko, S, Koltypin, Y, Palchik, O, Felner, I, Xu, X & Gedanken, A 2001, 'Synthesis of Highly Magnetic, Air-Stable Iron ± Iron Carbide Nanocrystalline Particles by Using Power Ultrasound`', *Angewandte Chemie International Edition*, vol 40, no. 23, p. 4447-4449.

Nuttall, S, Krishnan, U, Hattarki, M, De Gori, R, Irving, R & Hudson, P 2001, 'Isolation of the new antigen receptor from wobbegong sharks, and use as a scaffold for the display of protein loop libraries', *Molecular Immunology*, vol 38, p. 313–326.

Olichon, A, Schweizer, D, Muyldermans, S & de Marco, A 2007, 'Heating as a rapid purification method for recovering correctly-folded thermotolerant VH and VHH domains.', *BMC Biotechnology*, vol 7, p. 7-14.

Olichon, A & Surrey, T 2007, 'Selection of Genetically Encoded Fluorescent Single Domain Antibodies Engineered for Efficient Expression in Escherichia coli', *Journal of Biological Chemistry*, vol 282, p. 14-20.

Pearce, E & MacDonald, A 2002, 'The Immunobiology of Schistosomiasis', *Nature Reviews*, vol 2, p. 499-511.

Rahbarizadeh, F, Rasaee, M, Forouzandeh-Moghadam, M & Allameh, A 2005, 'High expression and purification of the recombinant camelid anti-MUC1 single domain antibodies in Escherichia coli', *Protein Expression and Purification*, vol 44, p. 32-38.

Rahbarizadeh, F, Rasaee, M, Forouzandeh-Moghadam, M & Allameh, A 2006, 'Over expression of anti-MUC1 single-domain antibody fragments in the yeast Pichia pastoris', *Molecular Immunology*, vol 43, p. 426–435.

Rajabi Bazl, M, Rasaee, M, Foruzandeh, M, Rahimpour, A, Kiani, J, Rahbarizadeh, F, Alirezapour, B & Mohammad, M 2007, 'Production of chimeric recombinant single domain antibody-green fluorescent fusion protein in Chinese hamster ovary cells', *Hybridoma*, vol 26, p. 1-9.

Ratier, L, Urrutia, M, Paris, G, Zarebski, L, Frasch, A & Goldbaum, F 2008, 'Relevance of the diversity among members of the Trypanosoma cruzi trans-sialidase family analyzed with camelids single-domain antibodies', *PLOS One*, vol 3, no. 10, p. e3524.

Reichert, J 2008, 'Monoclonal antibodies as innovative therapeutics', *Current Pharmaceutical Biotechnology*, vol 9, p. 423–430.

Rothbauer, U, Zolghadr, K, Tillib, S, Nowak, D, Schermelleh, L, Gahl, A, Backmann, N, Conrath, K, Muyldermans, S, Cardoso, MC & Leonhardt, L 2006, 'Targeting and tracing antigens in live cells with fluorescent nanobodies', *Nature Methods*, vol 3, p. 887–889.

Saerens, D, Ghassabeh, G & Muyldermans, S 2008, 'Single-domain antibodies as building blocks for novel therapeutics', *Current Opinion in Pharmacology* , vol 8, p. 600-608.

Saerens, D, Kinne, J, Bosmans, E, Wernery, U, Muyldermans, S & Conrath, K 2004, 'Single domain antibodies derived from dromedary lymph node and peripheral blood lymphocytes sensing conformational variants of prostate-specific antigen', *The Journal of Biological Chemistry*, vol 279, p. 1965–1972.

Sambrook, J, Fritsch, E & Maniatis, T 1989, *Molecular Cloning: A laboratory Manual*, 2nd edn, Cold Spring Harbor Laboratory Press, NY.

Schätz, A, Grass, R & Stark, W 2010, 'Winzig und mit metallischem Kern', *Nachrichten aus der Chemie*, vol 58, no. 1, p. 857-863.

Schirrmann, T, Meyer, T, Schütte, M, Frenzel, A & Hust, M 2011, 'Phage Display for the Generation of Antibodies for Proteome Research, Diagnostics and Therapy', *Molecules*, vol 16, p. 412-426.

Seligmann, M, Mihaesco, E, Preud'homme, J, Danon, F & Brouet, J 1979, 'Heavy chain diseases: current findings and concepts', *Immunological Reviews*, vol 48, no. 1, p. 145–167.

Sethuraman, N & Stadheim, T 2006, 'Challenges in therapeutic glycoprotein production', *Current Opinion in Biotechnology*, vol 17, p. 341–346.

Simmons, D, Abregu, F, Krishnan, U, Proll, D, Streltsov, V, Doughty, L, Hattarki, M & Nuttall, S 2006, 'Dimerisation strategies for shark IgNAR single domain antibody fragments', *Journal of Immunological Methods*, vol 315, p. 171–184.

Stijlemans, B, Conrath, K, Cortez-Retamozo, V, Van Xong, H, Wyns, L, Senter, P, Revets, H, De Baetselier, P, Muyldermans, S & Magez, S 2004, 'Efficient targeting of conserved cryptic epitopes of infectious agents by single domain antibodies. African trypanosomes as paradigm', *The Journal of Biological Chemistry*, vol 279, p. 1256–1261.

Stok, W, van der Linden, R, Frenken, L, de Geus, B, Harmsen, M & Ruuls, R 1999, 'Comparison of physical chemical properties of llama VHH antibody fragments and mouse monoclonal antibodies', *Biochimica et Biophysica Acta*, vol 1431, p. 37–46.

Strokappe, N, Szynol, A, Aasa-Chapman, M, Gorlani, A, Quigley, A, Hulsik, D, Chen, L, Weiss, R, de Haard, H & Verrips, T 2012, 'Llama Antibody Fragments Recognizing Various Epitopes of the CD4bs Neutralize a Broad Range of HIV-1 Subtypes A, B and C', *PLoS ONE*, vol 7, no. 3, p. e33298.

Tanaka, T, Lobato, M & Rabbitts, T 2003, 'Single domain intracellular antibodies: a minimal fragment for direct *in vivo* selection of antigen-specific intrabodies', *Journal of Molecular Biology*, vol 331, p. 1109–1120.

Tanha, J, Xu, P, Chen, Z, Ni, F, Kaplan, H & Narang, S 2001, 'Optimal design features of camelized human single domain antibody libraires', *The Journal of Biological Chemistry*, vol 276, p. 24774–24780.

Tasis, D, Tagmatarchis, N, Bianco, A & Prato, M 2006, 'Chemistry of Carbon Nanotubes', *Chemical Reviews*, vol 106, p. 1105-1136.

Taylor, A 2010, 'Engineering Carbon Encapsulated Nanomagnets towards Their Use for Magnetic Fluid Hyperthermia', PhD Thesis, Mathematics and Natural Sciences, Technical University of Dresden, Dresden.

Thomassen, Y, Meijer, W, Sierkstra, L & Verrips, C 2002, 'Large-scale production of VHH antibody fragments by Saccharomyces cerevisiae', *Enzyme and Microbial Technology*, vol 30, p. 273–278.

Thomassen, Y, Verkleij, A, Boonstra, J & Verrips, C 2005, 'Specific production rate of VHH antibody fragments by Saccharomyces cerevisiae is correlated with growth rate, independent of nutrient limitation', *Journal of Biotechnology*, vol 118, p. 270–277.

Tijink, B, Laeremans, T, Budde, M, Stigter-van Walsum, M, Dreier, T, de Haard, H, Leemans, C & van Dongen, G 2008, 'Improved tumor targeting of anti-epidermal growth factor receptor Nanobodies through albumin binding: taking advantage of modular Nanobody technology', *Molecular Cancer Therapeutics*, vol 7, no. 8, p. 2288–2297.

Tillib, S 2011, '"Camel Nanoantibody" is an Efficient Tool for Research, Diagnostics and Therapy', *Molecular Biology*, vol 45, p. 66–73.

Tillib, SV, Ivanova, T & Vasilev, L 2010, 'Fingerprint like analysis of "nanoantibody" selection by phage display method using two helper phage variants', *Acta Naturae*, vol 2, p. 100–108.

Tremblay, J, Kuo, C, Abeijon, C, Sepulveda, J, Oyler, G, Hu, X, Jin, M & Shoemaker, C 2011, 'Camelid single domain antibodies (VHHs) as neuronal cell intrabody binding agents and inhibitors of Clostridium botulinum neurotoxin (BoNT) proteases', *Toxicon*, vol 56, no. 6, p. 990–998.

Utsumi, S & Karush, F 1964, 'The subunits of purified rabbit antibody', *Biochemistry*, vol 3, p. 1329–1338.

Van Creveld, C, Ungar-Waron, H, Yagil, R, Brenner, J, Paz, R & Partoch, N 2003, 'Reactions of peripheral blood mononuclear cells of camels with monoclonal antibodies against ruminant leukocytes', *Comparative Immunology, Microbiology and Infectious Diseases*, vol 26, p. 137–143.

Van de Laar, T, Visser, C, Holster, M, López, C, Kreuning, D, Sierkstra, L, Lindner, N & Verrips, T 2007, 'Increased heterologous protein production by Saccharomyces cerevisiae growing on ethanol as sole carbon source', *Biotechnology and Bioengineering*, vol 96, p. 483–494.

Van der Linden, R, de Geus, B, Stok, W, Bos, W, van Wassenaar, D, Verrips, T & Frenken, L 2000, 'Induction of immune responses and molecular cloning of the heavy chain antibody repertoire of Lama glama', *Journal of Immunology Methods*, vol 240, p. 185–195.

Van der Linden, R, Frenken, L, de Gues, B, Harmsen, M, Ruuls, R, Stok, W, de Ron, L, Wilson, S, Davis, P & Verrips, T 1999, 'Comparison of physical chemical properties of llama VHH antibody fragments and mouse monoclonal antibodies', *Biochimica et Biophysica Acta*, vol 1431, p. 37–46.

Van der Vaart, J, Pant, N, Wolvers, D, Bezemer, S, Hermans, P, Bellamy, K, Sarker, S, van der Logt, C, Svensson, L, Verrips, C, Hammarstrom, L & van Klinken, B 2006, 'Reduction in morbidity of rotavirus induced diarrhoea in mice by yeast produced monovalent llama-derived antibody fragments', *Vaccine*, vol 24, p. 4130–4137.

van Vliet, C, Ledeboer, A, Bezemer, S, de Hiaard, J, Schaffers, I & Verrips, C 2002, 'Preventing phage lysis of Lactococcus lactis in cheese production using a neutralizing heavy-chain antibody fragment from llama', *Journal of Dairy Science*, vol 85, p. 1376–1382.

Vaneycken, I, D'huyvetter, M, Hernot, S, De Vos, J, Xavier, C, Devoogdt, N, Caveliers, V & Lahoutte, T 2011, 'Immuno-imaging using nanobodies', *Current Opinion in Biotechnology*, vol 22, p. 877–881.

Vaneycken, I, Devoogdt, N, Van Gassen, N, Vincke, C, Xavier, C, Wernery, U, Muyldermans, S, Lahoutte, T & Caveliers, V 2011, 'Preclinical screening of anti-HER2 nanobodies for molecular imaging of breast cancer', *The FASEB Journal*, vol 25, no. 7, p. 2433-2446.

Verheesen, P, Kluijver, A, van Koningsbruggen, S, de Brij, M, de Haard, H, van Ommen, C, van der Maarel, S & Verrips, T 2006, 'Prevention of oculopharyngeal muscular dystrophy-associated aggregation of nuclear poly(A)-binding protein with a single-domain intracellular antibody', *Human Molecular Genetics*, vol 15, p. 105–111.

Verrips, T, van der Linden, R, de Geus, B, Stok, W, Bos, W & van Wassenaar, D 2000, 'Induction of immune responses and molecular cloning of the heavy chain antibody repertoire of Lama glama', *Journal of Immunological Methods*, vol 240, p. 185–195.

Vincke, C, Gutiérrez, C, Wernery, U, Devoogdt, N, Hassanzadeh-Ghassabeh, G & Muyldermans, S 2012, 'Generation of single domain antibody fragments derived from camelids and generation of manifold constructs', in P Chames (ed.), *Antibody Engineering : Methods and Protocols, Second Edition*, 2nd edn, Marseille , France.

Vincke, C, Loris, R, Saerens, D, Martinez-Rodriguez, S, Muyldermans, S & Conrath, K 2009, 'General strategy to humanize a camelid single-domain antibody and identification of a universal humanized nanobody scaffold', *The Journal of Biological Chemistry*, vol 284, p. 3273–3284.

Vosjan, M, Perk, L, Roovers, R, Visser, G, Walsum, M, en Henegouwen, P & van Dongen, G 2011, 'Facile labelling of an anti-epidermal growth factor receptor Nanobody with 68Ga via a novel bifunctional desferal chelate for immuno-PET', *European Journal of Nuclear Medicine and Molecular Imaging*, vol 38, p. 753–763.

Vosjan, M, Vercammen, J, Kolkman, J, Stigter-van Walsum, M, Revets, H & van Dongen, G 2012, 'Nanobodies targeting the hepatocyte growth factor: potential new drugs for molecular cancer therapy', *Molecular Cancer Therapy*, vol 11, p. 1017-1025.

Vu, K, Ghahroudi, M, Wyns, L & Muyldermans, S 1997, 'Comparison of llama VH sequences from conventional and heavy chain antibodieS', *Molecular Immunology*, vol 34, p. 1121–1131.

Wang, Z, Choi, C, Kim, B, Kim, J & Zhang, Z 2003, 'Characterization and magnetic properties of carbon-coated cobalt nanocapsules synthesized by the chemical vapor-condensation process', *Carbon*, vol 41, no. 9, p. 1751-1758.

Wernery, U 2001, 'Camelid immunoglobulins and their importance for the new-born—a review', *Journal of Veterinary Medicine*, vol 48, no. 8, p. 561–568.

Wernery, U, Fowler, M & Wernery, R 1999, *Color atlas of camelid hematology*, Blackwell Wissenschafts-Verlag, Berlin ; Boston.

Wesolowski, J, Alzogaray, V, Reyelt, J, Unger, M, Juarez, K, Urrutia, M, Cauerhff, A, Danquah, W, Rissiek, B, Scheuplein, F, Schwarz, N, Adriouch, S, Boyer, O, Seman, M, Licea, A, Serreze, D, Goldbaum, F, Haag, F & Koch-Nolte, F 2009, 'Single domain antibodies: promising experimental and therapeutic tools in infection and immunity', *Medical Microbiology and Immunology*, vol 198, p. 157-174.

WHO 2010, 'Neglected Tropical Diseases Department', *WHO Fact Sheets*.

World.Health.Organization 1993, 'The Control of Schistosomiasis: Second Report of the WHO Expert Committee', WHO Technical Report Series, World Health Organization, 803.

Wu, H, Chang, X, Liu, L, Zhao, F & Zhao, Y 2009, 'Chemistry of Carbon Nanotubes in Biomedical Application', *Journal of Materials Chemistry*, vol 20, p. 1036-1052.

Xavier, C, Devoogdt, N, Hernot, S, Vaneycken, I, D'Huyvetter, M, De Vos, J, Massa, S, Lahoutte, T & Caveliers, V 2012, 'Site-Specific Labeling of His-Tagged Nanobodies with 99mTc: A Practical Guide', in D Saerens, S Muyldermans (eds.), *Single Domain Antibodies : Methods and Protocols*, 2012th edn, Humana Press, Brussels.

Xu, Y, Mahmood, M, Fejleh, A, Li, Z, Watanabe, F, Trigwell, S, Little, R, Kunets, V, Dervishi, E, Biris, A, Salamo, G & Biris, A 2010, 'Carbon-covered magnetic nanomaterials and their application for the thermolysis of cancer cells', *International Journal of Nanomedicine*, vol 5, p. 167–176.

Young, J, Wang, M & Brezovich, I 1980, 'Frequency/depth–penetration considerations in hyperthermia by magnetically induced currents', *Electronics Letters*, vol 16, p. 358–359.

Zhang, W, Feng, J, Li, Y, Guo, N & Shen, B 2005, 'Humanization of an anti-human TNF-a antibody by variable region resurfacing with the aid of molecular modeling', *Molecular Immunology*, vol 42, p. 1445–1451.

Zhang, J, Tanha, J, Hirama, T, Khieu, N, Tong-Sevinc, H, Stone, E, Brisson, J & MacKenzie, C 2003, 'Pentamerization of single-domain antibodies from phage libraries: a novel strategy for the rapid generation of high-avidity antibody reagents', *Journal of Molecular Biology*, vol 335, p. 49–56.

Web Sites:

CDC, 2010. *Schistosomiasis*. [Online] Available at:
http://www.dpd.cdc.gov/dpdx/HTML/Schistosomiasis.htm [Accessed 1 January 2012].

CDC, 2011. *Geographic Distribution of Schistosomiasis*. [Online] Available at:
http://wwwnc.cdc.gov/travel/images/map3-14-distribution-schistosomiasis.jpg [Accessed 1 January 2012].

Education, H., 2011. *Hope Education*. [Online] Available at: http://www.hope.edu/swimmersitch [Accessed 1 July 2012].

Pierce, T.S., 2012. *Pierce Protein Biology Products*. [Online] Available at:
http://www.piercenet.com/browse.cfm?fldID=F3305493-0FBC-93DA-2720-4412D198A9C9 [Accessed 12 November 2012].